RECOMBINANT ELASTIN-MIMETIC PROTEIN POLYMERS AS DESIGN ELEMENTS FOR AN ARTERIAL SUBSTITUTE

A Dissertation
Presented to
The Academic Faculty

by

Rory Elizabeth Sallach

In Partial Fulfillment
of the Requirements for the Degree
Doctor of Philosophy in Bioengineering

Georgia Institute of Technology
August 2008

RECOMBINANT ELASTIN-MIMETIC PROTEIN POLYMERS AS DESIGN ELEMENTS FOR AN ARTERIAL SUBSTITUTE

Approved by:

Dr. Elliot L. Chaikof, Advisor
School of Biomedical Engineering
Georgia Institute of Technology
Department of Surgery
Emory University School of Medicine

Dr. Robert M. Nerem
School of Mechanical Engineering
Georgia Institute of Technology

Dr. Vincent P. Conticello
School of Chemistry
Emory University

Dr. Yadong Wang
School of Biomedical Engineering
Georgia Institute of Technology

Dr. Marc E. Levenston
School of Mechanical Engineering
Stanford University

Date Approved: May 09, 2008

ACKNOWLEDGEMENTS

I would like to express my sincere appreciation to my advisor, Dr. Elliot Chaikof, for his continued guidance and support throughout my graduate career. His passion for science and research has inspired me. I would also like to thank Dr. Carolyn Haller for her encouragement, advice, and technical guidance, as well as Dr. Wanxing Cui for his technical assistance and personal investment in my work.

My sincere appreciation goes out to members of my committee: Dr. Vincent Conticello, Dr. Marc Levenston, Dr. Robert Nerem, and Dr. Yadong Wang for their contributions and investment in this project. I would also like to remember Dr. Robert Apkarian, whose zest for living and enthusiasm for science was truly contagious.

I would like to acknowledge the members of the Chaikof laboratory for all of their help, advice, and friendship, as well as members of the Conticello lab for their expertise and helpful guidance.

I would especially like to thank those who got me started on this journey many years ago: Mr. Wesley Kidd, who first taught me to love science, and to Dr. Dennis Maher, who introduced me to this field and encouraged me to pursue it. Lastly, I would like to extend my gratitude to those who have had the most profound impact on my life, my family, for their everyday love and support. To my parents who have taught me everything important in life and to my brilliant siblings, Lindsay, Megan, and Brett who have motivated me to set lofty goals and pushed me to achieve them.

This work has been supported by the National Science Foundation pre-doctoral research grant as well as a PEO Scholar Award.

TABLE OF CONTENTS

Acknowledgements ..... **iii**

List of Tables ..... **vi**

List of Figures ..... **vii**

Summary ..... **xiv**

Chapter 1-Introduction **1**

1.1 Central Hypothesis and Specific Aims 1

1.2 Motivation 2

1.3 Rational 4

1.4 Background 5

1.4.1 Current strategies in the design of an engineered vascular graft 6

1.4.2 The aortic media, a model system for the design of a vascular graft prosthesis 6

1.4.3 Native elastin, an introduction 9

1.4.4 Biochemistry of native elastin 10

1.4.5 Coacervation phenomena in native elastin and recombinant proteins 10

1.4.6 Elastin fiber assembly 11

1.4.7 Biosynthetic approach to the development of an engineered vascular graft 12

1.4.8 Elastin-mimetic proteins 13

1.5 Significance of Proposed Research 14

Chapter 2- Elastin-Mimetic Protein Polymers Capable of Physical and Chemical Crosslinking **15**

2.1 Introduction 15

2.2 Materials and Methods 17

2.3 Results and Discussion 39

2.4 Conclusions 60

Chapter 3- Biocompatibility of Recombinant Elastin-Mimetic Proteins **61**

3.1 Introduction 61

3.2 Materials and Methods 64

3.3 Results 73

3.3 Discussion 80

3.4 Conclusions 90

Chapter 4- Recombinant Elastin Protein Expression in *Pichia pastoris* **91**

4.1 Introduction 91

4.2 Materials and Methods 94

4.3 Results and Discussion 106
4.4 Conclusions 119
Chapter 5- Conclusions and Future Directions 120
Appendix A - DNA coding sequences 129
A.1 Coding sequences for DNA monomer repeat units of individual blocks of **LysB10** 130
A.2 Coding sequences for DNA monomer repeat units of individual blocks of **R4** 131
Appendix B- Electrospun Elastin and Collagen Nano-Fibers 132
B.1 Introduction 133
B.2 Electrospinning as a biomedical fabrication technology 134
B.2.1 The science of electrospinning 134
B.2.2 Generation of nanofibers with controlled structures and morphology 136
B.3 Generation of collagen and elastin small diameter fibers and fiber networks 137
B.3.1 Native collagen and biological function 138
B.3.2 Collagen as a biomaterial 139
B.3.3 Electrospun collagen nanofibers 140
B.3.4 Biological role of elastin 142
B.3.5 Elastin as a biomaterial 143
B.3.6 Recombinant elastin technologies 144
B.3.7 Generation of elastin and elastin-mimetic small diameter fiber networks 145
B.4 Generation of crosslinked fibers and fiber networks 148
B.4.1 Crosslinking collagen networks 149
B.4.2 Crosslinking elastin networks 149
B.5 Multicomponent electrospun assemblies 151
B.6 Elecrospun networks and the potential for the incorporation of living cells 152
B.7 Future Trends: Biomedical applications for electrospun collagen and elastin nanofiber networks 153
References 155

LIST OF TABLES

Table 2-1. Coding Sequences of Oligonucleotide Cassettes Employed for the Construction of Crosslinkable Protein Triblocks, **LysB10** ($AP_1IE_1IP_1A$) and **R4** (AP_2IE_2IPA) **19**

Table 2-2. Amino acid sequence of **LysB10** and related nucleic acid coding sequence $[VPAVGKVPAVG(IPAVG)_4][(IPAVG)_5]_{33}$ $[IPAVGKAAKVPGAG][(VPGAG)_2VPGEG(VPGAG)_2]_{28}$ $[VPAVGKAAKVPGAGVPAVG(IPAVG)_4][(IPAVG)_5]_{33}[IPAVGKAAKA]$ **31**

Table 2-3. Amino acid sequence of **R4** and related nucleic acid coding sequence $[VPAVGKVPAVG[(IPAVG)_5]_{16}$ (IPAVGIPAVG)KAAK(VPGAGVPGIG) $[(VPGIG)_5]_{15}$(VPGIGVPAVG)KAAK(VPGAGVPAVG) $[(IPAVG)_5]_{16}$ IPAVGVPAVGKAAKA] **32**

Table 2-4. Review of chemically crosslinkable elastin-mimetic systems and chemical crosslinking strategies **45**

Table 2-5. Summary of mechanical parameters in crosslinked and non-crosslinked films **48**

Table 3-1. Biocompatibility evaluation of elastin-mimetic polypeptides **84**

Table 3-2. Biostability in physically crosslinked systems **89**

Table 4-1. Amino acid sequence and related nucleic acid coding sequence for the **Yeast ELP** gene in *E coli* **(A)** and *P pastoris* **(B)** expression systems **95**

Table 4-2. Monomer Library. **97**

Table 4-3. Nucleic acid sequence of **Yeast ELP** adaptor with related amino acid coding sequence and restriction enzyme cut sites **100**

Table A-1. Coding sequences for DNA monomer repeat units of individual blocks of **LysB10** **130**

Table A-2. Coding sequences for DNA monomer repeat units of individual blocks of **R4**..... **131**

LIST OF FIGURES

Figure 2-1. Analytical restriction digests, 1% TAE (Tris-acetate-EDTA) agarose gel, depicting gene and vector sizes at each stage of the LysB10 assembly process with corresponding digestion schemes. DNA standard used was a 1Kb DNA ladder (NEB). **A.** Lane 1: *Bam*HI / *Hin*DIII digest pE1 (2.1 Kb), pZerO-2 (3.3 Kb). Lane 2: *Bam*HI / *Hin*DIII digest pP1 (2.5 Kb), pZerO-2 (3.3Kb). Lane 3: *Nsi* I / *Xma* I digest pP1I (2.56 Kb), pZerO-1 (1.3, 1.5 Kb). Lane 4: *Nsi* I / *Xma* I digest pIP1 (2.56 Kb), pZerO-1 (1.3, 1.5 Kb). **B.** Lane 1: Nsi I digest pP1IE1 (4.66 Kb), pZErO-1 (2.8 Kb). **C.** Lane 1: *Nsi* I digest pP1IE1IP1 (7.22 Kb), pZErO-1 (2.8 Kb). Lane 2: *Nsi* I digest LysB10 (7.28 Kb), pZErO-1 (2.8 Kb). Lane 3: *Bam*HI / *Hin*DIII digest LysB10 (7.28 Kb), pET 24a (5.3 Kb) **26**

Figure 2-2. Analytical restriction digests, 1% TAE (Tris-acetate-EDTA) agarose gel, depicting gene and vector sizes at each stage of the R4 assembly process with corresponding digestion schemes. DNA standard used was a 1Kb DNA ladder (NEB). **A.** Lane 1: Nsi I digest pE2 (1.1 Kb), pZerO-1 (2.8 Kb). Lane 2: Nsi I digest pP2 (1.2 Kb), pZerO-1 (2.8Kb). Lane 3: Nsi I digest pE2I (1.16 Kb), pZerO-1 (2.8 Kb). Lane 4: Nsi I digest pP2I (1.26 Kb), pZerO-1 (2.8 Kb). Lane 5: Nsi I digest pP2IE2I (2.42 Kb), pZerO-1 (2.8 Kb). **B.** Lane 1: Nsi I digest pP2IE2IP2 (3.62 Kb), pZerO-1 (2.8 Kb). Lane 2: Nsi I digest pR4 (3.7 Kb), pZerO-1 (2.8Kb). Lane 3: BamH I / HinD III digest pR4 (3.7 Kb), pET24-a (5.3 Kb).....**27**

Figure 2-3. Sodium dodecyl sulfate-polyacrylamide gel electrophoresis (SDS-PAGE) analysis of crosslinkable elastin-mimetic triblock copolymers. **A**. **LysB10**, run on 7.5% SDS-PAGE stained with Copper Stain (BioRad). Expected molecular weight: 209 KDa. **B**. **R4** run on 7.5% SDS-PAGE stained with Copper Stain. Expected molecular weight: 108 KDa. Marker lane: Precision Plus Protein Kaleidoscope (Bio-Rad). **C.** Assembly scheme for crosslinkable elastin-mimetic proteins, **LysB10** and **R4**. Both proteins are triblock copolymers with lysine-containing crosslinking domains flanking each plastic-like and elastic-like domain. Together, there are eight possible sites for chemical crosslinking afforded by the free amine moieties of the lysine residues and the N-terminal amine of the peptide chain. Plastic-like domain (grey), Elastic-like domain (white), Crosslinking domain (black) **33**

Figure 2-4. Rheological behavior of triblocks in water.**(A) LysB10** dynamic shear storage (G′), loss modulus (G″) are plotted as a function of temperature (γ 2%, ω 1Hz). **(B) LysB10** dynamic shear storage (G′), loss modulus (G″), and complex viscosity (η^*) are plotted as

a function of frequency (γ 2%, 37°C). **(C) R4** dynamic shear storage (G′), loss modulus (G″) are plotted as a function of temperature (γ 2%, ω 1Hz). **(D) R4** dynamic shear storage (G′), loss modulus (G″), and complex viscosity (η*) are plotted as a function of frequency (γ 2%, 37°C).....**43**

Figure 2-5. The influence of preconditioning on the resilience of water cast **LysB10** films with and without glutaraldehyde crosslinking (Figure **A** and **B**, respectively). A sample was cyclically stretched to 50% strain and then to 30% for 20 cycles, with an off-loading period of 5 minutes between cycles. This figure is representative of multiple data sets **49**

Figure 2-6. **A.** The influence of preconditioning on the resilience of water cast **LysB10** films with (left y-axis) and without glutaraldehyde crosslinking (right y-axis). The sample was cyclically stretched to 50% strain and then to 30% for 20 cycles, with an off-loading period of 5 minutes between cycles. This figure is representative of multiple data sets and illustrates cycle 20 of 30% stretch. **B.** Uniaxial stress-strain analysis performed on a Minimat 2000. The Young's modulus was 1.60 ± 0.48MPa for preconditioned glutaraldehyde crosslinked films and 0.53 ± 0.02 MPa for preconditioned non-crosslinked films measured from the linear region **50**

Figure 2-7. **A.** Creep behavior of water cast **LysB10** films GTA crosslinked examined as tensile stress was maintained at 45KPa and 450KPa. These figures are representative of multiple data sets in which variability was <10%. **B.** Comparison of the creep behaviors of water cast **LysB10** films with and without gluteraldehyde crosslinking at applied stresses of 45 KPa **51**

Figure 2-8. **A.** Uniaxial stress-strain analysis. The Young's modulus was determined from the linear region of the curve as 67.4± 5 MPa for glutaraldehyde crosslinked **R4** films measured on a Minimat 2000 and 48.6± 9 MPa for non-crosslinked **R4** films measured on a DMTA. **B.** Comparison of the creep behaviors of water cast **R4** films subjected to gluteraldehyde crosslinking. Creep was examined as tensile stress was maintained at 45KPa and 450KPa, and 800KPa. This figure is representative of multiple data sets. **R4** samples were not preconditioned **52**

Figure 2-9. FACS analysis of peritoneal implanted **LysB10** and **R4** cylindrical hydrogels one week post-implant (n=5 for each group). Experimental groups showed no statistical difference in cell number from normal and sham control groups **57**

Figure 2-10. Histological analysis of three subcutaneous **LysB10** implants retrieved 3 weeks post-implant. **(A)** H&E staining of formalin fixed, paraffin embedded subcutaneous **LysB10** implants demonstrates the presence of a mild foreign body reaction along the periphery of the sample. **(B)** F4/80 staining of formalin fixed, paraffin embedded subcutaneous **LysB10** implants demonstrate the presence of macrophages along the periphery of the fibrous capsule but no infiltration into the **LysB10** implant. Histological analysis of peritoneal **LysB10** implants retrieved 1 week post-implant. **(C)** H&E staining demonstrates the presence of a mild foreign body reaction along the periphery of the peritoneal **LysB10** implant . **(D)** F4/80 staining the presence of macrophages along the periphery of the fibrous capsule but no infiltration into the peritoneal **LysB10** implant. Images are oriented so that the **LysB10** gel is located in the bottom right corner…….....**58**

Figure 2-11. Histological analysis of three subcutaneous **R4** implants retrieved 3 weeks post-implant. **(A)** H&E staining of formalin fixed, paraffin embedded subcutaneous **R4** implants demonstrates the presence of a mild foreign body reaction along the periphery of the sample. **(B)** F4/80 staining of formalin fixed, paraffin embedded subcutaneous **R4** implants demonstrate the presence of macrophages along the periphery of the fibrous capsule but no infiltration into the **R4** implant. Histological analysis of peritoneal **R4** implants retrieved 1 week post-implant. **(C)** H&E staining demonstrates the presence of a mild foreign body reaction along the periphery of the peritoneal **R4** implant . **(D)** F4/80 staining the presence of macrophages along the periphery of the fibrous capsule but no infiltration into the peritoneal **R4** implant. Images are oriented so that the **R4** gel is located in the bottom right corner…….....**59**

Scheme 2-1. General cloning strategy in the assembly of crosslinkable triblock genes. Plasmids have been designated by the DNA cassette they contain. For example, the plasmid containing the lysine insert cassette is referred to as plasmid **I** (p**I**). **P** = Plastic-like cassette (blue), **E** = Elastic-like cassette (yellow), **I** = Insert cassette (black), **A** = Adaptor cassette (black). **22**

Figure 3-1. Syringe casting method for **B9** hydrogel implants. **(A)** 10wt% **B9** solution was drawn into syringe and allowed to gel at room temperature. **(B)** End of syringe was removed. **(C) B9** hydrogel was ejected from syringe into room temperature PBS. **(D)** Ejected sample equilibrated in PBS. This sample was sectioned into 8mm implants. **69**

Figure 3-2. **A.** A coronal view through the C57BL/6 mouse showing the location of the implant. Image is oriented with the mouse vertical. The green lines shown are the planing of the 23 transverse-oblique slices through the implant. **B.** MR scan slices through implant. **C.**

Transverse MR image of the subcutaneous **B9** implant. The light region on the outer surface is a cross section of the **B9** implant. Implant areas were assessed from individual images and summed to assess volume of the implant. Slice thickness of the scan is 0.5mm. (V = verterbra, M = Psoas Major muscle, I = Intestine cross-sections, **B9** = cross-section of **B9** implant). **71**

Figure 3-3. Transverse MR images of the subcutaneous **B9** implant. The light region on the outer surface is the cross section of **B9** implant. Slice thickness is 0.5mm. **72**

Figure 3-4. Structural Characterization of the B9 protein. **A**. Sodium dodecyl sulfate-polyacrylamide gel electrophoresis (SDS-PAGE) analysis revealed a single protein band at 170 KDa corresponding to **B9**. 10ug of the elastin-mimetic polypeptide was run on 7.5% gel and negatively stained with Copper stain (Bio-Rad). Molecular weight markers were Precision Plus Protein Kaleidoscope (Bio-Rad). **B.** Rheological behavior of 10 weight percent **B9** in water. Dynamic shear storage (G′) and loss modulus (G″) are plotted as a function of temperature (γ 2%, ω 1Hz). The gelation temperature was determined by heating samples from 4°C to 37°C at a rate of 1°C per minute. Experiments were repeated on 3 samples and representative data presented. **74**

Figure 3-5. Subcutaneous injection mouse model. 200 uL of a 10 weight percent solution of **B9** was injected subcutaneously, which gelled instantly. A group of samples were retrieved at one week for FACS analysis and histology. Another group of samples were retrieved three weeks for histology. **75**

Figure 3-6. H&E staining of formalin fixed, paraffin embedded **B9** implants demonstrates the presence of a mild foreign body reaction along the periphery of the sample. Histological analysis of subcutaneous **B9** implants retrieved 3 weeks post-implant, skin side **(A)** and muscle side **(B)**. Histological analysis of peritoneal **B9** implants retrieved 1 week post-implant **(C)**. All images were obtained at 20X magnification and are oriented such that the **B9** hydrogel is located in the bottom right corner……**76**

Figure 3-7. F4/80 staining of formalin fixed, paraffin embedded **B9** implants demonstrate the presence of macrophages along the periphery of the fibrous capsule but no infiltration into the **B9** implant. Histological analysis of subcutaneous **B9** implants retrieved 3 weeks post-implant **(A)** and peritoneal **B9** implants retrieved 1 week post-implant **(B)**. All images were obtained at 20X magnification and are oriented such that the **B9** hydrogel is located in the bottom right corner……..……**77**

Figure 3-8. FACS analysis of peritoneal implanted **B9** 1 week post-implant (n=5). Experimental group showed no statistical difference in cell number from control group, $p < 0.05$. Cells were immunostained for flow

cytometry with FITC-conjugated hamster anti-mouse CD3 for total T cells, FITC-conjugated rat monoclonal anti-mouse CD4 for helper T cells, FITC-conjugated rat monoclonal anti-mouse CD8 for cytotoxic T cells, FITC-conjugated rat monoclonal anti-mouse CD19 for B cells, PE-conjugated rat monoclonal anti-mouse CD11b for macrophage, and FITC-conjugated rat monoclonal anti-mouse Gr-1 for neutrophils (BD Biosciences Pharmingen)……**78**

Figure 3-9. Biostability of **B9** implants assessed by MRI. Implant cross-sectional areas and lenths were obtained through image analysis over 7 months and data is currently being compiled. Four month biostability data is presented in this figure……..**79**

Figure 4-1. Codon Usage Table for *P.pastoris* (Codon Usage Database, NCBI GenBank) **108**

Figure 4-2. **A.** 1% TAE (Tris-acetate-EDTA) agarose gel. Ladder of concatamerization products, each band indicates different sized concatamers, differing by 75 bp (addition of one monomer cassette). Seven unique monomer units were pooled in equal amounts in the concatamerization reaction for random incorporation of the monomer units in the concatamerization of the **Yeast ELP** gene. **B.** 1% TAE (Tris-acetate-EDTA) agarose gel. *Xho* I / *Xba* I digested **Yeast ELP** (1575bp), pPICZα-A (3.6 kb). DNA standard used was a 1Kb DNA ladder (NEB). **110**

Figure 4-3. pPICZα-A expression vector (Invitrogen). The **Yeast ELP** gene was cloned into the vector at the *Xho* I and *Xba* I restriction sites within the multiple cloning region. Vector was linearized with *Pme* I digestion for integration into the *P. pastoris* genome at the AOX1 crossover sites. The expressed elastin product has an α-factor signal sequence for secretion which is subsequently cleaved. Additionally, the protein retains a 5' *c-myc* epitope and 5' 6XHis-tag which can be used for purification or identification via Western blotting. **113**

Figure 4-4. pPICZα-A expression vector multiple cloning region (MCR) (Invitrogen). The **Yeast ELP** gene was cloned into the vector at the *Xho* I and *Xba* I restriction sites ( ) within the multiple cloning region. Verification of gene insertion through PCR amplification employed the 5' and 3' AOX1 primers. **114**

Figure 4-5. Plasmid integration in *P. Pastoris*. pPICZα-A vector containing the **Yeast ELP** gene of interest was linearized within the 5' AOX1 region through digestion with restriction enzyme *Pme* I. Linearized plasmid was integrated by gene insertion into the host AOX1 region. **115**

Figure 4-6. **A.** 1% TAE (Tris-acetate-EDTA) agarose gel of PCR products using AOX1 5' and AOX1 3' primers. Note incomplete amplification of the **Yeast ELP** gene as observed with the smear and ladder

product (Lane 1). Lane 1: Positive Control, Yeast ELP miniprep DNA. Lane 2: Negative Control, empty X-33 colony stab, note the yeast chromosome has PCR product of 2.2 kb. Lane 3: Colony PCR product of X-33 transformed cells containing **Yeast ELP**, note that the smear and ladder product is also observed. **B.** 1.5% TAE (Tris-acetate-EDTA) agarose gel of PCR products utilizing the Yeast ELP 3'-2 primer and AOX1 5' primer. Target product, approximately 400bp in size, was excised from the gel, purified, and correct sequence verified through DNA sequence analysis using the AOX1 5' primer. Lane 1: Positive control, **Yeast ELP** miniprep DNA, 400bp PCR product observed. Lane 2: Colony PCR product of X-33 transformed cells containing **Yeast ELP**, 400bp product observed. Lane 3: Negative Control, empty X-33 colony stab, no 400bp product observed. **117**

Figure 4-7. Western blotting of elastin-mimetic protein **Yeast ELP** run on a 4-20% SDS-PAGE gel. **A**. c-myc primary antibody, goat-anti-mouse secondary antibody. **B**. anti-His primary antibody, goat-anti-mouse secondary antibody. **C.** Deglycosylation of **Yeast ELP**. Western blotting of elastin-mimetic protein **Yeast ELP** run on a 4-20% SDS-PAGE gel, anti-His primary antibody, goat-anti-mouse secondary antibody. Marker lane: Precision Plus Protein Kaleidoscope (Bio-Rad). Lane 1: Purified Yeast ELP, Lane 2: Purified and deglycosylated **Yeast ELP**. Analysis indicates no deglycosylation of the **Yeast ELP** protein. **118**

Scheme 4-1. Cloning strategy in the construction of the **Yeast ELP** gene. The seven unique double stranded DNA monomer cassettes were ligated together to form concatamer of random sequence. A target multimer of 1575bp was selected, cloned into the recombinant plasmid, pPICZα-A and integrated into the *Pichia* host's DNA. **102**

Figure B-1. Experimental evidence summary plots of the relationship of electrospinning parameters to fiber morphology. **(A)** Fiber diameter as a function of deposition distance at constant applied voltage, flow rate and protein concentration, **(B)** Fiber diameter as a function of applied voltage at constant flow rate, depositon distance, and protein concentration**, (C)** fiber diameter as a function of flow rate at constant applied voltage, deposition distance, and protein concentration**, (D)** Fiber diameter as a function of protein concentration at constant applied voltage, deposition distance, and flow rate. (adapted from Bowlin, VCU, http://www.egr.vcu.edu/bme/faculty/bme-bowlin.html).....**137**

Figure B-2. SEM micrographs of PEO-collagen blended fibers spun from 2 wt% acid solution (34 mM NaCl) at a flow rate of 100 µl min^{-1} and at different collagen–PEO weight ratios: **(A)** 30 : 1, 50 000x magnification, **(B)** 10 : 1, 50 000x magnification **(C)** 5 : 1, 50 000x magnification, **(D)** 2: 1, 50 000x magnification, **(E)** 1 : 1, 20 000x

magnification, **(F)** 1 : 2, 50 000x magnification. Fibers of uniform morphology and ultrastructure, with average diameters of 100-150 nm, were generated (adapted from [278])..... **141**

Figure B-3. First reported fiber formation from an elastin-like analog utilizing a 81 kDa recombinant elastin peptide polymer. SEM micrographs of elastin-mimetic peptide fibers spun from 15 wt % solution at 50 **(A),** 100 **(B),** 150 **(C),** and 200 µl min^{-1} **(D)** flow rate. Electrospinning of a 15-wt% solution afforded a fabric with a unimodal distribution of fiber diameters (adapted from [41])…….. **148**

SUMMARY

Genetic engineering has been employed in the design of novel protein polymers composed of repetitive amino acid sequences or peptide blocks whose structural complexity imparts distinct mechanical, chemical or biological properties. Recently, we have reported the synthesis of elastin-mimetic multiblock copolymer composed of identical endblocks derived from self-associating, hydrophobic sequences that display plastic-like mechanical responses (Ile-Pro-Ala-Val-Gly), separated by a central block that is both hydrophilic and elastomeric (Val-Pro-Gly-Glu-Gly). Significantly, these multiblock systems afford the ability to form physical or virtual crosslinked networks through the self-association of chemically similar domains under physiologically relevant conditions (pH 7.4, 37°C).

Recombinant synthesis of elastin-mimetic proteins has been employed for several decades, however, long-term biocompatibility and biostability of such proteins was not fully defined. We present virtually crosslinked elastin-mimetic proteins which exhibit exceptional biocompatibility and long-term biostability over a period of at least seven months. This report is the first evidence of a non-chemically or ionically crosslinked system that exhibits long-term *in vivo* stability.

Although, physically crosslinked protein-based materials possess a number of advantages over their chemically crosslinked counterparts, physical crosslinks and the related domains so formed may be deformed or damaged at applied stresses lower than those required to disrupt covalent crosslinks. In this regard, we have synthesized a new class of recombinant elastin-mimetic triblock copolymer capable of both physical and chemical crosslinking. We have demonstrated that chemical crosslinking provides an independent mechanism for control of protein mechanical

responses. Specifically, elastic modulus was enhanced and creep strain reduced through the addition of chemical crosslinking sites.

A number of reports have described the design of synthetic genes, which encode elastin-like proteins for bacterial expression in *Escherichia coli*. Although advantages with this expression system exist, significant limitations including the lack of eukaryotic post-translational systems, the tendency to sequester mammalian proteins into inclusion bodies, difficult purification protocols, and endotoxin contamination have been noted. We demonstrate the expression of a recombinant elastin-mimetic protein from *P. pastoris*. A novel synthetic strategy, monomer library concatamerization, was utilized in designing non-repetitive elastin genes for highly repetitive protein sequences. It is likely that this strategy will be useful for creating large, repetitive genes for a variety of expression systems in order to more closely approach the genetic diversity inherent to native DNA sequences.

All told, elastin-based protein polymers are a promising class of material characterized by high degree of biocompatibility, excellent biostability, and a tunable range of mechanical properties from plastic to elastic. A variety of options facilitate the processing of these biopolymers into chemically crosslinked or non-crosslinked gels, films, or nanofibers for any of a number of implant applications including structural components of artificial organs and engineered living tissues, carriers for controlled drug release, or biocompatible surface coatings.

CHAPTER I

INTRODUCTION

1.1 CENTRAL HYPOTHESIS AND SPECIFIC AIMS

The central hypothesis encompassing the work described in this manuscript states that recombinant elastin proteins can be engineered to exhibit enhanced biostability and mechanical properties that closely match those of native elastin thus providing a rational approach for generating the elastin component of a tissue engineered vascular graft.

The *Central Hypothesis* was investigated by pursuing the following specific aims. The goal of **Specific Aim 1** was to synthesize recombinant elastin-mimetic protein polymers that have the capacity to form both physical and chemical crosslinks. We hypothesized that using genetic engineering approaches elastin-mimetic materials can be produced with controlled elastomeric properties and enhanced biostability through appropriate choice of recombinant peptide sequences that facilitate both chemical and physical crosslink formation. For this aim, two novel elastin-mimetic triblock copolymers were engineered, **LysB10** and **R4**. These results are presented in Chapter 2.

The goal of **Specific Aim 2** was to characterize the mechanical properties of crosslinkable elastin-mimetic triblock copolymers. We anticipated that the presence of chemical and physical crosslinks would act synergistically to improve the modulus of elasticity and resilience of elastin films. Target property endpoints for crosslinkable elastin-mimetic triblock copolymers have been defined as exhibiting a modulus of elasticity of 0.3-1.3 MPa and greater than 80% resilience over a strain of 30-45%. Additionally, we hypothesized that creep responses of elastin films can be improved with the incorporation of chemical crosslinks. Target property endpoints for crosslinkable

elastin-mimetic triblock copolymers have been defined as exhibiting less than 10% creep above physiologic stresses (45 kPa). Both **LysB10** and **R4** proteins were evaluated as water-cast films with and without glutaraldehyde (GTA) crosslinking. Uniaxial stress-strain responses and creep responses were evaluated. These results are presented in Chapter 2.

The goal of **Specific Aim 3** was to define the short- and long-term biocompatibility and biostability of crosslinkable elastin-mimetic triblock copolymers after *in vivo* implantation. We hypothesized that elastin-mimetic crosslinked hydrogels would exhibit sufficient biocompatibility and enhanced biostability to be used in a vascular construct. Biocompatibility was examined through histological evaluation of the fibrous capsule surrounding implanted materials as well as florescent activated cell sorting (FACS) analysis of number and type of inflammatory cells present at the implant site. These results are presented in Chapters 2 and 3. Biostability was monitored using magnetic resonance imaging (MRI) over a period of seven months. The methodology for assessing biostability was developed using a model protein system and these results are presented in Chapter 3.

1.2 MOTIVATION

The work presented herein was motivated by previous investigations in our laboratory and others. In particular, we have developed a class of recombinant elastin-mimetic proteins which have the capacity to form physically or virtually crosslinked systems [1-3]. These self-assembling triblock elastin copolymers have demonstrated that through selective engineering of block structure, a wide range of mechanical responses can be produced. In recent studies we have demonstrated that relatively limited changes in chemistry, including midblock size or amino acid sequence, provide an additional mechanism for tailoring protein elasticity, resilience, tensile strength, or

strain at failure [1, 4, 5]. Specifically, an elastin-mimetic protein was designed with midblock and endblocks that were approximately equal in size and displayed significant increases in both tensile strength and creep resistance as compared to an elastin-mimetic protein with endblocks approximately half the size of the midblock [5, 6]. We have demonstrated these proteins can find application as gels, films and fiber networks.

We have demonstrated elastin-mimetic triblock coplymers can be used to generate a non-thrombogenic hydrogel coating on the luminal surface of an ePTFE vascular prosthesis, and display excellent short-term blood contacting properties of this material [7]. Extensive biocompatibility characterization is necessary to assess the behavior of these proteins *in vivo*. Using a model protein which has been extensively characterized *in vitro*, the methods for assessing biocompatibility and biostability have been developed as presented in Chapter 3.

Additionally, we have explored alternative expression systems for the expression of recombinant elastin-mimetic proteins as a method for simplifying purification protocols. In particular, through genetic engineering we have developed elastin-mimetic proteins for expression in the methylotrophic yeast, *Pichia pastoris*. Of note, we have developed a novel genetic engineering strategy to create repetitive elastin polypeptides with non-repetitive nucleotide sequences using a concatamerization strategy employing random ligation of a library of monomer repeat units. These results are presented in Chapter 4.

Collectively, these studies demonstrate the need for the development of recombinant elastin proteins capable of both physical and chemical crosslinking and characterization of their mechanical behaviors, biocompatibility, and biostability.

1.3 RATIONAL

According to the American Heart Association Heart Disease and Stroke Statistics-2008 Updates, cardiovascular disease (CVD) is unmistakably a growing concern with statistics indicating approximately 500,000 procedures for coronary bypass surgery performed in over 250,000 patients each year. Since 1900 CVD has been the leading cause of death in the United States, killing nearly 2,400 American each day, or one person every 37 seconds. Specifically, coronary artery disease accounts for 54% of the CVD deaths annually [8].

Consequently, the need for a small diameter arterial prosthesis is apparent. Although employing polymers such as polytetrafluorethylene have been successful in the development of large diameter vascular grafts, the fabrication of a durable small diameter prosthesis remains an elusive goal. Biological reactions at the tissue material interface resulting from mechanical or compliance mismatch between native artery and the arterial replacement material lead to their ultimate failure. Presently, autologous vessels (i.e. saphenous veins and internal mammary arteries) are choice vascular replacements, though even these vessels are not sufficient for long term patency. Significantly, of the 600,000 coronary bypass operations performed annually, 10-20% of patients will require a second operation within 10 years [9].

In response to these limitations, strategies to mimic some or all of the characteristics of the arterial wall have been pursued. Current tissue engineering strategies provide an opportunity to circumvent maladaptive responses, though adequate replacements could be decades away. Alternatively, the generation of protein polymers that mimic native structural proteins offers a replacement strategy to develop a vascular graft with clinical performance results that match or exceed those of a native vessel. The reformulation of these proteins into nanofiber networks provides an opportunity to optimize the mechanical properties of an arterial bioprosthesis, as well as

other biologically related characteristics, thus creating an optimal vascular replacement material.

The long-term goal encompassing this work can be divided into three areas: (i) to synthesize a family of recombinant elastin-mimetic proteins capable of physical and chemical crosslinking (ii) to define their structure-property relationships; and (iii) to characterize the capacity of these artificial proteins for the generation of biocompatible small diameter blood vessel substitutes with mechanical properties that closely match those of native blood vessels. We anticipate that utilizing recombinant proteins based on consideration of the structural properties of the native matrix will lead to the creation of vascular conduits with better defined mechanical properties and enhanced biodegradation with improved clinical performance characteristics.

1.4 BACKGROUND

Current pursuits in the discipline of biomedicine, including artificial organs and engineered living tissues, are dependent on the ability to generate novel materials, fabricate or assemble materials into appropriate 2-D or 3-D structures, and to precisely tailor material-related properties in order to achieve a desired clinical response [10]. To that end, of profound importance is the development of artificial extracellular matrices (ECM). These structures are integral to the fashioning of microenvironments that are engineered for ideal mechanical and biological performance. It is likely this design will require the mimicry of many, if not all, morphological or physiologic features of native tissues. Decades of research have indeed demonstrated that as our ability to control the physical and biological properties of scaffolding materials improves, the quality of the tissues thus formed is enhanced.

More specifically, molecular and supramolecular organization of Type I collagen and elastin fiber assemblies establishes and important paradigm for the design in the

development of novel scaffolds. In the body, both tissues and organs are organized into 3-D structures, each having specific architectures, directly dependent upon its biological function. This architecture is believed to foster cellular ingrowth and proliferation by providing appropriate channels for mass transport and spatial cellular organization, thus directing new tissue formation.

The primary focus of our investigation is to engineer a material for vascular graft replacements. However, the strategies employed and materials thus generated can be utilized in biosynthetic design of many different artificial organs and tissues.

1.4.1 Current strategies in the design of an engineered vascular graft

Development of a small diameter vascular replacement for coronary bypass procedures has been described as the 'Holy Grail' for cardiovascular tissue engineering [11]. Developing an adequate replacement material has the potential to transform the treatment of coronary heart disease. It is recognized that adverse events leading to vascular graft failure are related to destructive biological reactions at the blood-material and tissue-material interface. Specifically, synthetic materials which have been successfully applied to large diameter replacements fail when applied to the small diameter with insufficient patency rates limited by thrombosis and compliance mismatch [12-16]. Over the past three decades, vascular graft design has adapted more of a tissue engineering approach with new graft design inspired by characteristics of the arterial wall.

Earliest efforts endeavored to functionalize synthetic graft prostheses with a luminal layer of endothelial cells. Though this strategy has several limitation; issues with cell sourcing, cell retention, and procoagulant tendencies, it has found success as larger peripheral artery replacements [17-20]. The inherent limitations of synthetic polymers

have motivated investigation to take a completely biological approach to the development of vascular grafts. Early work explored collagen gel technology in which constructs were developed consisting of cell populated collagen gels [21]. This research has served as the foundation for subsequent innovation. Extensions of this technology have incrementally enhanced the material integrity of the construct, through strategies to increase fiber alignment of the collagen [22-24], strength via mechanical conditioning [25, 26], crosslinking [27], and others, yet constructs exhibit inferior mechanical properties as compared to native vessels. Other approaches have utilized native vascular cells in the production of 'cell secreted scaffolds' [28-31]. Though these tissue engineering strategies have reported promising results, some even progressing from bench to human studies [31, 32], each poses unique challenges. Specifically, the duration of incubation time, immunologic challenges associated with the use of allogeneic cells, and suboptimal compliance has limited the application of these strategies to create a clinically applicable small diameter replacement.

Decellularized allo- and xenogeneic tissue have alternatively been investigated as materials for vascular grafts. These decellularized natural matrices contain the intact extracellular matrix and associated attachment proteins and have been used to produce structures with increase degradation resistance, decreased thromobgenicity, and decreased inflammatory reactions. Human umbilical vein, bovine procine carotid artery and small intestine submucosa, chemically crosslinked using gluteraldehyde, have been employed in clinical application though their use has been limited due to suboptimal patency rates via dilation and aneurysm formation [33-40].

Protein fiber spinning has recently been investigated for the development of tubular constructs for vascular applications. It has been postulated that the versatility of structural proteins as a scaffold will be significantly enhanced when reformulated into fiber networks. In this regard, electrospinning has been investigated as a mechanism for

generating fibers with diameters < 1 μm. Briefly, the electrospinning technique relies on electrostatic forces to produce sub-micron diameter fibers from protein solutions. A high voltage is applied to a spinneret while a protein solution is slowly being pumped through which induces evenly dispersed charges in a pendent drop at the tip of the spinneret, relaxing the fluid surface. This surface charge and the external Coulombic forces from the electric field combine to form a tangential stress which results in the drop becoming distorted into a shape referred to as a Taylor cone. At a threshold value, the electric field strength will overcome that of surface tension and the protein solution is ejected as a charged jet from the spinneret tip. As the jet travels to the grounded collector it undergoes stretching and whipping phenomena which reduces the diameter of this fiber. It is then collected, usually in a random orientation, on the grounded collector, creating a nonwoven fiber networks. Accordingly, a tubular construct can be fabricated using a rotating mandrel as a collector. Materials such as soluable elastin, Type I and III collagen, collagen-elastin-PLGA blends and recombinant elastin-mimetic materials have fabricated into electrospun fiber conduits [1, 41-46]. Reformulating proteins into fiber networks provides an additional level of control over the properties of the system. Specifically, studies have indicated electrospun fabrics composed of small diameter fibers (≤ 1um) demonstrated decreased porosity, increased fiber density, increased mechanical strength, as well as an optimized biological environment for promoting endothelial cell adhesion as compared to larger diameter fibers (7um) [42, 47].

1.4.2 The aortic media, a model system for the design of a vascular graft prosthesis

The native blood vessel is composed of three main structural layers containing unique cell and matrix components. The inner most layer of the blood vessel is the tunica intima which is composed of a single layer of endothelial cells with an underlying

basement membrane consisting of Type IV collagen, glycosaminoglycans, elastin and laminin. The outermost layer of the blood vessel, the tunica adventitia, forms a connective sheath around the vessel consisting of Type I and Type III collagen, elastin and fibroblasts. The adventitia functions to stabilize and anchor the blood vessel and maintain longitudinal tension. The middle layer of the native blood vessel is the tunica media which is composed of concentric sheets of elastic lamellar units each composed of smooth muscle cells within a fibrillar matrix of Type I and Type III collagen, elastin and proteoglycans. The inherent elasticity of blood vessels arises from the structure of the medial layer. Elastin and collagen function in a concerted action in response to imposed deformations. Elastin is primarily responsible for distensibility and elastic recovery of the vessel in the low-strain regime while collagen responds by limiting deformation during excessive strain [48-52]. The elastin protein network appears to be integral to mechanically match the native blood vessel and for the prevention of intimal hyperplasia and potential graft failure. Additionally, the pores of the elastic lamina are important for the exchange of nutrients and metabolites. Thus, the lamellar unit of the aortic media serves as a foundation in the design of a vascular graft prosthetic [53-55].

1.4.3 Native elastin, an introduction

Native elastin is a highly insoluable matrix protein that is responsible for providing extensibility and resilience to most tissues of the body. Insoluable elastin has a 70 year half-life making it one of the most stable proteins discovered [56]. In the vascular system, elastin fiber networks appear in large densities (over 50%) and function to provide resilience to the artery to absorb dynamic systolic stresses of the cardiac cycle and to release energy in the form of blood pressure during diastole [57]. Therefore, elastin networks maximize the durability of tissues that are loaded by repetitive forces by

minimizing the conversion of mechanical energy to heat which would ultimately result in tissue damage [52]. In addition to its structural role, elastin creates an environment which promotes proper cell function. Specifically within the vascular system, elastin regulates smooth muscle cell phenotype and proliferation, and in this way is responsible for stabilizing arterial structure [57-60].

1.4.4 Biochemistry of native elastin

Human elastin is synthesized as a 72 kDa soluble precursor, tropoelastin. The distinctive composition of tropoelastin affords unique physical properties of this structural protein. Tropoelastin is rich in glycine (33%), proline (10-13%), and other hydrophobic residues (44%) rendering elastin an extremely hydrophobic protein [61]. Tropoelastin contains distinct crosslinking and hydrophobic domains. Crosslinking domains are alanine rich, containing pairs of lysine residues facilitating intermolecular crosslinking. Specifically, lysine residues are separated by either two or three alanine residues (eg. Ala-Ala-Ala-Lys-Ala-Ala-Lys-Ala-Ala) allowing for retention of an α-helical conformation in this region. The sequence within the crosslinking domains appears to be conserved as a consequence of the conformational constraints of crosslinking [62]. Alternatively, the hydrophobic domains within tropoelastin are composed of three-quarters of valine, glycine, proline, and alanine which occur in repeat units like Gly-Val-Gly-Val-Pro, Gly-Val-Pro-Gly-Val, and Gly-Val-Gly-Val-Ala-Pro. The total size of the protein polymer, 750-800 residues, is highly conserved among species, however, investigations have elucidated that precise sequence and size of this region are not critical for appropriate function [62].

1.4.5 Coacervation phenomena in native elastin and recombinant elastin proteins

Coacervation is a self assembly process thought to align tropoelastin molecules in preparation for intermolecular crosslinking [63-65]. At ambient temperatures, tropoelastin is soluble in aqueous solutions. However, as the temperature is raised, the molecules begin to aggregate through hydrophobic interactions. Coacervation is a lower critical solution temperature (LCST) phenomenon in which the protein forms a more ordered system upon increasing temperature. The same phenomena has been observed with recombinant elastin proteins where precise control over the temperature at which coacervation occurs has been correlated to amino acid sequence [66, 67]. Recombinant elastin proteins which lack hydrophobic domains do not have the ability to coacervate [68].

1.4.6 Elastin fiber assembly

Elastin fibers appear to exist as two morphologically different components, a highly isotropic amorphous elastin constituent within an organized microfibrilar scaffold primarily composed of fibrillin [69, 70]. Understanding of the complex mechanism of fiber assembly in native elastin is limited. Fiber assembly appears to take place in the extracellular space in proximity to the cell membrane where microfibrils appear first, grouped in small bundles. Tropoelastin, synthesized by smooth muscle cells, is secreted within each fiber bundle. Tropoelastin exhibits the ability to self-assemble under physiological conditions through coacervation. It is likely that this phenomena is responsible for the alignment of tropoelastin in preparation of intermolecular crosslinking [62-65]. Intermolecular crosslinking occurs between four lysine residues from two tropoelastin molecules. Briefly, crosslinks are formed through the deamination of the ε-amino group of the lysine side chains by the enzyme lysyl oxidase. The reaction occurs in two ways: the reactive aldehyde residue condenses with a second aldehyde residue

to form an allysine aldol or it reacts with a lysine residue to form lysinonorleucine. These two precursors condense to form desmosine and isodesmosine crosslinks [71]. Crosslinking appears to take place every 65-70 residues [72].

1.4.7 Biosynthetic approach to the development of an engineered vascular graft

Allogeneic and xenogeneic strategies indicate native fiber networks can be used to fabricate a vascular graft prosthetic, though the inability to tailor matrix composition and content, fiber size and architecture, limits the applicability of these materials. As a result, strategies to design a prosthesis with precisely defined mechanical and biological properties has been pursued via a 'ground-up' design. Recent developments in recombinant protein engineering now offer the opportunity to construct new proteins with near absolute control over molecular architecture [73-76]. Employing biosynthetic routes to the design of structural proteins for vascular prosthetics afford the ability to modulate material properties at the level of the primary amino acid sequence, thus affording the capability to engineer recombinant proteins to meet physiologic requirements. Additionally, this strategy enables the elucidation of structure-property relationships and ultimately, control over these properties. Currently, structural proteins have been generated in this way consisting of sequentially repeated amino acid blocks derived from analysis of native protein molecular structure [77, 78]. This strategy not only allows for control of sequence and size, it also facilitates incorporation of additional functional groups, in particular, the placement of crosslinks at well defined intervals along the peptide chain allowing for the additional control over material properties of the protein. Thus, recombinant proteins that mimic structural matrix proteins can be engineered with a precisely tailored design to modulate tensile strength, elastic modulus, viscoelasticity, and in vivo stability, as well as desired host response.

1.4.7 Elastin-Mimetic Proteins

Limitations to the use of elastin in biomedical and tissue engineering applications are a consequence of its intrinsic insolubility and inability to be processed. But through the structural characterization of the hydrophobic domains, the ability to base synthetic protein polymers on native elastin sequences is feasible. The pioneering work of Dan W. Urry elucidated the elastomeric pentapeptide repeat, VPGVG, from human elastin which now serves as the basic sequence extensively investigated by both chemical methodologies and recombinant technology [79, 80]. This repeat unit within found the hydrophobic domain of human elastin is responsible for resultant elastic properties. Additionally, this domain is responsible for facilitating fiber formation through coacervation phenomena, behaviors consistent with native elastin. Spectroscopic analysis has revealed that native elastin, and likewise, protein polymers containing this repeat, exhibit β-turns and helical β-spiral conformations and display an inverse temperature transition defined by the generation of a more ordered system upon increasing temperature. This loss of entropy is a consequence of protein folding into β-spiral conformation and the subsequent reorientation of water from the elastin chain [81].

Studies have indicated that the amino acid in the fourth (X) position (VPGXG) modulates the coacervation temperature with more polar amino acids increasing transition temperature [66, 67, 82]. As long as glycine and proline residues are preserved the structure and function of elastin is maintained [83]. This discovery has led to the generation of recombinant elastin analogs designed for biomedical applications. For instance, recombinant techniques have been employed to design amphiphilic elastin protein polymers consisting of hydrophobic and hydrophilic domains. Through precise sequence design and control of processing conditions, these elastin analogs exhibit a wide range of properties advantageous for biomedical applications, as micelles or physically crosslinked films [2-5, 84]. Additionally, groups have incorporated cell binding

domains, RGD or REDV, into elastin sequences to functionalize elastin matrix components for endothelial cell attachment [85-87]. Furthermore, incorporation of reactive lysine residues into recombinant elastin design provides the ε-amino moiety of lysine for crosslinking using a variety of approaches. Crosslinking of synthetic elastin-mimetic protein polymers has been investigated using solution phase systems; either gamma irradiation [82, 88-90], chemical [91-102] , or enzymatic based approaches [100], as well as solid state photocrosslinking [103].

1.5 SIGNIFICANCE OF PROPOSED RESEARCH

It is proposed that employing a biosynthetic strategy, elastin-mimetic protein polymers can be designed to facilitate both covalent and physical crosslink formation thus enhancing static and dynamic material behavior. Specifically, it is hypothesized that these protein polymers will exhibit improved compliance, resilience, creep, and biostability as compared to allogeneic or xenogeneic tissue. Additionally, these proteins may be reformulated into gels, films or nano-fiber networks. Significantly, this strategy can be integrated into schemes which are ultimately driven either by a desire to generate a cell containing arterial construct or a non-thrombogenic acellular conduit.

CHAPTER 2

Elastin-mimetic protein polymers capable of physical and chemical crosslinking

2.1 INTRODUCTION

Genetic engineering provides a facile route for the design of novel protein polymers composed of repetitive amino acid sequences or peptide blocks whose structural complexity imparts distinct mechanical, chemical or biological properties. To date, the majority of recombinant multiblock protein polymers have been designed with relatively short block sequences that limit structural polymorphism. As a consequence, opportunities to access diverse polymer morphologies are limited and the potential to tune a wide range of functional responses reduced [74, 104]. Recently, we have reported a new class of elastin-mimetic multiblock copolymer composed of identical endblocks derived from self-associating, hydrophobic sequences that display plastic-like mechanical responses (Ile-Pro-Ala-Val-Gly), separated by a central block that is both hydrophilic and elastomeric (Val-Pro-Gly-Glu-Gly) [1, 2]. Block sizes, typically, exceed 35 kDa, which has allowed us to explore the production of protein-based materials that are structurally polymorphic [1-5, 84].

Significantly, multiblock systems afford the ability to form physical or virtual crosslinked networks through the self-association of chemically similar domains. In the case of elastin-mimetic proteins [1-5, 84], repeat peptide sequences of self-associating blocks are chosen such that coacervation or phase separation of these domains occurs in water under physiologically relevant conditions (pH 7.4, 37°C), which maximizes hydrophobic interactions that drive self-assembly. In turn, the sequence of the non-crosslinking domain is selected in a manner that precludes coacervation. This typically has required the incorporation of hydrophilic residues in the fourth position of the pentapeptide repeat sequence (Val-Pro-Gly-Xaa-Gly), such as glutamic acid, which

limits the tendency for block aggregation. Physically crosslinked protein-based materials possess a number of advantages over their chemically crosslinked counterparts, including ease of processability, the ability to avoid the addition or removal of reagents or unreacted intermediates needed for chemical crosslinking, and the capacity to incorporate biologically or chemically active agents or cells that might otherwise be sensitive to covalent crosslinking schemes. Moreover, if blocks are of sufficient size and chemical diversity the potential to access diverse polymer morphologies exists. This provides the capacity to tune a wide range of functional responses, such as mechanical behavior, permeability or drug elution characteristics, as well as the potential to design templated materials [74, 86, 91]. Notwithstanding these desirable features, physical crosslinks and the related domains so formed may be deformed or damaged at applied stresses lower than those required to disrupt covalent crosslinks.

Native elastin is enzymatically crosslinked upon proper alignment of two pairs of lysine residues between adjacent tropoelastin chains with formation of desmosine or isodesmosine linkages [105, 106]. Likewise, most recombinant elastin analogues that have been designed to date have relied on crosslinking through available amino groups, albeit with most reports describing the use of chemical crosslinkers, including isocyanates, NHS-esters, phosphines, aldehydes, or genipin [91-102]. In this regard, we have previously reported the design of a synthetic elastin sequence, (Val-Pro-Gly-Val-Gly)$_4$(Val-Pro-Gly-Lys-Gly), in which lysine residues were chemically crosslinked using bis(sulfosuccinimidyl) suberate and disuccinimidyl suberate [99]. Subsequent studies have reported the application of transglutaminase or lysyl oxidase for enzymatic crosslinking [107]. In addition, we have also explored solid-state crosslinking of recombinant elastin-mimetic proteins using both UV and visible light activated photoinitiators [103]. In tropoelastin, lysine residues are often interspersed among

alanine repeats (eg. Ala-Ala-Ala-Lys-Ala-Ala-Lys-Ala-Ala), which has suggested that self-association of alanine-rich sequences facilitates crosslinking [108, 109]. Several elastin-like proteins have been designed in similar manner [86, 91, 110].

The capacity of chemical crosslinks to provide an independent mechanism for control of protein mechanical responses and biostability is well established. However, in this report we postulated that by chemically locking a multiblock protein assembly in place, functional responses that are linked to specific domain structures and morphologies may be preserved over a broader range of loading conditions that would otherwise disrupt microphase structure solely stabilized by physical crosslinking. We report herein the synthesis of a new class of recombinant elastin-mimetic triblock copolymer capable of both *physical* and *chemical* crosslinking. These investigations were motivated by a desire to capture features unique to both physical and chemical crosslinking schemes so as to exert optimal control over a wide range of potential properties afforded by protein-based mutiblock materials.

2.2 MATERIALS and METHODS

Synthetic gene construction of elastic- and plastic-like domains. Synthetic methods used to produce the DNA inserts that encode the various elastin-mimetic block copolymers have been described previously [2-5]. Genes encoding two distinct chemically crosslinkable protein triblock copolymers were synthesized. Briefly, oligonucleotide cassettes encoding elastic- (**E**) and plastic-like (**P**) repeat units **(Table 2-1, Appendix A)** were independently synthesized and inserted into the *BamH* I and *Hin*D III sites within the polylinker of pZErO cloning vectors. Specifically, $\mathbf{P_1}$ and $\mathbf{E_1}$ encode the monomer repeat unit for plastic- and elastic-like domains designated for the triblock protein polymer, referred to as **LysB10**. A second set of oligonucleotide cassettes, $\mathbf{P_2}$

and **E_2**, were designed to encode monomer repeat units for plastic- and elastic-like domains for a second protein triblock copolymer, designated **R4**. Recombinant clones were isolated after propagation in *E. coli* strain TOP10F' and the identity of the DNA inserts **E** and **P** verified by double-stranded DNA sequence analysis. DNA monomers **E** and **P** were liberated from the respective plasmids via sequential restriction digestion with *Bbs* I and *Bsm*B I, respectively. Multimerization, or self-ligation in a head-to-tail fashion of each DNA cassette afforded a population of multimers. This procedure was repeated separately for the four multimers synthesized in this report (**P_1**, **E_1**, **P_2**, and **E_2**).

Multimers derived from DNA monomers were inserted into the *Bsm*B I site of their original plasmid containing the monomer cassette. Multimers encoding 33 repeats of the **P_1** monomer, 16 repeats of the **P_2** monomer, 28 repeats of the **E_1** monomer, and 15 repeats of the **E_2** monomer were isolated and identified via restriction cleavage with *Bam*H I and *Hin*D III. Double-stranded DNA sequence analysis confirmed the integrity of the concatemers within the recombinant plasmids, which were labeled p**P_1**, p**P_2**, p**E_1**, and p**E_2**, respectively. p**P_1** and p**E_1** were utilized in the construction of the **LysB10** gene, p**P_2** and p**E_2** for the **R4** gene.

Table 2-1. Coding Sequences of Oligonucleotide Cassettes Employed for the Construction of Crosslinkable Protein Triblocks, **LysB10** ($AP_1IE_1IP_1A$) and **R4** ($AP_2IE_2IP_2A$)

E_1 Block (LysB10 Elastic-like Block)

Val	**Pro**	**Gly**	**Ala**	**Gly**	**Val**	**Pro**	**Gly**	**Ala**	**Gly**	**Val**	**Pro**	**Gly**	**Glu**	**Gly**
GTT	CCA	GGT	GCA	GGC	GTA	CCG	GGT	GCT	GGC	GTT	CCG	GGT	GAA	GGT
Val	**Pro**	**Gly**	**Ala**	**Gly**	**Val**	**Pro**	**Gly**	**Ala**	**Gly**					
GTT	CCA	GGC	GCA	GGT	GTA	CCG	GGT	GCG	GGT					

E_2 Block (R4 Elastic-like Block)

Val	**Pro**	**Gly**	**Ile**	**Gly**	**Val**	**Pro**	**Gly**	**Ile**	**Gly**	**Val**	**Pro**	**Gly**	**Ile**	**Gly**
GTT	CCA	GGT	ATT	GGC	GTT	CCG	GGT	ATC	GGT	GTG	CCA	GGC	ATC	GGT
Val	**Pro**	**Gly**	**Ile**	**Gly**	**Val**	**Pro**	**Gly**	**Ile**	**Gly**					
GTA	CCG	GGT	ATT	GGC	GTT	CCA	GGC	ATT	GGC					

P_1 Block (LysB10 Plastic-like Block)

Ile	**Pro**	**Ala**	**Val**	**Gly**	**Ile**	**Pro**	**Ala**	**Val**	**Gly**	**Ile**	**Pro**	**Ala**	**Val**	**Gly**
ATT	CCG	GCT	GTT	GGT	ATC	CCA	GCT	GTT	GGT	ATC	CCA	GCT	GTT	GGC
Ile	**Pro**	**Ala**	**Val**	**Gly**	**Ile**	**Pro**	**Ala**	**Val**	**Gly**					
ATT	CCG	GCT	GTA	GGT	ATC	CCG	GCA	GTG	GGC					

P_2 Block (R4 Plastic-like Block)

Ile	**Pro**	**Ala**	**Val**	**Gly**	**Ile**	**Pro**	**Ala**	**Val**	**Gly**	**Ile**	**Pro**	**Ala**	**Val**	**Gly**
ATT	CCA	GCT	GTT	GGT	ATC	CCA	GCT	GTT	GGT	ATC	CCA	GCT	GTT	GGC
Ile	**Pro**	**Ala**	**Val**	**Gly**	**Ile**	**Pro**	**Ala**	**Val**	**Gly**					
ATT	CCG	GCT	GTA	GGT	ATC	CCG	GCA	GTG	GGC					

I Block (Lysine Insert)

Ile	**Pro**	**Ala**	**Val**	**Gly**	**Lys**	**Ala**	**Ala**	**Lys**	**Val**	**Pro**	**Gly**	**Ala**	**Gly**
ATT	CCA	GCT	GTT	GGT	AAG	GCG	GCC	AAG	GTT	CCA	GGT	GCA	GGC

A Block (Modified Lysine Adaptor)

Val	**Pro**	**Ala**	**Val**	**Gly**	**Lys**	**Val**	**Pro**	**Ala**	**……**	**Ile**	**Pro**	**Ala**	**Val**
GTT	CCA	GCT	GTT	GGT	AAG	GTT	CCA	GCT	……	ATT	CCA	GCT	GTT
Gly	**Lys**	**Ala**	**Ala**	**Lys**	**Ala**	**Stop**							
GGT	AAG	GCG	GCC	AAG	GCG	TAA							

Synthetic gene construction of chemical crosslinking domains. Single stranded oligonucleotides encoding the sense and anti-sense strands of the Lysine Insert (**I**) and Lysine Adaptor (**A**) were chemically synthesized (Sigma Genosys, Inc.) **(Appendix A, Table 2-1).** The Lysine Insert is a 60 bp DNA cassette encoding the crosslinking sequence, Lys-Ala-Ala-Lys, which was inserted between the plastic- and elastic-like domains. The Lysine Adaptor is a 50 bp DNA cassette designed with restriction enzyme cut sites midway through the cassette to allow for insertion of the assembled triblock gene. The Lysine Adaptor encodes for a single N-terminal lysine residue and two C-terminal lysine residues. Additionally, it allows for facile cloning into the pET24-a expression vector within the multiple cloning region. This ensures correct insertion of the gene in frame with the N-terminal polyhistidine tag.

The following procedure detailing the protocol to generate double stranded DNA was implemented for both the Lysine Insert and Lysine Adaptor. The DNA was suspended in 10 mM Tris buffer (pH 8) to a final concentration of 0.5 µg/uL. A solution of 10 µg of each corresponding oligonucleotide, 4µL 5M NaCl, 4µL 1M $MgCl_2$, 152 µL of sterile ddH2O was subjected to an annealing procedure initiated at a reaction temperature of 99°C with temperature decrements of 1°C every 5 minutes to a final reaction temperature of 30°C. The resultant double stranded DNA cassette was analyzed by agarose gel electrophoresis (4% GTG NuSieve agarose, 1X TBE buffer).

Double stranded synthetic DNA was phosphorylated through a 2-hour incubation with T4 Poynucleotide Kinase (New England Biolabs) in the presence of T4 DNA ligase buffer with 10mM ATPs (New England Biolabs). The enzymes were removed with phenol/chloroform/isoamyl alcohol (25:24:1) and the double stranded DNA (dsDNA) was recovered through an ethanol precipitation.

The pZErO-1 acceptor plasmid (1 µg), was prepared via *Bam*H I and *Hin*D III double digestion, followed by heat inactivation of the enzymes at 65°C and a dilution of

the digested plasmid to 10 ng/μL. The Lysine Insert and Lysine Adaptor were designed with *Bam*H I and *Hin*D III overhangs to enable cloning into pZErO-1 at these restriction sites.

The DNA cassette and respective acceptor plasmid were ligated together in the presence of T4 DNA Ligase at 16°C for 30 minutes. A 2 μL aliquot of the ligation reaction mixture was used to transform 40 μL of electrocompetent TOP10F' *E. coli* cells. A total of 100 μL of the transformation mixture was spread onto low salt (LSLB) agar supplemented with Zeocin (50 μg/μL). The plates were incubated for 12 hours at 37°C. Five transformants were selected from each plate to inoculate individual 7 mL cultures of LSLB/Zeocin. Cultures were rotary incubated for 12 hours at 37°C. Plasmid DNA was isolated following a Qiagen Spin Miniprep protocol (Quiagen, Inc.). DNA was initially screened by a *Bam*H I and *Hin*D III double digestion. Positive transformants were verified by agarose gel electrophoresis (4% GTG NuSieve agarose, 1X TBE buffer). Automated DNA sequencing utilizing the M13 forward and M13 reverse primers confirmed correct DNA products. Plasmids containing the correct sequence for the Lysine Insert and Lysine Adaptor are identified as p**I** and p**A,** respectively.

Assembly of elastin-mimetic triblock copolymers. The proteins, **LysB10** and **R4** were designed to contain the Lysine Insert between each plastic-like and elastic-like blocks and to be flanked by the Lysine Adaptor (-Lysine Adaptor-Plastic-like Domain-Lysine Insert-Elastic-like Domain-Lysine Insert-Plastic-like Domain-Lysine Adaptor-) (**Scheme 2-1**). All subcloning steps were performed in the pZErO-1 plasmid using LSLB media under Zeocin antibiotic selection. **Scheme 2-1** summarizes the general cloning strategy employed in the assembly of these genes.

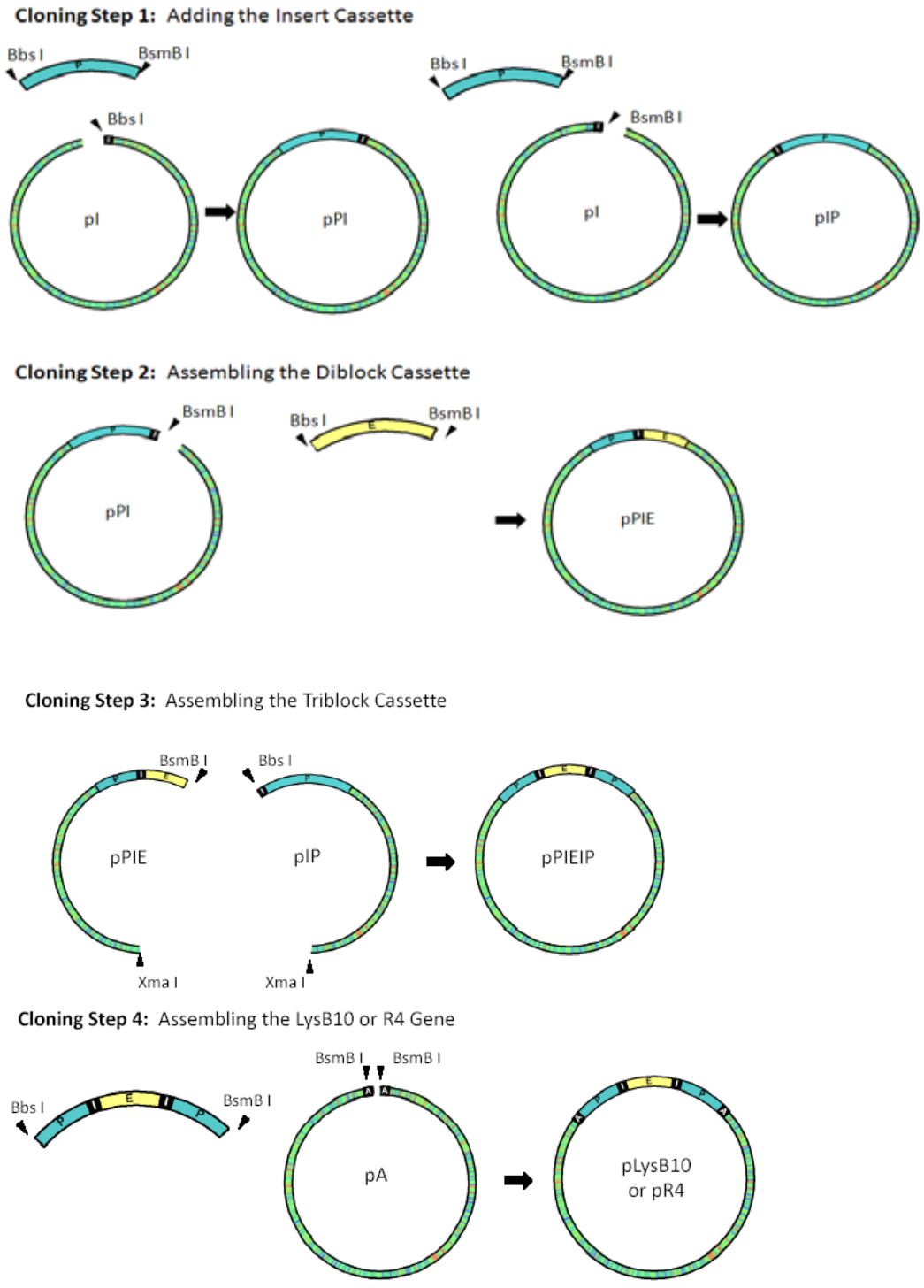

Scheme 2-1. General cloning strategy in the assembly of crosslinkable triblock genes. Plasmids have been designated by the DNA cassette they contain. For example, the plasmid containing the Lysine Insert cassette is referred to as plasmid **I** (p**I**). **P** = Plastic-like cassette (blue), **E** = Elastic-like cassette (yellow), **I** = Insert cassette (black), **A** = Adaptor cassette (black).

Recombinant plasmids encoding the elastic-like (p**E**) (**E_1**=2.1 kB, **E_2**=1.1 kB) and plastic-like (p**P**) (**P_2**=2.5 kB, **P_2**=1.2 kB) domains were constructed, as described above. Each gene was isolated from its respective plasmid with *Bbs* I and *Bsm*B I sequential digestion. The gene fragment was isolated via preparative gel electrophoresis (1% agarose, 0.5X TBE) and purified using Zymoclean Gel Recovery (ZymoResearch, Inc). Preparative amounts of p**I** DNA was isolated for two separate reactions. A total of 5 µg of p**I** was digested with restriction enzyme *Bbs* I and Shrimp Alkaline Phosphatase (SAP) dephosphorylated (1 U SAP per 1 pmol strand ends) to prevent re-ligation. A separate 5 µg of p**I** was digested with the restriction enzyme *Bsm*B I and SAP dephosphorylated. The linearized plasmids were isolated via preparative gel electrophoresis (1% agarose, 0.5X TBE) and purified using Zymoclean Gel Recovery.

Similar protocols for ligation, transformation, and propagation were followed, as previously described. Two separate ligation reactions were performed between *Bbs* I digested p**I** and **P** and *Bsm*B I digested p**I** and **P (Scheme 2-1, Cloning Step 1)**. Isolated DNA from clones were screened by a *Bam*H I and *Hin*D III double digestion and cleavage fragments analyzed by agarose gel electrophoresis. Correct ligation was confirmed by automated DNA sequence analysis using M13 forward and reverse primers. Plasmids containing the correct sequences are identified as p**IP** and p**PI**.

Analogously, 5 µg of p**PI** was digested with restriction enzyme *Bsm*B I and Shrimp Alkaline Phosphatase (SAP) dephosphorylated (1U SAP per 1 pmol strand ends) to prevent relegation. The linearized plasmid was isolated via preparative gel electrophoresis (1% agarose, 0.5X TBE) and purified using Zymoclean Gel Recovery. Linearized p**PI** was ligated with **E**, followed by transformation and propagation **(Scheme 2-1, Cloning Step 2)**. Isolated DNA from transformants were screened by a *Bam*H I and *Hin*D III double digestion and cleavage fragments analyzed by agarose gel electrophoresis. Correct ligation was confirmed by automated DNA sequence analysis

using M13 forward and reverse primers. The plasmid containing the correct sequence was termed p**PIE**.

Recombinant plasmids p**IP** and p**PIE** were digested with *Bbs* I / *Xma* I and *Bsm*B I / *Xma* I, respectively. The gene fragment from each of these digestions was isolated via preparative gel electrophoresis (1% agarose, 0.5 x TBE) and purified using Zymoclean Gel Recovery. **IP** and **PIE** fragments were ligated by T4 DNA ligase, transformed into TOP10F' and plated on LSLB/Zeocin plates **(Scheme 2-1, Cloning Step 3)**. As the *Xma* I site cuts within the Zeocin coding region, only clones containing the correctly assembled triblock (**PIEIP**), and thus, the correctly reassembled antibiotic coding region, were able to propagate. Transformants were confirmed by analysis of *Bam*H I and *Hin*D III restriction digest fragments with agarose gel electrophoresis (1% agarose, 0.5 x TBE) and automated DNA sequence analysis using M13 forward and reverse primers. The plasmid containing the correct sequence for the triblock was termed, p**PIEIP**.

p**A**, containing the Lysine Adaptor, was assembled, as described above. This plasmid was digested with restriction enzyme *Bsm*B I and SAP dephosphorylated. The triblock, **PIEIP**, was excised from the pZErO-1 plasmid via sequential digestion using restriction enzymes *Bbs* I and *Bsm*B I and purified via gel isolation. A ligation reaction was performed to relocate the **PIEIP** gene from p**PIEIP** to p**A (Scheme 2-1, Cloning Step 4)**. The ligation mixture was transformed into competent TOP10F' cells and plated on LSLB media under Zeocin antibiotic selection. Isolated DNA from transformants were screened via agarose gel electrophoresis analysis of a *Bam*H I and *Hin*D III double digestion. Automated DNA sequence analysis using M13 forward and reverse primers confirmed correct insertion of the gene p**AP$_1$IE$_1$IP$_1$A** and p**AP$_2$IE$_2$IP$_2$A**. p**AP$_1$IE$_1$IP$_1$A** was identified as the cloning plasmid, p**LysB10** and p**AP$_2$IE$_2$IP$_2$A** as the cloning plasmid, p**R4**.

The pET24-a plasmid (1 µg, Invitrogen) was prepared via *Bam*H I and *Hin*D III double digestion, followed by gel isolation and purification. The **APIEIPA** gene was

released from the pZErO-1 vector at analogous sites. Adaptor and plasmid were ligated together in the presence of T4 DNA ligase at 16°C for 30 minutes. A 2 µL aliguot of the ligation reaction mixture was used to transform 40 µL of electrocompetent TOP10F' *E. coli* cells. A 100 µL aliquot of the transformation mixture was spread onto LB agar supplemented with kanamycin (50 µg/µL). The plates were incubated for 12 hours at 37°C. Five transformants were selected from each plate to inoculate individual 7 mL cultures of LB/kanamyacin media. Cultures were rotary incubated for 12 hours at 37°C. Plasmid DNA was isolated following a Qiagen Spin Miniprep protocol (Quiagen, Inc.). DNA was screened by a *Bam*H I and *Hin*D III double digestion. Positive transformants were verified by agarose gel electrophoresis (4% GTG NuSieve agarose, 1X TBE buffer). Automated DNA sequencing utilizing the T7 promoter and T7 terminator primers confirmed the correct DNA product. The resultant plasmid was identified as expression plasmids, p**LysB10 ($AP_1IE_1IP_1A$)** and p**R4 ($AP_2IE_2IP_2A$).** DNA agarose gels in **Figures 2-1 and 2-2** depicts gene products at each subcloning step in the assembly of p**LysB10** and p**R4**, respectively.

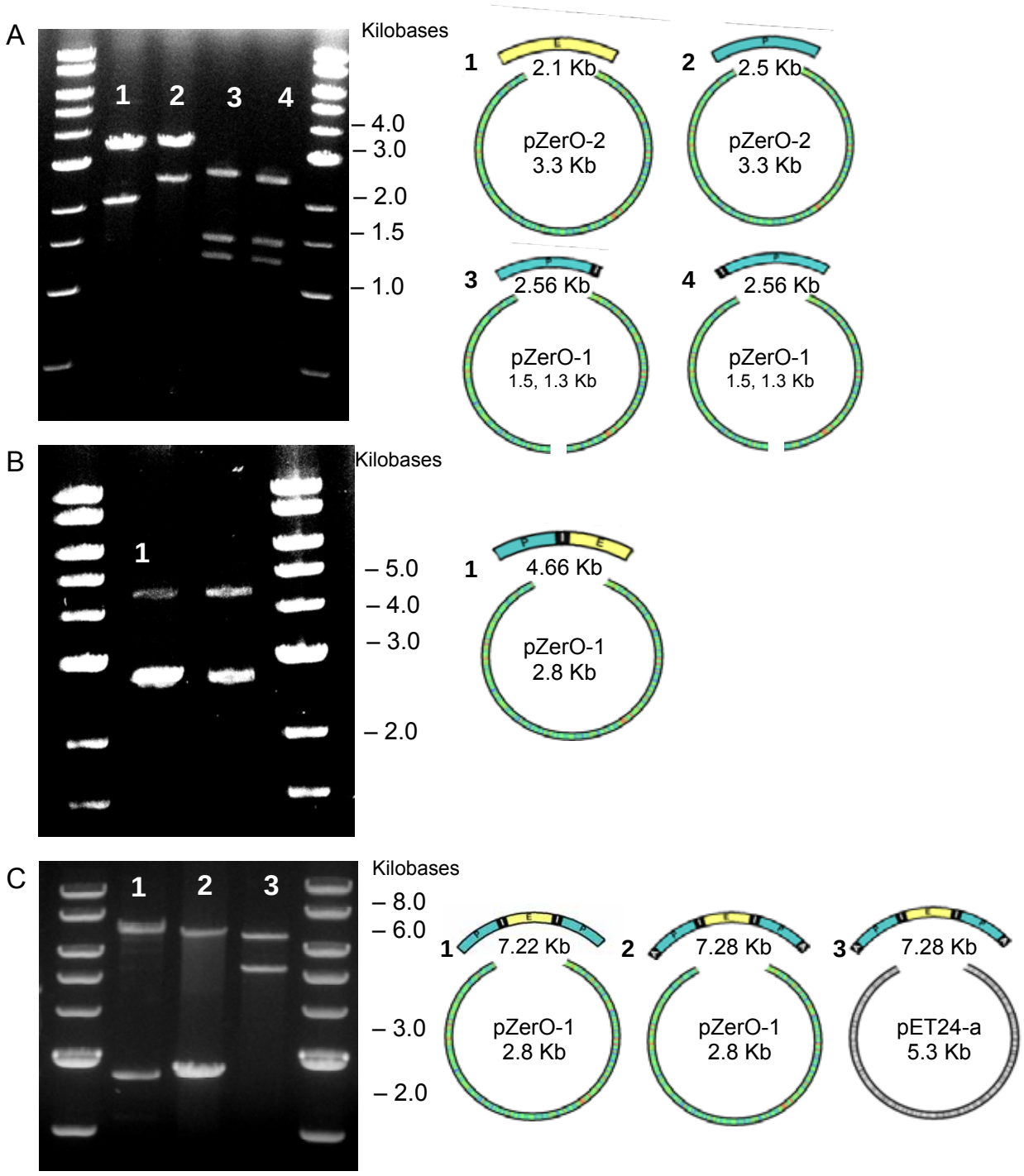

Figure 2-1. Analytical restriction digests, 1% TAE (Tris-acetate-EDTA) agarose gel, depicting gene and vector sizes at each stage of the **LysB10** assembly process with corresponding digestion schemes. DNA standard used was a 1Kb DNA ladder (NEB). **A.** Lane 1: *Bam*HI / *Hin*DIII digest p**E$_1$** (2.1 Kb), pZerO-2 (3.3 Kb). Lane 2: *Bam*HI / *Hin*DIII digest p**P$_1$** (2.5 Kb), pZerO-2 (3.3Kb). Lane 3: *Nsi* I / *Xma* I digest p**P$_1$I** (2.56 Kb), pZerO-1 (1.3, 1.5 Kb). Lane 4: *Nsi* I / *Xma* I digest p**IP$_1$** (2.56 Kb), pZerO-1 (1.3, 1.5 Kb). **B.** Lane 1: *Nsi* I digest p**P$_1$IE$_1$** (4.66 Kb), pZErO-1 (2.8 Kb). **C.** Lane 1: *Nsi* I digest p**P$_1$IE$_1$IP$_1$** (7.22 Kb), pZErO-1 (2.8 Kb). Lane 2: *Nsi* I digest **LysB10** (7.28 Kb), pZErO-1 (2.8 Kb). Lane 3: *Bam*HI / *Hin*DIII digest **LysB10** (7.28 Kb), pET 24a (5.3 Kb).

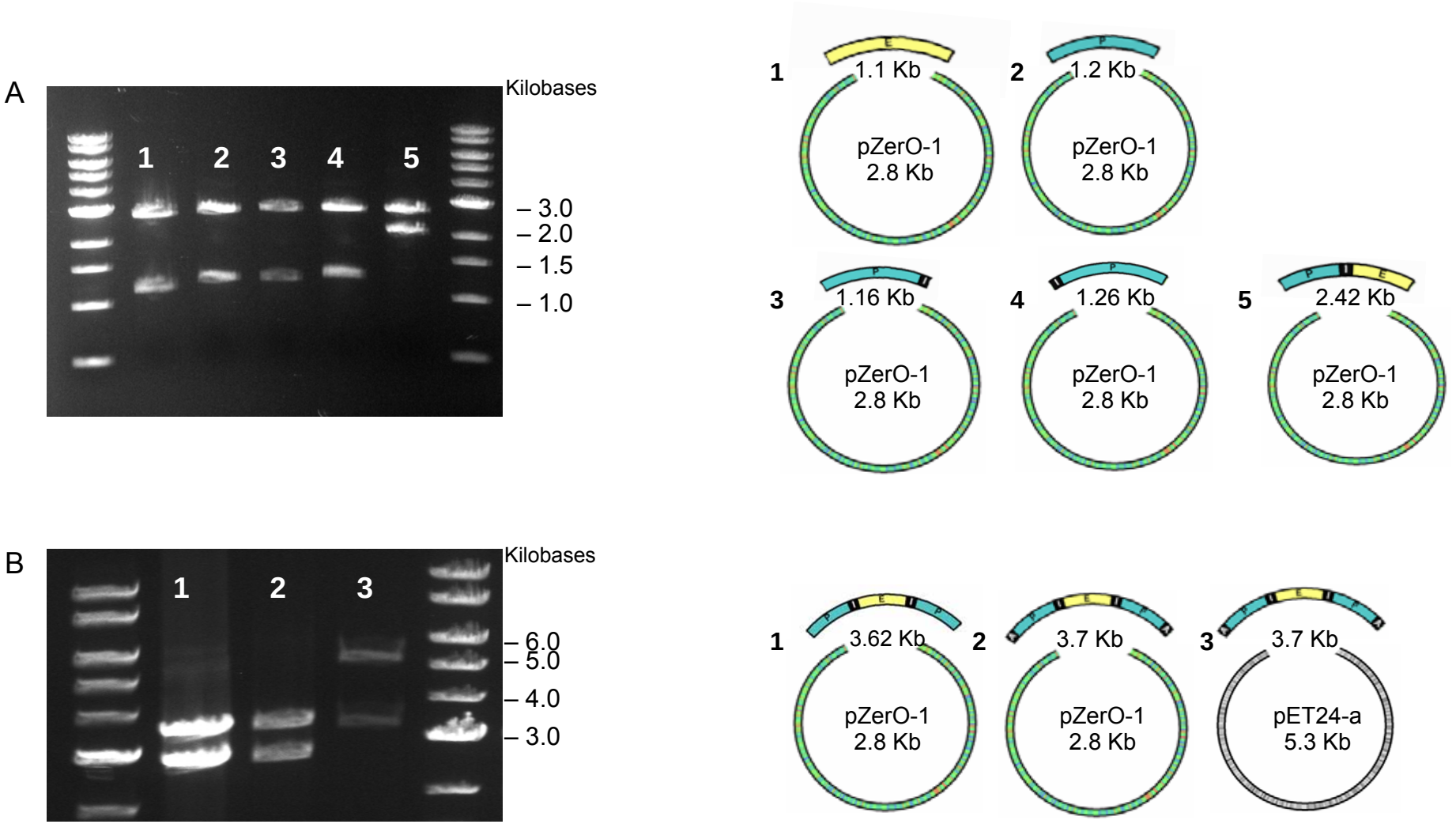

Figure 2-2. Analytical restriction digests, 1% TAE (Tris-acetate-EDTA) agarose gel, depicting gene and vector sizes at each stage of the **R4** assembly process with corresponding digestion schemes. DNA standard used was a 1Kb DNA ladder (NEB). **A.** Lane 1: *Nsi* I digest p**E$_2$** (1.1 Kb), pZerO-1 (2.8 Kb). Lane 2: *Nsi* I digest p**P$_2$** (1.2 Kb), pZerO-1 (2.8Kb). Lane 3: *Nsi* I digest p**E$_2$I** (1.16 Kb), pZerO-1 (2.8 Kb). Lane 4: *Nsi* I digest p**P$_2$I** (1.26 Kb), pZerO-1 (2.8 Kb). Lane 5: *Nsi* I digest p**P$_2$IE$_2$I** (2.42 Kb), pZerO-1 (2.8 Kb). **B.** Lane 1: *Nsi* I digest p**P$_2$IE$_2$IP$_2$** (3.62 Kb), pZerO-1 (2.8 Kb). Lane 2: *Nsi* I digest p**R4** (3.7 Kb), pZerO-1 (2.8Kb). Lane 3: *Bam*H I / *Hin*D III digest p**R4** (3.7 Kb), pET24-a (5.3 Kb).

Isolation and purification of protein triblock copolymers. The plasmid, p**LysB10**, encoding the protein **LysB10** as a single contiguous reading frame within plasmid pET24-a was used to transform the *E. coli* expression strain BL21(DE3). This afforded a protein triblock of sequence **(Table 2-2)**:

N-terminal endblock: VPAVGK[(VPAVG)(IPAVG)$_4$][(IPAVG)$_5$]$_{33}$

Midblock: (IPAVG)KAAK(VPGAG)[(VPGAG)$_2$VPGEG(VPGAG)$_2$]$_{28}$(VPAVG)KAAK(VPGAG)

C-terminal endblock: [(VPAVG)(IPAVG)$_4$][(IPAVG)$_5$]$_{33}$IPAVGKAAKA

The plasmid, p**R4**, encoding the protein **R4** as a single contiguous reading frame within plasmid pET24-a was used to transform the *E. coli* expression strain BL21(DE3). This afforded a protein triblock of sequence **(Table 2-3)**:

N-terminal endblock: VPAVGKVPAVG[(IPAVG)$_5$]$_{16}$ (IPAVG)

Midblock: (IPAVG)KAAK(VPGAG)(VPGIG) [(VPGIG)$_5$]$_{15}$(VPGIG)(VPAVG)KAAK(VPGAG)

C-terminal endblock: (VPGAG) [(IPAVG)$_5$]$_{16}$ (IPAVG)VPAVGKAAKA

Large-scale fermentation (100 L) was performed at 37°C in Circle Grow (Q-BIOgene) medium supplemented with kanamycin (50 µg/mL) at the Bioexpression and Fermentation Facility, University of Georgia. The fermentation cultures were incubated under antibiotic selection for 24 hours at 37°C.

Cells were harvested through centrifugation in sterile tubes at 1660 RCF for 20 minutes at 4°C. The supernatant was carefully decanted, cell pellets were resuspended in cold, sterile PBS (phosphate buffered saline, 20 mL per large culture flask pellet) and frozen at -80°C. Three freeze (-80°C) / thaw (25°C) cycles were employed for the initial cell fracture with equilibration back to cold temperatures following the cycles. Once cells were completely resuspended, six cycles of sonication, consisting of 20 second bursts followed by a 20 second rests in an ice bath, was employed to thoroughly break the

cells. To recover any unbroken cells, a preparative centrifugation step was used (1660 RCF for 10 minutes at 4°C). Unbroken cells, which pelleted out during the spin were resuspended in cold, sterile PBS and re-sonicated, as described above.

The cold cell lysate was centrifuged at 20,000g for 40 minutes at 4°C. The supernatant was transferred to a cold, sterile tube and poly(ethyleneimine) (PEI) was added to a final concentration of 0.5%. This solution was centrifuged again at 20,000g for 40 minutes at 4°C to remove all nucleic acids and contaminating cellular material precipitated by the PEI. The supernatant was transferred to new sterile 50 mL tubes and NaCl was added to a 2M final concentration. The elastin-mimetic protein was salted out of solution at 25°C for 30-45 minutes. This solution was centrifuged at 9500g for 15 minutes at 25°C to recover the protein product ('hot-spin'). The supernatant was discarded and the protein pellet was resuspended in cold, sterile PBS on ice for only 10-20 minutes to avoid solubilizing unwanted contaminates. The resuspended protein solution was then subjected to a 'cold spin' at 20,000g for 40 minutes at 4°C. The supernatant was transferred to sterile 50 mL tubes and salting precipitation was repeated. The hot (25°C) / cold (4°C) spin cycles were repeated until no contaminating pellet was observed after the cold spin. The number of cycles ranged between 6 to 10 and ended with a hot spin. Dialysis and lyophillization afforded proteins **LysB10** and **R4** as fibrous solids in isolated yield of 150 mg/L and 200 mg/L of culture, respectively.

For *in vivo* studies, **LysB10** and **R4** proteins underwent a secondary treatment with sodium hydroxide (NaOH). The protein pellets were resuspended in cold, sterile PBS at approximately 50mg/20mL. Sterile NaOH was added to a 0.4N final concentration and mixed gently by hand. The mixture was incubated on ice for fifteen minutes, after which 5M sodium chloride was added to a final concentration of 2M. The protein was precipitated from solution at 25°C, centrifuged at 8500g for 20 minutes at 25°C, and resuspended in cold PBS. This treatment was repeated for a total of three

times. Following the third treatment, the protein solution was adjusted to pH 6-8. A cold spin was performed at 20,000 rpm for 40 minutes at 4°C and the supernatant was sterilely desalted using PD-10 desalting columns (GE Healthcare Lifesciences) with molecular grade water (Cellgro). The end product was filtered through a 0.2 μm filter, eluted into autoclaved Lyoguard freeze drying trays (Gore), frozen at -80°C, and lyophilized. This procedure afforded **Lys B10** and **R4** as white fibrous protein products with isolated yields of 75 mg/L and 100 mg/L of expression culture, respectively.

Lyophilized protein was resuspended in sterile molecular grade water at 1 mg/mL and endotoxin levels were assessed according to manufacturer instructions using the Limulus Amoebocyte Lysate (LAL) assay (Cambrex). Levels of 0.1 EU/mg were obtained (1 EU = 100 pg of endotoxin), which corresponds to endotoxin levels for clinically used alginate (Pronova sodium alginate, endotoxin $\leq$ 100 EU/gram).

Table 2-2. Amino acid sequence of **LysB10** and related nucleic acid coding sequence
[VPAVGKVPAVG(IPAVG)$_4$][(IPAVG)$_5$]$_{33}$ [IPAVGKAAKVPGAG][(VPGAG)$_2$VPGEG(VPGAG)$_2$]$_{28}$
[VPAVGKAAKVPGAGVPAVG(IPAVG)$_4$][(IPAVG)$_5$]$_{33}$[IPAVGKAAKA]

Val	**Pro**	**Ala**	**Val**	**Gly**	**Lys**	**Val**	**Pro**	**Ala**	**Val**	**Gly**	**Ile**	**Pro**	**Ala**	**Val**
GTT	CCA	GCT	GTT	GGT	AAG	GTT	CCA	GCT	GTT	GGT	ATC	CCA	GCT	GTT
Gly	**Ile**	**Pro**	**Ala**	**Val**	**Gly**	**Ile**	**Pro**	**Ala**	**Val**	**Gly**	**Ile**	**Pro**	**Ala**	**Val**
GGT	ATC	CCA	GCT	GTT	GGC	ATT	CCG	GCT	GTA	GGT	ATC	CCG	GCA	GTG
Gly	**[Ile**	**Pro**	**Ala**	**Val**	**Gly**	**Ile**	**Pro**	**Ala**	**Val**	**Gly**	**Ile**	**Pro**	**Ala**	**Val**
GGC	ATT	CCG	GCT	GTT	GGT	ATC	CCA	GCT	GTT	GGT	ATC	CCA	GCT	GTT
Gly	**Ile**	**Pro**	**Ala**	**Val**	**Gly**	**Ile**	**Pro**	**Ala**	**Val**	**Gly]$_{33}$**	**Ile**	**Pro**	**Ala**	**Val**
GGC	ATT	CCG	GCT	GTA	GGT	ATC	CCG	GCA	GTG	GGC]$_{33}$	ATT	CCA	GCT	GTT
Gly	**Lys**	**Ala**	**Ala**	**Lys**	**Val**	**Pro**	**Gly**	**Ala**	**Gly**	**[Val**	**Pro**	**Gly**	**Ala**	**Gly**
GGT	AAG	GCG	GCC	AAG	GTT	CCA	GGT	GCA	GGC	GTT	CCA	GGT	GCA	GGC
Val	**Pro**	**Gly**	**Ala**	**Gly**	**Val**	**Pro**	**Gly**	**Glu**	**Gly**	**Val**	**Pro**	**Gly**	**Ala**	**Gly**
GTA	CCG	GGT	GCT	GGC	GTT	CCG	GGT	GAA	GGT	GTT	CCA	GGC	GCA	GGT
Val	**Pro**	**Gly**	**Ala**	**Gly]$_{28}$**	**Val**	**Pro**	**Ala**	**Val**	**Gly**	**Lys**	**Ala**	**Ala**	**Lys**	**Val**
GTA	CCG	GGT	GCG	GGT]$_{28}$	GTT	CCA	GCT	GTT	GGT	AAG	GCG	GCC	AAG	GTT
Pro	**Gly**	**Ala**	**Gly**	**Val**	**Pro**	**Ala**	**Val**	**Gly**	**Ile**	**Pro**	**Ala**	**Val**	**Gly**	**Ile**
CCA	GGT	GCA	GGC	GTT	CCA	GCT	GTT	GGT	ATC	CCA	GCT	GTT	GGT	ATC
Pro	**Ala**	**Val**	**Gly**	**Ile**	**Pro**	**Ala**	**Val**	**Gly**	**Ile**	**Pro**	**Ala**	**Val**	**Gly**	**[Ile**
CCA	GCT	GTT	GGC	ATT	CCG	GCT	GTA	GGT	ATC	CCG	GCA	GTG	GGC	ATT
Pro	**Ala**	**Val**	**Gly**	**Ile**	**Pro**	**Ala**	**Val**	**Gly**	**Ile**	**Pro**	**Ala**	**Val**	**Gly**	**Ile**
CCG	GCT	GTT	GGT	ATC	CCA	GCT	GTT	GGT	ATC	CCA	GCT	GTT	GGC	ATT
Pro	**Ala**	**Val**	**Gly**	**Ile**	**Pro**	**Ala**	**Val**	**Gly]$_{33}$**	**Ile**	**Pro**	**Ala**	**Val**	**Gly**	**Lys**
CCG	GCT	GTA	GGT	ATC	CCG	GCA	GTG	GGC]$_{33}$	ATT	CCA	GCT	GTT	GGT	AAG
Ala	**Ala**	**Lys**	**Ala**	**Stop**										
GCG	GCC	AAG	GCG	TAA										

Table 2-3. Amino acid sequence of **R4** and related nucleic acid coding sequence
[VPAVGKVPAVG[(IPAVG)$_5$]$_{16}$ (IPAVGIPAVG)KAAK(VPGAGVPGIG) [(VPGIG)$_5$]$_{15}$
(VPGIGVPAVG)KAAK(VPGAGVPAVG) [(IPAVG)$_5$]$_{16}$ IPAVGVPAVGKAAKA]

Val	**Pro**	**Ala**	**Val**	**Gly**	**Lys**	**Val**	**Pro**	**Ala**	**Val**	**Gly**	**[Ile**	**Pro**	**Ala**	**Val**
GTT	CCA	GCT	GTT	GGT	AAG	GTT	CCA	GCT	GTT	GGT	[ATT	CCG	GCT	GTT
Gly	**Ile**	**Pro**	**Ala**	**Val**	**Gly**	**Ile**	**Pro**	**Ala**	**Val**	**Gly**	**Ile**	**Pro**	**Ala**	**Val**
GGT	ATC	CCA	GCT	GTT	GGT	ATC	CCA	GCT	GTT	GGC	ATT	CCG	GCT	GTA
Gly	**Ile**	**Pro**	**Ala**	**Val**	**Gly]$_{16}$**	**Ile**	**Pro**	**Ala**	**Val**	**Gly**	**Ile**	**Pro**	**Ala**	**Val**
GGT	ATC	CCG	GCA	GTG	GGC]$_{16}$	ATT	CCG	GCT	GTT	GGT	ATT	CCA	GCT	GTT
Gly	**Lys**	**Ala**	**Ala**	**Lys**	**Val**	**Pro**	**Gly**	**Ala**	**Gly**	**Val**	**Pro**	**Gly**	**Ile**	**Gly**
GGT	AAG	GCG	GCC	AAG	GTT	CCA	GGT	GCA	GGC	GTT	CCA	GGT	ATT	GGT
[Val	**Pro**	**Gly**	**Ile**	**Gly**	**Val**	**Pro**	**Gly**	**Ile**	**Gly**	**Val**	**Pro**	**Gly**	**Ile**	**Gly**
[GTA	CCT	GGT	ATT	GGC	GTT	CCG	GGT	ATC	GGT	GTG	CCA	GGC	ATC	GGT
Val	**Pro**	**Gly**	**Ile**	**Gly**	**Val**	**Pro**	**Gly**	**Ile**	**Gly]$_{15}$**	**Val**	**Pro**	**Gly**	**Ile**	**Gly**
GTA	CCG	GGT	ATT	GGC	GTT	CCA	GGC	ATT	GGC]$_{15}$	GTA	CCT	GGT	ATT	GGT
Val	**Pro**	**Ala**	**Val**	**Gly**	**Lys**	**Ala**	**Ala**	**Lys**	**Val**	**Pro**	**Gly**	**Ala**	**Gly**	**Val**
GTT	CCA	GCT	GTT	GGT	AAG	GCG	GCC	AAG	GTT	CCA	GGT	GCA	GGC	GTT
Pro	**Ala**	**Val**	**Gly**	**[Ile**	**Pro**	**Ala**	**Val**	**Gly**	**Ile**	**Pro**	**Ala**	**Val**	**Gly**	**Ile**
CCA	GCT	GTT	GGT	[ATT	CCG	GCT	GTT	GGT	ATC	CCA	GCT	GTT	GGT	ATC
Pro	**Ala**	**Val**	**Gly**	**Ile**	**Pro**	**Ala**	**Val**	**Gly**	**Ile**	**Pro**	**Ala**	**Val**	**Gly]$_{16}$**	**Ile**
CCA	GCT	GTT	GGC	ATT	CCG	GCT	GTA	GGT	ATC	CCG	GCA	GTG	GGC]$_{16}$	ATT
Pro	**Ala**	**Val**	**Gly**	**Ile**	**Pro**	**Ala**	**Val**	**Gly**	**Lys**	**Ala**	**Ala**	**Lys**	**Ala**	**Stop**
CCG	GCT	GTT	GGT	ATT	CCA	GCT	GTT	GGT	AAG	GCG	GCC	AAG	GCG	TAA

Identification of elastin-mimetic proteins. Sodium dodecyl sulfate-polyacrylamide gel electrophoresis (SDS-PAGE) analysis revealed a single protein band at 250 kDa and 100 kDa corresponding to **LysB10 (Figure 3A)** and **R4 (Figure 3B)**, respectively. A total of 10 µg of the elastin-mimetic polypeptide along with molecular weight markers (Precision Plus Protein Kaleidoscope, Bio-Rad) were run on a 7.5% gel and negatively stained with a Copper stain (Bio-Rad). As previously reported, molecular weights observed by SDS-PAGE for elastin-mimetic proteins are approximately 20% greater than calculated molecular weights [75, 97] .

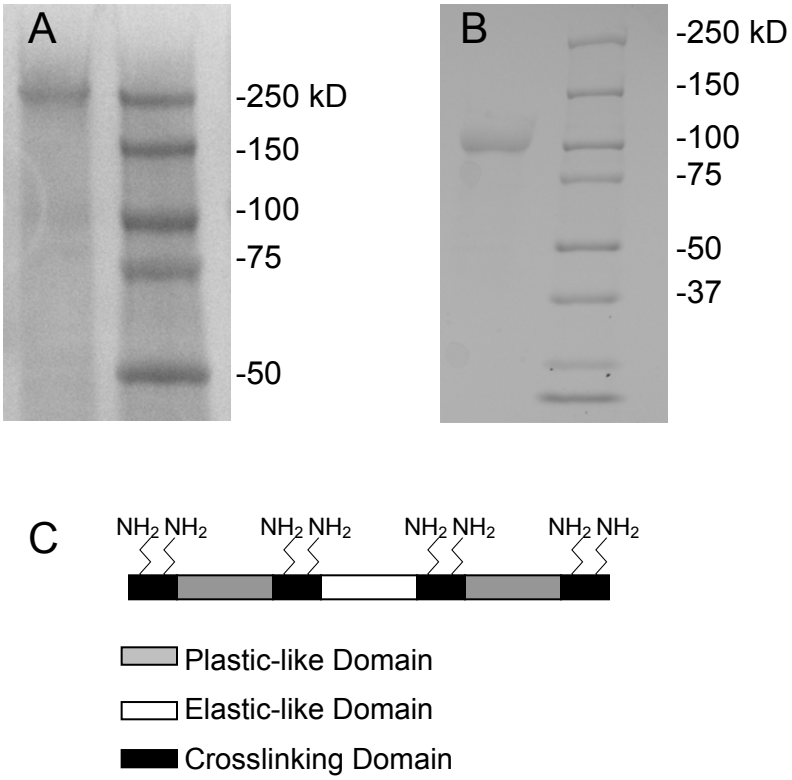

Figure 2-3. Sodium dodecyl sulfate-polyacrylamide gel electrophoresis (SDS-PAGE) analysis of crosslinkable elastin-mimetic triblock copolymers. **A**. **LysB10**, run on 7.5% SDS-PAGE stained with Copper Stain (BioRad). Expected molecular weight: 209 KDa. **B**. **R4** run on 7.5% SDS-PAGE stained with Copper Stain. Expected molecular weight: 108 KDa. Marker lane: Precision Plus Protein Kaleidoscope (Bio-Rad). **C.** Assembly scheme for crosslinkable elastin-mimetic proteins, **LysB10** and **R4**. Both proteins are triblock copolymers with lysine-containing crosslinking domains flanking each plastic-like and elastic-like domain. Together, there are eight possible sites for chemical crosslinking afforded by the free amine moieties of the lysine residues and the N-terminal amine of the peptide chain. Plastic-like domain (grey), Elastic-like domain (white), Crosslinking domain (black).

Amino acid composition analysis was performed by the Microchemical Facility at Harvard University. Lyophilized protein was resuspended in HPLC grade water and dialyzed against the same water at 4°C with buffer changes. Solutions of 1 mg/mL were submitted for analysis. Amino acid compositional analysis of **LysB10**. Calc. (mol.-%): Ala, 19; Glu, 1; Gly, 25.7; Ile, 13.9; Pro, 19.8; Val, 19.9. Obs. (mol.-%): Ala, 18.7; Glu, 2.3; Gly, 23; Ile, 13.5; Pro, 18.1; Val, 18. **R4**. Calc. (mol.-%): Ala, 14.2; Gly, 26.1; Ile, 19.2; Pro, 19.8; Val, 20.2. Obs. (mol.-%): Ala, 15.6; Gly, 24.3; Ile, 17.5; Pro, 19.4; Val, 18.9.

Rheological analysis of concentrated protein polymer solutions.

Rheological data were acquired on an Advanced Rheological Expansion System III rheometer (ARES III, TA instrument, NJ) in parallel plate geometry with a plate diameter of 25 mm. The testing protocol for rheological analysis has been detailed elsewhere [1]. In brief, 100 mg/mL protein solutions were prepared by adding distilled, deionized water to lyophilized protein at 4°C, shaking the solution for 48 hours, and then allowing the solution to equilibrate for 72 hours. The gap between parallel plates was adjusted between 0.2 and 0.35 mm and dynamic mechanical experiments were performed in shear deformation mode. An initial strain amplitude sweep was performed at 4°C and 37°C at a frequency of 1 Hz to confirm the linear viscoelastic range for the protein polymer.

The gelation temperature was determined by heating samples from 4°C to 37°C at a rate of 1°C per minute. Following temperature equilibration at 37°C, viscoelastic properties were examined by a strain sweep at a fixed frequency of 1Hz and a frequency sweep at fixed strain amplitude of 2%. Experiments were repeated on six samples and representative data presented.

Fabrication of water cast protein films. For mechanical property analysis, films were cast from protein solutions in water at room temperature. In brief, lyophilized proteins were dissolved at a concentration of 100 mg/mL in water at 4°C. The protein solution was then poured into Teflon casting molds and regulated solvent evaporation performed at 23°C for 48 hours. After complete solvent evaporation, films were subjected to glutaraldehyde (GTA) vapor phase crosslinking. Specifically, films were enclosed in a 2 L chamber containing a 10 mL of 25% gluteraldehyde (GTA) solution. Films were placed on a platform 4 cm above the GTA solution and exposed to GTA vapor for 24 hours. Subsequently, the films were rinsed in PBS for 48 hours with a change of PBS at 24 hours. Test samples were referred to as crosslinked or non-crosslinked indicating whether GTA treatment was used. Prior to testing, films were hydrated in PBS at 37°C, which contained NaN_3 at 0.2 mg/mL to prevent biological contamination. Samples were cut into a dumbbell shape using a stainless steel die with gauge dimensions of 13 mm x 4.75 mm. Hydrated film thickness, as measured by optical microscopy, was typically 0.07 mm for non-crosslinked and crosslinked **Lys B10** films and 0.1 mm for **R4** films.

Evaluation of water content in protein films. For evaluation of water content, 200 µL of a 10 wt% protein solution was cast as a disk measuring 1 cm in diameter. Dried films were vapor phase crosslinked with a 25% GTA solution for 24 hours, fully dehydrated under vacuum, and the dehydrated weight obtained using a Mettler balance. Films were subsequently incubated in PBS at 37°C for 24 hours and fully hydrated weights were obtained. A total of six films were evaluated for each protein. The equilibrium water content and equilibrium swelling ratio were determined according to equations (1) and (2), respectively [111].

$$\text{Equilibrium Water Content} = \frac{\text{hydrated weight - dehydrated weight}}{\text{hydrated weight}} \quad (1)$$

$$\text{Equilibrium Swelling Ratio} = \frac{\text{hydrated weight}}{\text{dehydrated weight}} \quad (2)$$

Characterization of non-crosslinked extractables. To determine the percent of potentially extractable protein polymer, 200 µL of a 10-wt% protein solution was cast as a disk measuring 1 cm in diameter. Dried films were vapor phase crosslinked with a 25% GTA solution for 24 hours, rinsed in PBS and incubated at 4°C, below the inverse transition temperature of the protein, for a period of seven days. Every 48 hours films were dehydrated and dry weight was monitored for material losses. Six films were investigated for each protein. The percent extractable was determined by equation (3).

$$\%\ \text{Extractables} = 1 - \frac{\text{dehydrated weight}}{\text{hydrated weight}} \times 100 \quad (3)$$

Mechanical analysis of hydrated protein films. A preconditioning protocol was employed for **LysB10** samples that consisted of a single cyclic stretch to 50% strain for one cycle followed by 20 cycles of 30% strain with off-loading periods of 5 minutes between each cycle. Due to the plasticity of **R4** protein films, preconditioning was not conducted. Uniaxial stress-strain properties of protein films were determined on at least five to six individual specimens using a dynamic mechanical thermal analyzer (DMTA V, Rheometric Scientific Inc., Newcastle, DE) with a 15 N load cell in the inverted orientation, so that samples could be immersed in a jacketed beaker filled with PBS at 37°C. The maximum travel distance of the drive shaft was 23 mm, which limited maximum strain to 70% of engineering strain. Given the extensibility of these materials, uniaxial stress-strain responses were also characterized using a miniature materials tester (Minimat 2000, Rheometric Scientific) in tensile deformation mode at a rate of 5

mm/min conducted in air at room temperature. All samples were coated with a thin layer of mineral oil to prevent dehydration. For both DMTA and Minimat testing, samples were cut into a dumbbell shape using a stainless steel die with gauge dimensions of 13 mm x 4.75 mm. In addition, to calculating Young's modulus (E), ultimate tensile stress (UTS), and strain at failure (ε), resilience was determined from equation (4).

$$\%\ \text{Resilience} = 1 - \frac{\text{area under loading curve} - \text{area under unloading curve}}{\text{area under loading curve}} \times 100 \qquad (4)$$

Creep analysis was performed on 6 to 12 specimens for each film type subjected to varying levels of constant engineering stress for periods of up to 11 hours.

In vivo evaluation of crosslinked protein gels. *Syringe casting method for creating cylindrical implants.* In order to minimize sample manipulation and the risk of cross-contamination, the following protocol was used for preparation of samples for in vivo implant studies. A 10 wt% cold protein solution was drawn into a chilled sterile 1 mL syringe (Becton Dickenson) and subsequently gelled at 37°C. The tip of the syringe was removed with a sterile scalpel and the molded protein gel extruded into room temperature PBS. Gel samples, 4.75 mm in diameter by 8 mm in length, were incubated in 0.5% GTA for 24 hours. Following crosslinking, samples were washed in sterile PBS for 48 hours with 20 buffer exchanges.

Subcutaneous and peritoneal implant models. All animal experiments were approved by the Institutional Animal Care and Use Committee (IACUC) at Emory University. Eight-week-old inbred male C57BL/6 mice weighing 25–30 g were obtained from the Jackson Laboratory (Bar Harbor, ME). Under ketamine (95 mg/kg, IM) and xylazine (5 mg/kg, IM) anesthesia, a 1 cm dorsal midline incision was performed and a single test sample implanted in the subcutaneous space, parallel to the longitudinal body

axis of each mouse. Each implant type was implanted in at least three separate mice. Three weeks after implantation, animals were sacrificed and samples explanted with overlying skin. For peritoneal implants, a 1 cm long midline incision was made along the linea alba of the abdominal wall and a single implant placed into the peritoneal cavity. After closing the abdominal muscle with 4-0 absorbable surgical suture (Vicryl, Ethicon, Inc, NJ), the skin incision was closed with wound clips. Each recombinant protein was implanted in at least five mice. Mice were sacrificed one week later and, prior to sample removal, a peritoneal saline lavage was performed to harvest cells for FACS analysis.

Histological examination. Retrieved samples were processed for histological and immunohistochemical evaluation to characterize the local cellular response and to determine the extent and thickness of fibrous capsule formation. All samples were fixed in 10% neutral buffered formalin overnight and processed for parafin embedding. Sections were prepared at a thickness of 5 μm and stained with hematoxylin and eosin (H&E) or rat anti-mouse monoclonal F4/80 (CI:A3-1, Abcam) to identify infiltrating macrophages. In all cases, multiple sections were examined in three to five separate samples for each protein polymer type.

Fluorescent-activated cell sorting (FACS) of peritoneal lavage. Prior to harvesting implants, each peritoneal cavity was initially lavaged with 10 mL of cold Hank's Balanced Salt Solution containing 10 U/mL heparin and 1% BSA (Mediatech, Inc). Typically, 6 to 7 mL of lavage solution was retrieved and cells immunostained for flow cytometry with PE-conjugated rat monoclonal anti-mouse CD11b for macrophages, FITC-conjugated hamster anti-mouse CD3 for total T cells, FITC-conjugated rat monoclonal anti-mouse CD4 for helper T cells, FITC-conjugated rat monoclonal anti-mouse CD8 for cytotoxic T cells, FITC-conjugated rat monoclonal anti-mouse CD19 for B cells, and FITC-conjugated rat monoclonal anti-mouse Gr-1 for neutrophils (BD Biosciences Pharmingen). Typically, antibodies were diluted to 1 μg/50 μL/10^6 cells in

PBS containing 1% BSA and 0.1% sodium azide. Cells were incubated in the dark for 30 minutes on ice, then washed three times in staining buffer, and fixed in 1% paraformaldehyde. Analysis was performed on a FACScan using Cellquest (Becton Dickinson) and FlowJo software (Tree Star) [112]. Comparison between groups was analyzed via a Student's t-test and $p < 0.05$ were considered to be significant. Results are presented as mean ± SEM. Two control groups were employed; one that did not undergo surgery and another in which surgery was performed without sample implantation. At least five mice were enrolled in each experimental and control group.

2.3 Results and Discussion

Synthesis of triblock protein copolymers capable of both chemical and physical crosslinking. We have recently reported the design of a new class of recombinant elastin-mimetic triblock copolymer that has the capacity to form physical or virtual crosslinks, which stabilize protein network structure [1-3]. Moreover, through selective engineering of block structure, including the design of block size or sequence, and choice of film casting conditions, microphase structure can be manipulated and, as a consequence, material properties, such as drug elution characteristics and mechanical behavior tailored over a wide range of responses [1, 4, 5]. However, physical crosslinks formed as a result of hydrophobic aggregation may be deformed or disrupted under external stresses lower than that required to disrupt covalent crosslinks. This feature may limit the capacity of physically crosslinked protein-based materials to retain material integrity under loading conditions operative for a number of potential applications in tissue engineering or regenerative medicine. Given these considerations, we have postulated that chemically locking a multiblock protein assembly in place may provide a strategy to preserve functional responses that are linked to specific domain structures and morphologies over a broader range of externally applied loads. Further, it would also

provide an additional approach for altering material strength and compliance, as well as stress induced creep behavior.

In this report, elastin-mimetic triblock copolymers were designed with endblock sequences, encoded by a hydrophobic repeat sequence, (IPAVG), that exhibits plastic-like mechanical responses, and a central elastomeric block of varying amino acid structure. The endblock sequence was selected to display an inverse temperature transition in water below 37°C, thereby mediating protein self-assembly due to endblock coacervation at or above this temperature. Sites for covalent crosslinking were engineered at positions flanking each block. Two target proteins were genetically engineered. A 209 kDa triblock, **LysB10,** was designed with hydrophobic endblocks with a mass of approximately 75 kDa each, which contained 33 repeats of the pentapeptide sequence $[IPAVG]_5$, separated by a 58 kDa hydrophilic midblock comprised of 28 repeats of the pentapeptide sequence $[(VPGAG)_2VPGEG(VPGAG)_2]$ **(Table 2-2)**. Crosslinking sites that contained a pair of lysine residues (KAAK) flanked each block, such that a total of eight crosslinkable residues were potentially accessible. The presence of glutamic acid residues (E) was responsible for the hydrophilic character of the midblock.

In addition, a 108 kDa triblock protein polymer, designated as **R4,** was synthesized with flanking hydrophobic plastic-like endblocks, each with a mass of approximately 37 kDa that contained 16 repeats of $[IPAVG]_5$, separated by a 35 kDa midblock comprised of 15 repeats of $[VPGIG]_5$ **(Table 2-3)**. Likewise, a total of eight potential crosslinking sites were engineered into the protein sequence; positioned predominantly as lysine pairs (KAAK) that flank each block. The substitution of isoleucine for glutamic acid in the midblock yielded a protein that was largely hydrophobic with little difference in block polarity. While VPGEG and VPGIG are both reported to form β-spiral structures that display elastic responses when crosslinked as

gels, polypeptides from each sequence differ significantly in their inverse transition temperature. Specifically, by incorporating the hydrophobic residue, isoleucine, into the fourth position of the repeat sequence, the inverse transition temperature of VPGIG is much lower than that associated with VPGEG [66, 67, 81-83].

Lysine crosslinking domains were engineered with an appreciation of the structure of similar crosslinking sites in native elastin and a consideration of the 'N-end rule', such that the identity of the N-terminal residue of a recombinant protein may influence degradation in bacterial expression systems. In native elastin, crosslinking domains contain paired lysines within polyalanine repears (eg. Ala-Ala-Ala-Lys-Ala-Ala-Lys-Ala-Ala) [108, 109], which promotes formation of an alpha-helix that has been reported to facilitate intermolecular crosslinking [62-65]. Thus, for both protein triblock copolymers, a lysine containing insert was designed encoding two lysine residues separated by two alanine residues (Lys-Ala-Aal-Lys) that was inserted between component blocks. Additionally, lysine containing adaptor sequences were designed to encode for two C-terminal, as well as a single lysine residue near the N-terminus. Lysine was not incorporated as an N-terminal residue, as previous efforts to encode lysine in this position have lead to a 10-fold decrease in protein yield [74, 85, 86, 113]. This design afforded eight free amines for crosslinking, seven from lysine and one from the N-terminal amine **(Figure 2-3C)**.

Rheological analysis confirms formation of viscoelastic protein gels. The gelation point of protein solutions can be determined by measurement of G' and G" as a function of temperature at a fixed frequency. Above 13°C, the shear storage (G') and loss (G") modulus of concentrated aqueous solutions of LysB10 increased by a factor of approximately 10^3 and 10 (Pa), respectively, while tan δ (G'/G") decreased, consistent

with the formation of a viscoelastic gel **(Figure 2-4A).** Above 15 °C, R4 solutions displayed an increase in shear storage (G') and loss (G") modulus to 10^4 and 10^3 (Pa), respectively, with only a modest reduction in tan δ **(Figure 2-4C).** For both LysB10 and R4 protein solutions at 37°C, G' and G" were independent of frequency between 1 to 10 rad/s at a fixed strain amplitude of 2% **(Figure 2-4B, 2-4D).** In addition, the complex viscosity (η*) was a linear function of the logarithm of frequency with a slope of -1. However, as evident by a significantly higher tan δ and complex viscosity, aqueous gels of R4 were more viscous than those of LysB10. This difference highlights the significance of the midblock structure in triblock design. Despite similar endblock structure and the presence of an elastomeric midblock sequence in both R4 and LysB10 triblocks, the R4 midblock is considerably more hydrophobic and coacervates along with the endblock at 37°C. Indeed, when expressed as single blocks the inverse transition temperatures of the R4 endblock and midblock proteins were 26°C and 16°C, respectively, while the comparable transition temperatures for LysB10 blocks were 21°C and >80°C (data not shown). Thus, significant mixing of the elastomeric and plastic-like blocks occurs only in the case of gels produced from the R4 protein polymer, which limits its elastomeric response. We have previously demonstrated that selected changes in midblock size and amino acid sequence result in significant changes in viscoelastic mechanical properties. Indeed, a more viscous response, similar to that observed for R4, was displayed by a protein composed entirely of hydrophobic plastic-like endblock sequences [1].

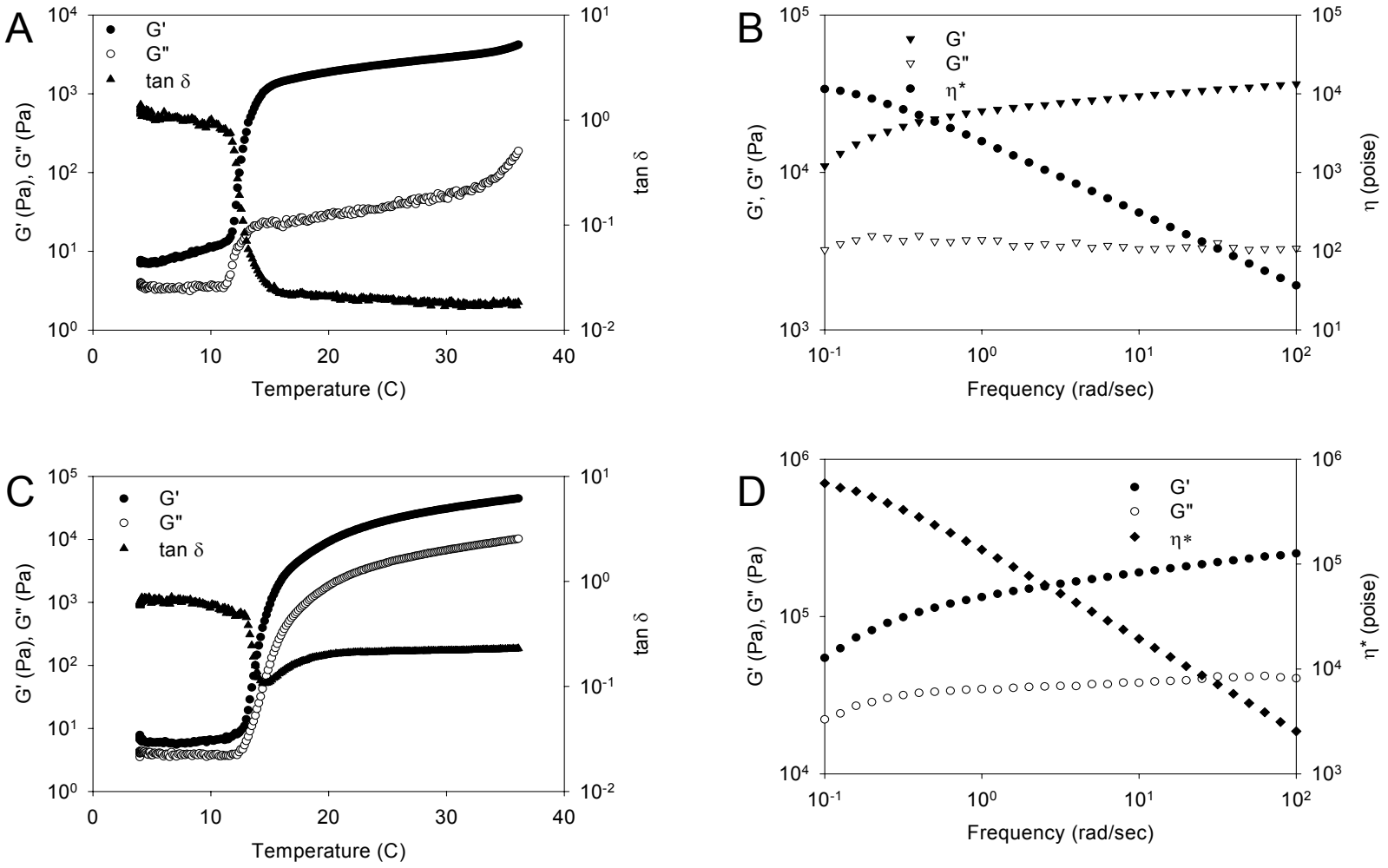

Figure 2-4. Rheological behavior of triblocks in water. **(A) LysB10** dynamic shear storage (G′), loss modulus (G″) are plotted as a function of temperature (γ 2%, ω 1Hz). **(B) LysB10** dynamic shear storage (G′), loss modulus (G″), and complex viscosity (η*) are plotted as a function of frequency (γ 2%, 37°C). **(C) R4** dynamic shear storage (G′), loss modulus (G″) are plotted as a function of temperature (γ 2%, ω 1Hz). **(D) R4** dynamic shear storage (G′), loss modulus (G″), and complex viscosity (η*) are plotted as a function of frequency (γ 2%, 37°C).

***Glutaraldehyde crosslinking of elastin-mimetic triblock copolymer films*.**

Investigations by our group and others have demonstrated that covalent crosslinks can enhance the mechanical stability of a variety of elastin analogues **(Table 2-4).** Aldehyde crosslinking agents, such as glutaraldehyde, have been commonly used to process implanted tissues and proteins because of their capacity for efficient crosslink formation with an associated reduction in tissue antigenicity and enhanced mechanical strength [114, 115]. While limitations of glutaraldehyde exist [96, 107], since it remains an industry standard and its effects are otherwise well established, it was used in this study as a model crosslinking system.

As a measure of the extent of crosslinking, the percent of extractable protein was examined after incubating samples at 4°C for seven days. Below the inverse transition temperature, non-crosslinked films dissolved immediately due to disruption of physical crosslinks. After vapor phase GTA crosslinking, films retained approximately 86% (**LysB10**) and 88% (**R4**) of their mass consistent with a high degree of chemical crosslinking, despite a relatively limited number of crosslink sites per protein species. The equilibrium water content observed for **R4** and **LysB10** films was 32.0 ± 3.7% and 54.3 ± 3.8%, respectively; values that are similar to the 32% water content reported for hydrated elastin at 36°C [116]. Likewise, water swelling ratios were 1.5 ± 0.1 for **R4** and 2.4 ± 0.2 for **LysB10**, consistent with the higher proportion of hydrophobic amino acids in **R4**.

Table 2-4. Review of chemically crosslinkable elastin-mimetic systems and chemical crosslinking strategies

Crosslinkable Recombinant Elastin-Mimetic Proteins	Molecular Weight (kDa)	Crosslinking Agent	Fabrication Technique	Mechanical Evaluation	Biocompatibility Evaluation	Reference
Poly(KGGVG) (polydisperse)	6.5-14 (polydisperse)	GTA and DSG	hydrogel	-	-	[94]
$VPGIG_2VPGKGVPGIG_2$-CS5-$VPGIG_2VPGKGVPGIG_2$	80.7	GTA	film	-	-	[93]
CS5-$(VPGIG)_{20}$ $[CS5\text{-}(VPGIG)_{20}]_3$ $[CS5\text{-}(VPGIG)_{20}]_5$	14, 36.6, 59	GTA	film	E = 0.099-0.32 MPa σ = 0.5-0.9 MPa ε = 251-393 %	-	[86]
$[VPGVG_4VPGKG]_{25}$	80.6	BS3 and DSS	hydrogel	-	-	[98]
CS5-$(VPGIG)_{25}$ $[CS5\text{-}(VPGIG)_{25}]_3$ $[CS5\text{-}(VPGIG)_{25}]_5$	14, 36.6, 59	Isocyanate	hydrogel	E = 0.4-0.9 MPa G = 0.13-0.31 MPa E = 340-570 %	-	[96]
ELP[KV_6]-102, ELP[KV_{16}]-112	42.7, 47	TSAT	hydrogel	G* = 1.6-15 kPa	-	[97]
ELP[KV_6-112]	47.1	TSAT	Hydrogel + cells	G* = 0.28-1.7 kPa	non-cytotoxic *in vitro*	[107]
KV_7F-72 AND KV_2F-64	31, 28.3	THPP	Hydrogel	G* = 5.8-45.8 kPa	non-cytotoxic *in vitro,* 3 days	[101, 102]
Exons 20-24	10	Genipin	Film	E = 1.8 MPa ε = 0.68 mm/mm	-	[65, 92]
		PQQ	Film	E = 0.4 MPa ε = 0.90 mm/mm	-	
CS5-$[(VPGIG)_2(VPGKG)(VPGIG)_2]_4$	37	BS3	Film	E = 0.08-0.7 MPa G = 0.022-0.060 MPa	-	[100]
		DSS	Film	E = 0.3-0.97 MPa G = 0.12-0.32 MPa	-	

Abbreviations: CS5-RGD cell binding domain, GTA-glutaraldehyde, DSG-disuccinimidyl glutarate, HMDI-hexamethylene diisocyanate, BS3-bis(sulfosuccinimidyl) suberate, DSS-disuccinimidyl suberate, TSAT-tris-succinimidyl aminotriacetrate, THPP-tris(hydroxymethyl)phosphino-propionic acid, PQQ-pyrroloquinoline quinine, E= elastic modulus, σ = ultimate tensile strength, ε = elongation at break, G* = complex modulus, G = shear modulus

Mechanical responses of LysB10 copolymer films. Most biomolecular constructs represent dynamic systems of hydrated biopolymer chains whose entanglements and structural interrelationships may be altered in response to an external load. As a consequence, initial mechanical properties may change in response to repetitive loading forces until stable behavior is observed. Thus, mechanical preconditioning is presumed to induce changes in microstructure that lead to fixed structural rearrangements of the constituent polymer chains and, as a consequence, stable material properties under a given loading environment [117-120]. Preconditioned, non-crosslinked **LysB10** films were robust and elastomeric; displaying an elastic modulus of 0.49 ± 0.03 MPa, an ultimate tensile strength of 2.88 ± 0.71 MPa, a strain at failure of 463 ± 43%, and a resilience of 53 ± 2%. In contrast, preconditioned crosslinked samples exhibited a three-fold increase in Young's modulus (1.10 ± 0.45 MPa) and a 50% decrease in strain at failure (223 ± 30%) along with no significant change in ultimate tensile strength compared to their non-crosslinked counterparts **(Table 2-5, Figures 2-5, 2-6)**. We speculate that these differences are largely related to the stabilization of semi-rigid endblocks by chemical crosslinking. While crosslinking enhanced strength and modulus, a modest reduction in resilience was noted. Since crosslinking was performed prior to preconditioning, the capacity of chain entanglements between midblock and endblock sequences to structurally rearrange in response to the conditioning protocol may have been restricted. In other words, crosslinked-fixed mixing between rigid and elastomeric domains, in addition to restricting the mobility of the elastomeric phase, may have contributed to this effect.

The approximate hoop stress of a blood vessel with an inner diameter of 4.5 mm and wall thickness of 0.8 mm is 45 kPa, when subjected to an intraluminal pressure of 16 kPa (120 mmHg). Crosslinked **LysB10** films demonstrated limited creep (<10%) over 11 hours at stress levels at or below 45 kPa. Increasing the applied stress by a factor of

ten increased creep to ~30% **(Figure 2-7A)**. In contrast, non-crosslinked films showed a four-fold greater level of creep strain in response to 45 kPa loading stress **(Figure 2-7B)**.

Mechanical responses of R4 copolymer films. Hydrated **R4** films revealed plastic-like deformation behavior. Specifically, stress increased linearly with increasing strain until a yield point was observed at 1.72 MPa and 4.49 MPa in non-crosslinked and crosslinked films, respectively **(Figure 2-8A)**. Corresponding values of Young's modulus were 48.6 ± 0.9 MPa and 67 ± 5.14 MPa for non-crosslinked and crosslinked samples, respectively. These values are four- to ten-fold greater than those noted for **LysB10 (Table 2-5).** As compared to **LysB10**, the more hydrophobic character of **R4** is associated with reduced water uptake, which contributes to an increase in material rigidity and tensile strength. Moreover, given the similarity of endblock and midblock polarity, size, and transition temperature, we speculate that a greater degree of block mixing occurs in films composed of **R4** with rigid, plastic-like domains sustaining a higher level of the external load. Crosslinking appears to have a relatively greater effect on the yield point (2.6-fold increase) than Young's modulus (1.4-fold increase). Likely, the effect of block mixing has a more profound effect on the mobility of the elastomeric phase than crosslinking, which predominantly stabilizes the semi-rigid endblocks. Consistent with these observed uniaxial stress-strain properties, crosslinked **R4** films demonstrated limited creep strain (<10%) over an 11-hour period, despite applied stresses as high as 400 kPa. Substantial deformation, however, was noted at stresses of nearly 1 MPa **(Figure 2-8B)**.

Table 2-5. Summary of mechanical parameters in crosslinked and non-crosslinked films

Protein	Treatment	Resilience (%)	Young's Modulus DMTA (MPa)	Young's Modulus Minimat (MPa)	UTS (MPa)	Strain at Failure (%)
LysB10	GTA Xlinked	39 ± 1*	1.10 ± 0.45*	1.60 ± 0.48*	3.62 ± 0.98	223 ± 30*
LysB10	Non-Xlinked	52 ± 2*	0.49 ± 0.03*	0.53 ± 0.02*	2.88 ± 0.71	463 ± 43*
R4	GTA Xlinked	-	67.4 ± 5.14*	-	4.49 ± 0.27*	8 ± 2*
R4	Non-Xlinked	-	48.6 ± 0.90*	-	1.72 ± 0.30*	4.9 ± 1*
B10[§]	Water-25	67± 1	0.71 ± 0.12	-	-	-

Average values obtained from 3-10 replicates. Resilience and Young's Modulus determined from DMTA testing. Young's modulus, UTS, and % Strain determined from Minimat testing. *($p < 0.05$ between crosslinked and non-crosslinked samples)

[§]B10 Data obtained from Wu et al, *Biomacromolecules*, in review [6].

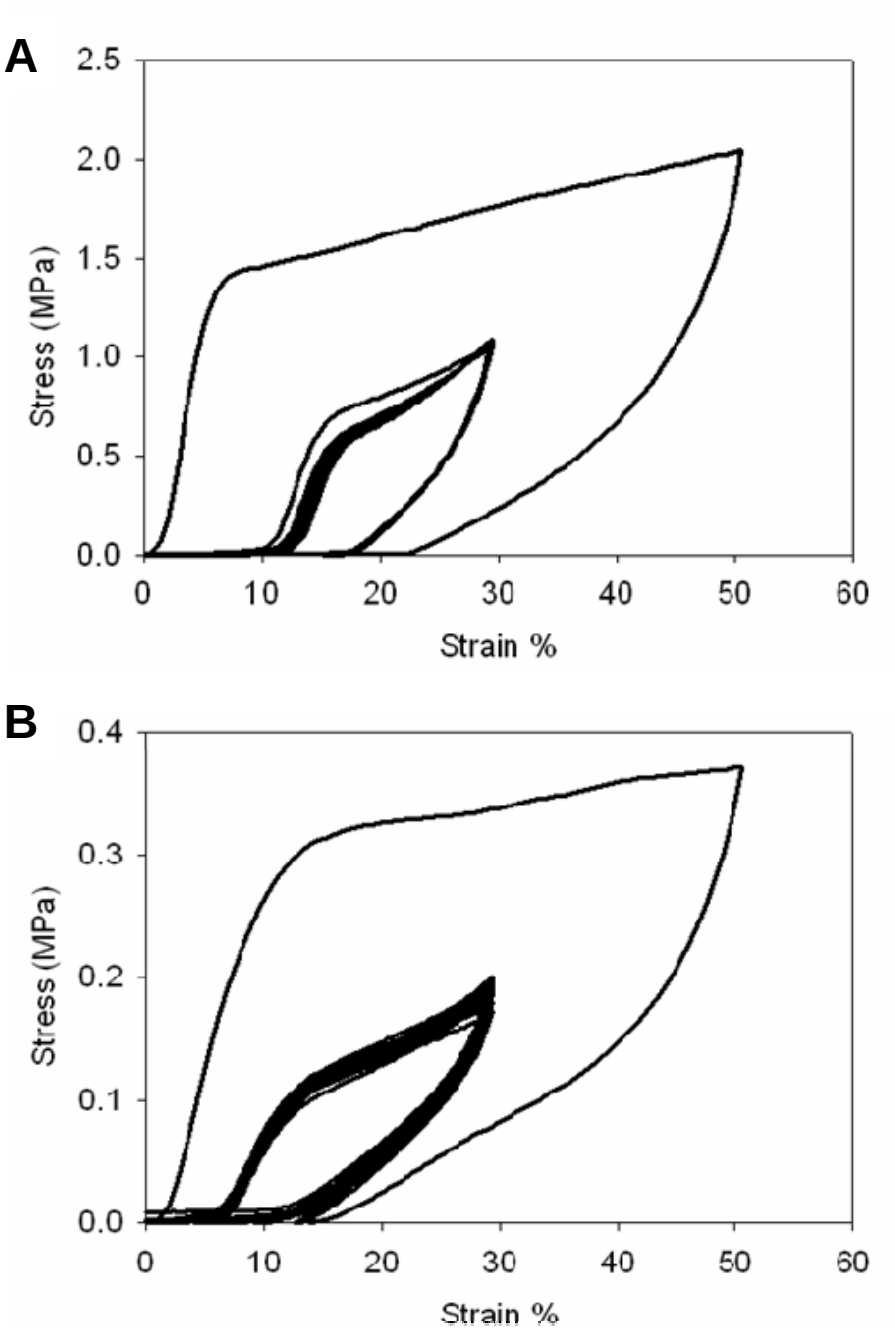

Figure 2-5. The influence of preconditioning on the resilience of water cast **LysB10** films with and without glutaraldehyde crosslinking (Figure **A** and **B**, respectively). A sample was cyclically stretched to 50% strain and then to 30% for 20 cycles, with an off-loading period of 5 minutes between cycles. This figure is representative of multiple data sets.

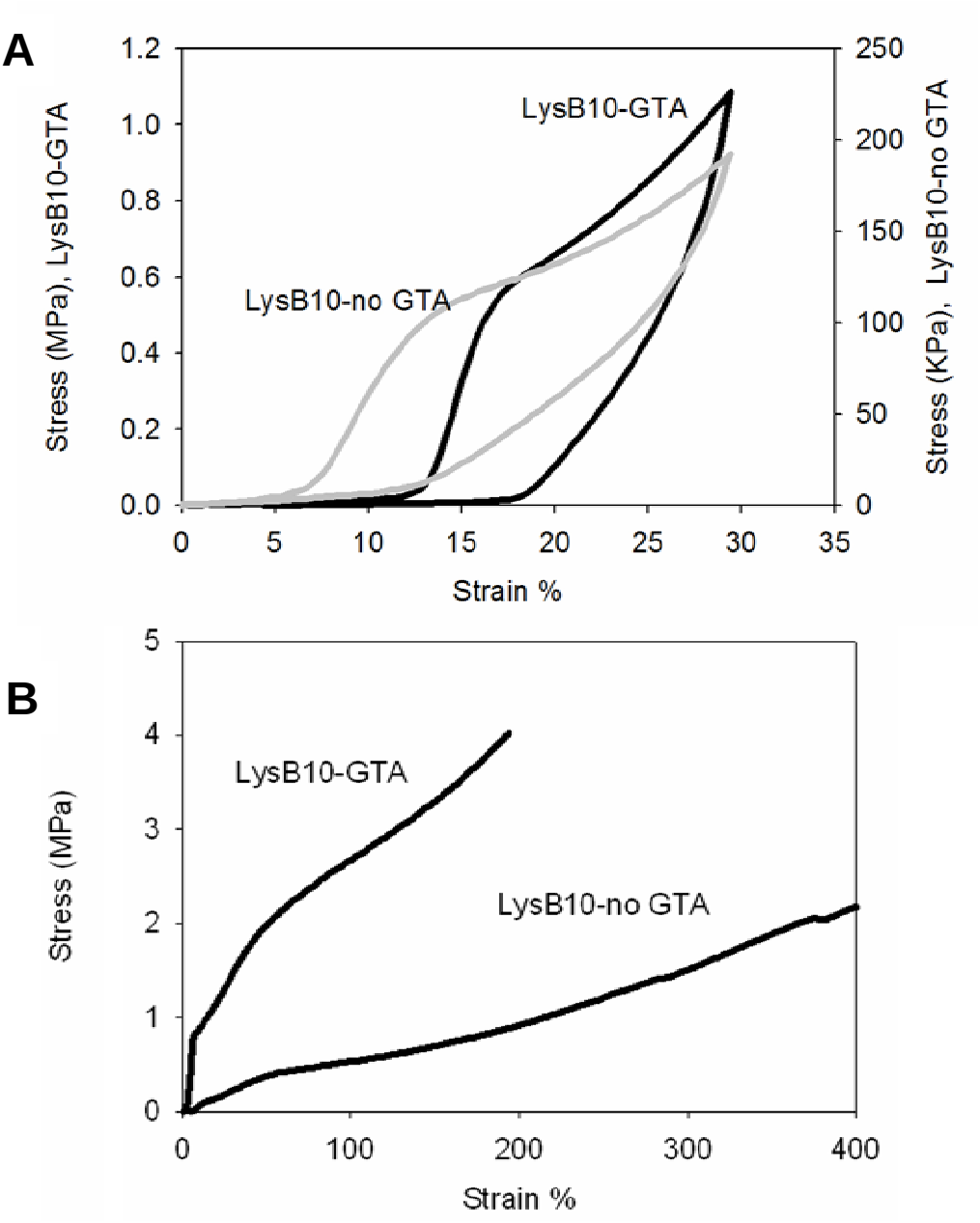

Figure 2-6. A. The influence of preconditioning on the resilience of water cast **LysB10** films with (left y-axis) and without glutaraldehyde crosslinking (right y-axis). The sample was cyclically stretched to 50% strain and then to 30% for 20 cycles, with an off-loading period of 5 minutes between cycles. This figure is representative of multiple data sets and illustrates cycle 20 of 30% stretch. **B.** Uniaxial stress-strain analysis performed on a Minimat 2000. The Young's modulus was 1.60 ± 0.48MPa for preconditioned glutaraldehyde crosslinked films and 0.53 ± 0.02 MPa for preconditioned non-crosslinked films measured from the linear region.

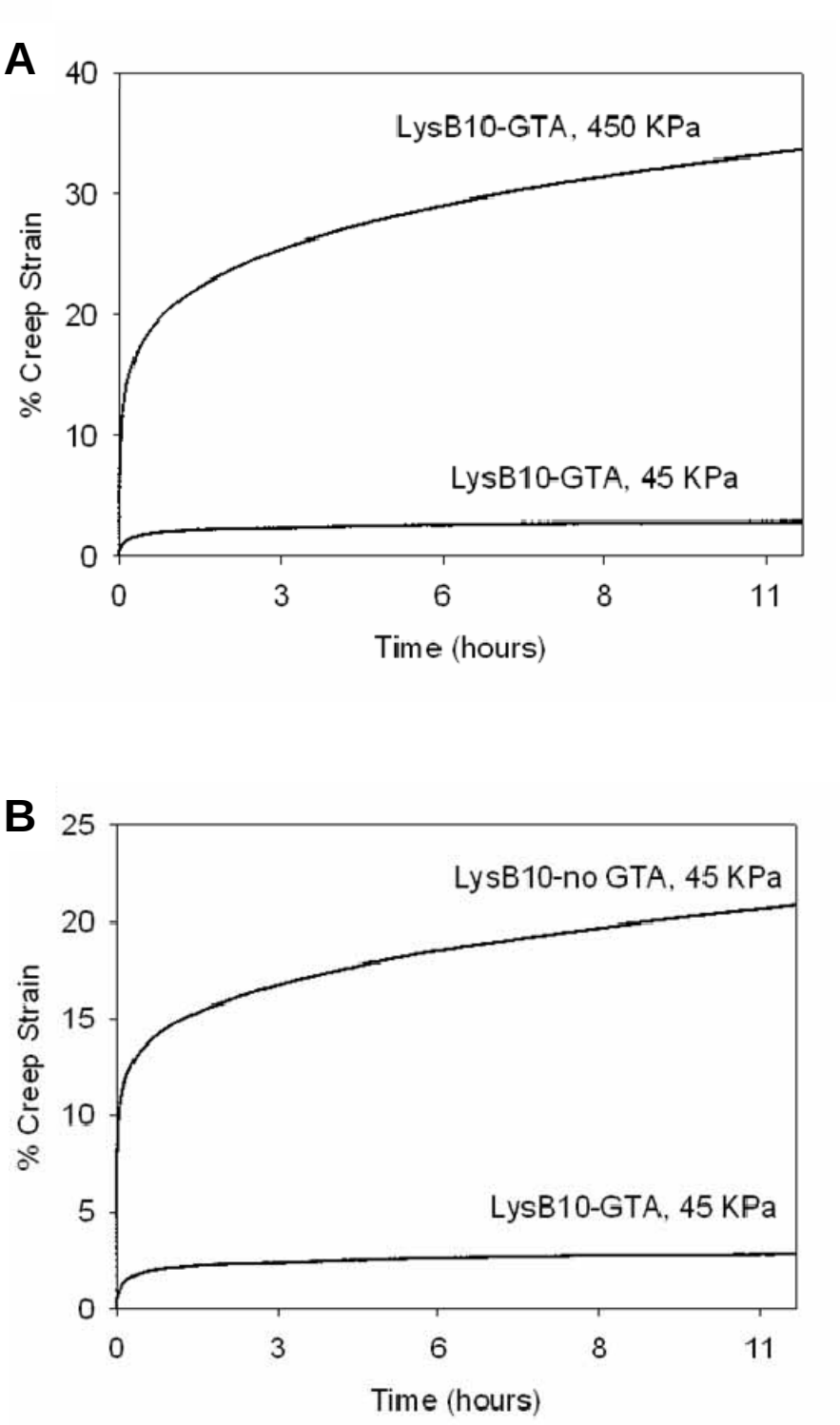

Figure 2-7. **A.** Creep behavior of water cast **LysB10** films GTA crosslinked examined as tensile stress was maintained at 45KPa and 450KPa. These figures are representative of multiple data sets in which variability was <10%. **B.** Comparison of the creep behaviors of water cast **LysB10** films with and without gluteraldehyde crosslinking at applied stresses of 45 KPa.

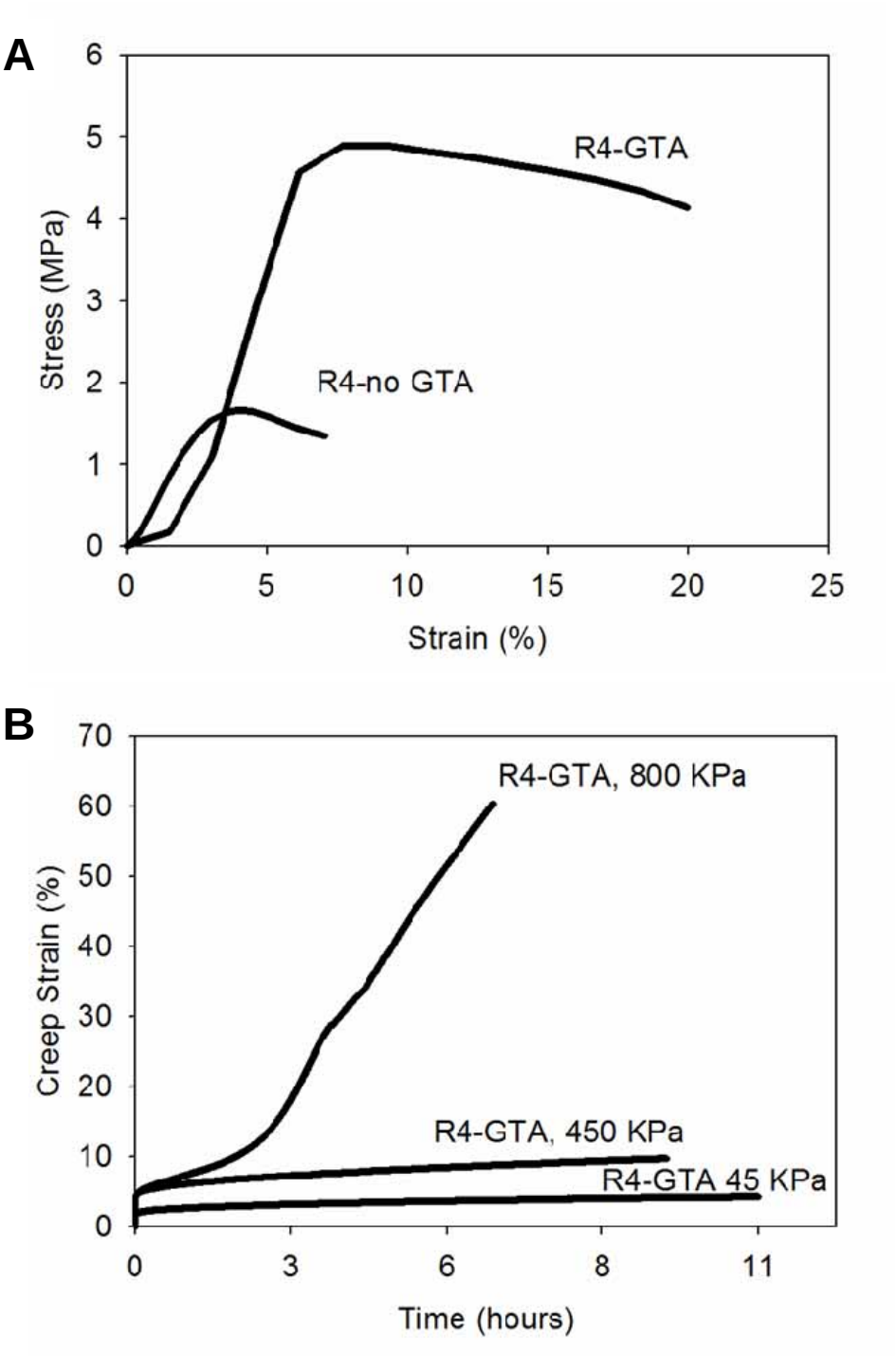

Figure 2-8. **A.** Uniaxial stress-strain analysis. The Young's modulus was determined from the linear region of the curve as 67.4± 5 MPa for glutaraldehyde crosslinked **R4** films measured on a Minimat 2000 and 48.6± 9 MPa for non-crosslinked **R4** films measured on a DMTA. **B.** Comparison of the creep behaviors of water cast **R4** films subjected to gluteraldehyde crosslinking. Creep was examined as tensile stress was maintained at 45KPa and 450KPa, and 800KPa. This figure is representative of multiple data sets. **R4** samples were not preconditioned.

In vivo responses to crosslinked elastin-mimetic protein hydrogels. Using a murine model, crosslinked **LysB10 and R4** hydrogels were implanted into either the subcutaneous space or the peritoneal cavity. FACS analysis demonstrated no difference in either the cell number or cell type identified within peritoneal lavage fluid, harvested one week after either sham surgery or protein polymer implantation **(Figure 2-9)**. Samples implanted within the peritoneal cavity and subcutaneous tissue were explanted one and three weeks after implantation, respectively **(Figures 2-10, 2-11).** Macrophages were identified along the periphery of the fibrous capsule and in the surrounding tissue without infiltration into the implant. The fibrous capsule thickness of **LysB10** samples within the subcutaneous space was 25.3 ± 16.1 μm, while the capsule measured 14.5 ± 5.3 μm for those placed in the peritoneal cavity. **R4** implants displayed a similar response, with a fibrous capsule thickness of 24.2 ± 6.0 μm and 8.4 ± 1.2 μm for subcutaneous and peritoneal cavity implants, respectively.

Tissue-material interactions, including biopolymer stability, are integral to assessing the suitability of elastin-like protein polymers for implant related applications. To date, reports documenting in vivo responses to elastin-mimetic protein implants have been limited; largely confined to studies performed 15 to 20 years ago on proteins synthesized chemically and subject to radiation crosslinking [82, 121]. In these investigations, homopolymers or copolymers composed of VPGVG, VPGKG, VPGEG, IPAVG, and VPAVG reportedly did not induce significant inflammatory or allergic reactions [121-124]. The most thoroughly characterized elastin variant, chemically synthesized poly(GVGVP), was subjected to in vitro toxicity and mutagenicity assays and was administered via intravenous, intraocular, intramuscular, intraperitoneal, and subcutaneous routes without toxic effect [82, 121]. A fibrous capsule was noted three weeks after intramuscular implantation of a radiation crosslinked sample [82]. In a more

recent report, elastin microparticles prepared from chemically synthesized poly(VPAVG) were evaluated following subcutaneous and intravitreal injection. No inflammatory response was observed after 28 days. However, tractional retinal detachment was noted [122]. The failure to detect an immune mediated reaction to these polymers is consistent with other studies that have sought to identify potentially immunogenic epitopes on native elastin. While polyclonal and monoclonal antibodies can be raised against peptides derived from the hydrolysis of native elastin, neither VPGVG nor VPAVG peptides have been among the recognized sequences [124]. Moreover, VPGVG peptides were unable to competitively inhibit the binding of any of the antibodies raised against native elastin, which further supports the notion that this pentapeptide is not present among antigenic elastin epitopes [124].

Recently, genetically engineered elastin-mimetic protein polymers have been investigated in vivo as non-thrombogenic coatings [7, 125], targeted drug delivery vehicles [126-128], and as an implantable material [129]. In the latter instance, after a 13 week implant period in the subcutaneous space, recombinant human tropoelastin 'sponges', chemically crosslinked with bis(sulfosuccinimidyl) suberate, were surrounded by a fibrous capsule with a minimal to moderate inflammatory response [129]. Non-chemically crosslinked recombinant elastin-like proteins have also been administered within the intra-articular space as a 650 μM protein solution [129]. Although the biological response was not evaluated, this study revealed a three hour half-life for non-aggregating VPGVG proteins and a three day half-life for aggregating VPG**X**G proteins, where **X** = V:G:A at a ratio of 1:7:8. As a related material, a 47 kDa recombinant silk-elastin-like protein (SELP), comprised of GAGAS silk-like [S] and GVGVP elastin-like [E] amino acid sequences ($[S]_4[E]_4[EK][E]_3$) has been studied after injection into the subcutaneous space. Histological analysis revealed minimal fibrous encapsulation after four weeks with a mild degree of inflammation that included the presence of

macrophages in the surrounding tissue [130]. SELPs have been also used for adenoviral gene delivery and demonstrate prolonged and localized expression of adenoviruses for up to 15 days, suggesting the potential for cancer therapy [131, 132]. A summary of in vivo biocompatibility studies conducted on elastin-mimetic proteins is presented in **Table 2-6**.

The evaluation of in vivo biocompatibility is largely based on characterizing local tissue responses to subcutaneously implanted materials where the intensity and duration of inflammation and wound healing, including capsule formation, is evaluated histologically [133, 134]. Although histological studies of biopolymers containing elastin-mimetic sequences have previously noted the presence of 'mild inflammation' [121, 122] and 'a reaction that was limited to a typical cell mediated response to the presence of a foreign body', the extent of fibrous capsule formation has not been reported [129]. Fibrous capsule thickness has been investigated for a variety of polymeric and ceramic implants designed for tissue repair, cell encapsulation, or as drug delivery systems [135-138]. Capsule thicknesses are dependent on implant site and material type and typically varies between 2 and 150 μm over implantation periods of one to three months. For example, greater capsule thickness has been observed for materials within intraperitoneal sites compared to those in subcutaneous sites over identical implant durations [136]. As an illustration of the effects of surface chemistry, implants comprised of poly(alkyl methacrylate) (PAMA) with short alkyl side chains exhibited a thicker fibrous capsule than those with long side chains (140 μm vs 120 μm) [135]. Additionally, self-assembled monolayers (SAMs) of alkanethiols on gold with different terminal functional groups displayed surface dependent inflammatory responses after one week with extremely hydrophobic methyl terminated surfaces inducing thick fibrous capsules (130 μm) and higher recruitment of inflammatory cells compared to hydrophilic COOH- and OH- terminated surfaces (80 μm and 70 μm, respectively) [139]. Likewise,

functionalized polypropylene implants revealed similar foreign body reactions to surface modifications, with –OH surfaces triggering a stronger response (~100 μm) compared to –COOH rich surfaces (37 μm) [140]. In contrast, surface topography does not appear to have a significant effect on capsule thickness, although it may influence local inflammatory responses [141]. In this report, there were no observable differences in biological responses for either chemically crosslinked triblock elastin-mimetic protein polymer. Both **R4** and **LysB10** implants initiated limited local inflammatory activity and displayed relatively thin fibrous capsules.

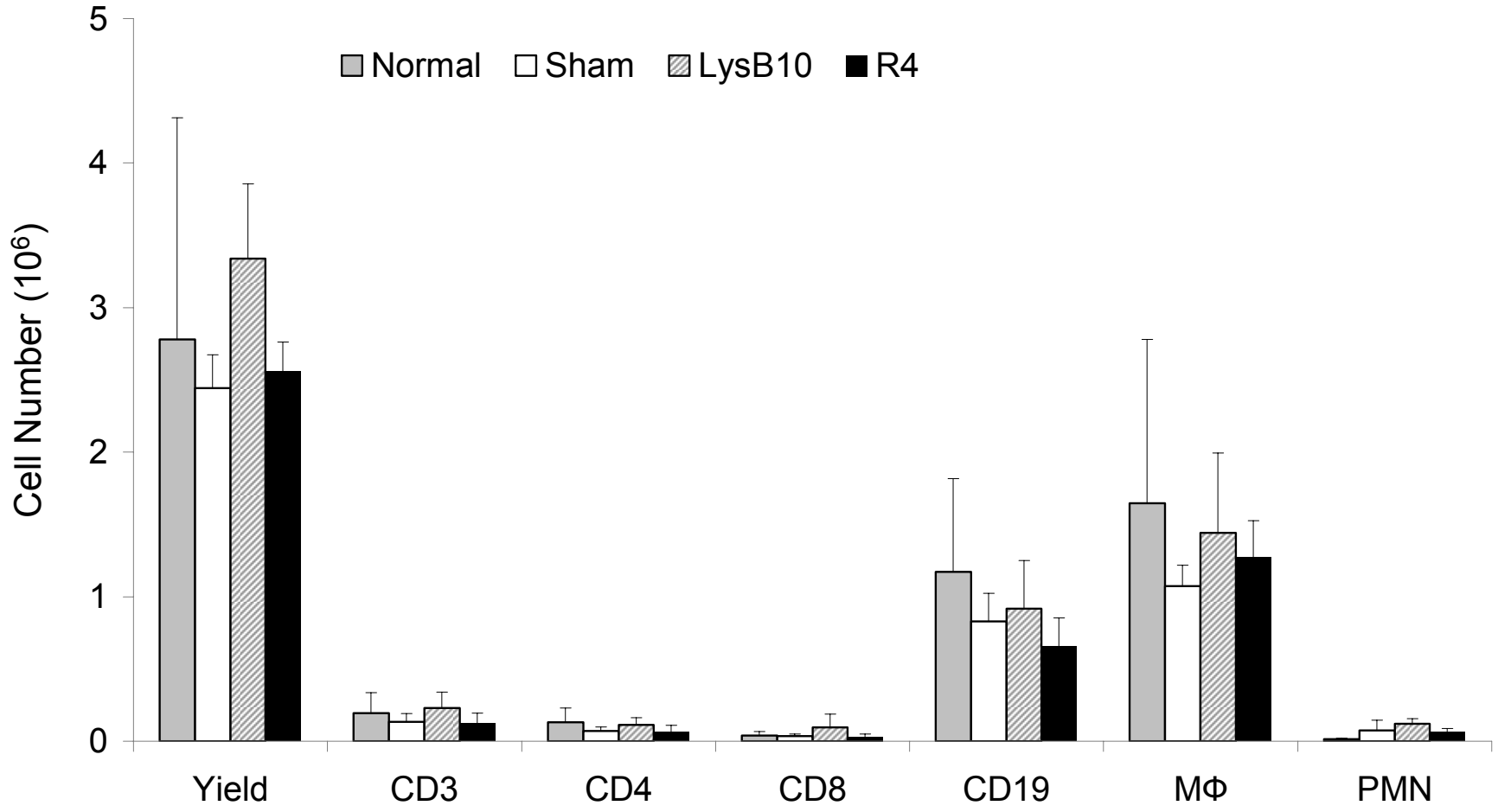

Figure 2-9. FACS analysis of peritoneal implanted **LysB10** and **R4** cylindrical hydrogels one week post-implant (n=5 for each group). Experimental groups showed no statistical difference in cell number from normal and sham control groups

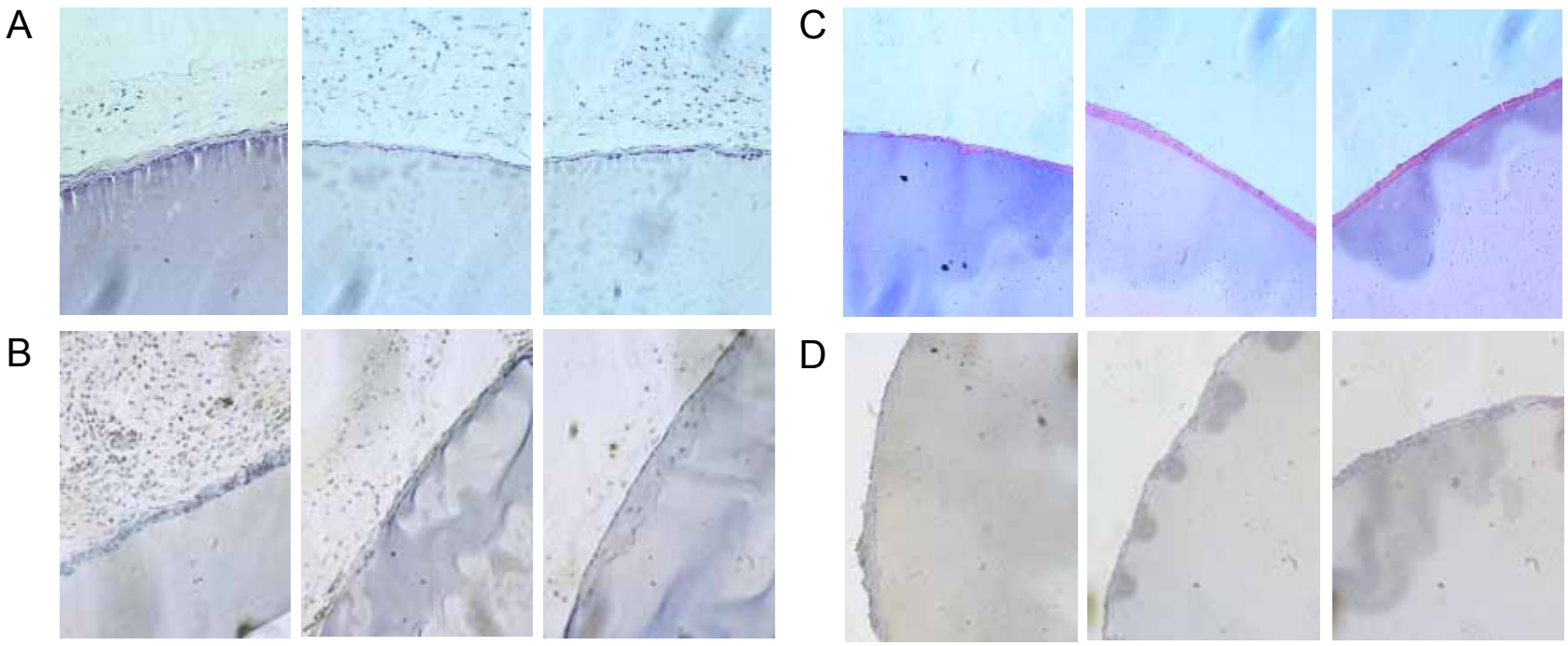

Figure 2-10. Histological analysis of three subcutaneous **LysB10** implants retrieved 3 weeks post-implant. **(A)** H&E staining of formalin fixed, paraffin embedded subcutaneous **LysB10** implants demonstrates the presence of a mild foreign body reaction along the periphery of the sample. **(B)** F4/80 staining of formalin fixed, paraffin embedded subcutaneous **LysB10** implants demonstrate the presence of macrophages along the periphery of the fibrous capsule but no infiltration into the **LysB10** implant. Histological analysis of peritoneal **LysB10** implants retrieved 1 week post-implant. **(C)** H&E staining demonstrates the presence of a mild foreign body reaction along the periphery of the peritoneal **LysB10** implant . **(D)** F4/80 staining the presence of macrophages along the periphery of the fibrous capsule but no infiltration into the peritoneal **LysB10** implant. Images are oriented so that the **LysB10** gel is located in the bottom right corner.

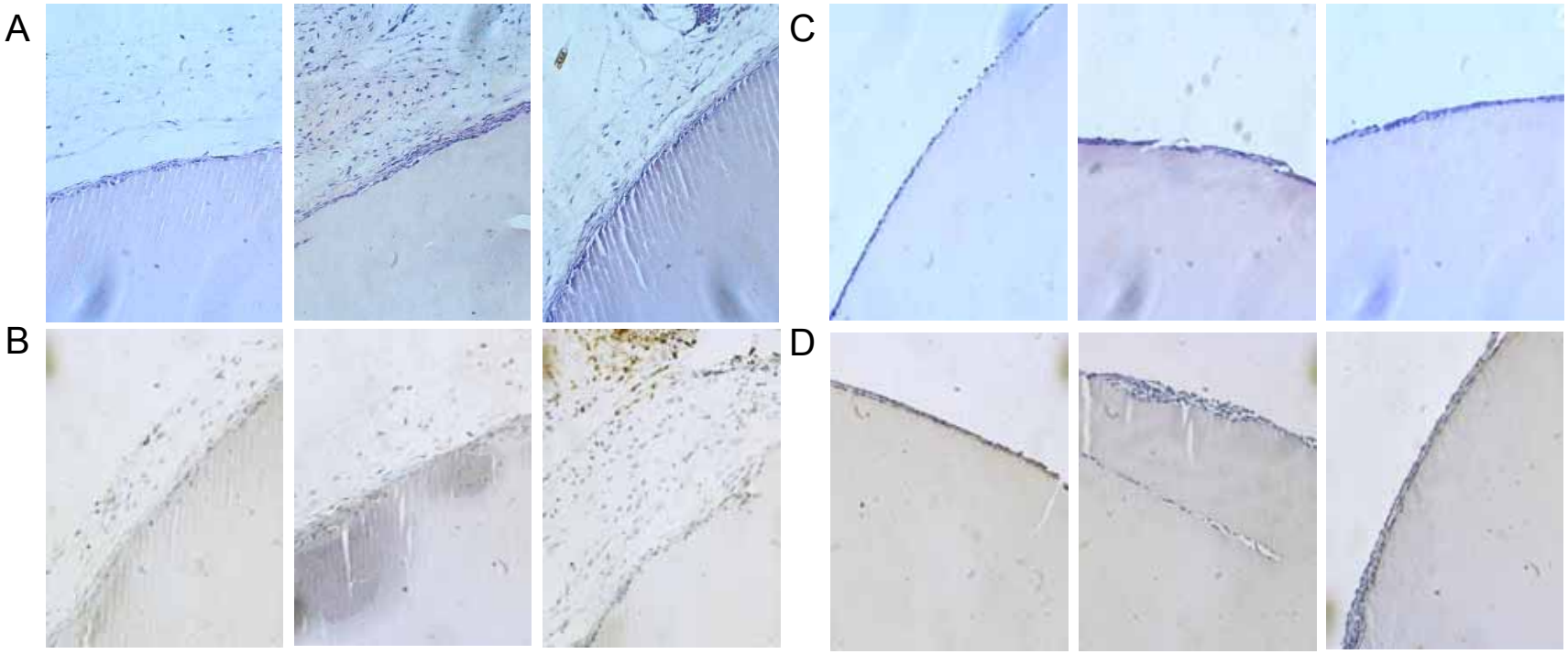

Figure 2-11. Histological analysis of three subcutaneous **R4** implants retrieved 3 weeks post-implant. **(A)** H&E staining of formalin fixed, paraffin embedded subcutaneous **R4** implants demonstrates the presence of a mild foreign body reaction along the periphery of the sample. **(B)** F4/80 staining of formalin fixed, paraffin embedded subcutaneous **R4** implants demonstrate the presence of macrophages along the periphery of the fibrous capsule but no infiltration into the **R4** implant. Histological analysis of peritoneal **R4** implants retrieved 1 week post-implant. **(C)** H&E staining demonstrates the presence of a mild foreign body reaction along the periphery of the peritoneal **R4** implant . **(D)** F4/80 staining the presence of macrophages along the periphery of the fibrous capsule but no infiltration into the peritoneal **R4** implant. Images are oriented so that the **R4** gel is located in the bottom right corner.

2.4 Conclusions

A new class of recombinant elastin-mimetic protein polymer has been designed that is capable of both physical and chemical crosslinking. We have demonstrated that chemical crosslinking provides an independent mechanism for control of protein mechanical responses. Specifically, elastic modulus can be enhanced and creep strain reduced through the addition of chemical crosslinking sites. Additionally, we have demonstrated exceptional biocompatibility of gluteraldehyde treated multiblock systems. By chemically locking a multiblock protein assembly in place, unique structures and morphologies are preserved and stabilized, which provides the capacity to modulate a wide range of functional responses, such as mechanical behaviors, permeability, and drug elution characteristics. We anticipate that these materials will find utility in a number of vascular and non-vascular biomedical applications.

CHAPTER 3

Biocompatibility of Recombinant Elastin-Mimetic Proteins

3.1 INTRODUCTION

Elastin-based protein polymers, genetically engineered with or without cell binding motifs, crosslinking domains, or non-natural amino acids, represent a promising new class of biomaterial [86, 102, 107, 142, 143]. Their capacity to be processed as gels [2-4], films [5, 6], or nanofibers [1, 103] demonstrate the versatility of these recombinant proteins with potential applications in drug delivery [2, 144-146], tissue engineering [86, 147-149], or as constituents of implanted medical devices [7, 125]. The majority of these proteins have been examined as covalently crosslinked networks [91-103].

Recently, we have reported the synthesis of amphiphilic elastin-mimetic protein polymers composed of complex block sequences that self-assemble through the formation of robust physical crosslinks [1, 4, 5, 150]. The biosynthetic scheme for generating self-assembling recombinant proteins has been based upon a convergent strategy for integrating multiple blocks of concatemerized DNA cassettes by sequential ligation [1, 2, 98]. To date, this strategy has been used to design diblock, triblock, and tetrablock copolymers ranging from 100 to 200 kDa in molecular weight [1, 4-7, 84, 150]. The segregation of protein blocks into compositionally, structurally, and spatially distinct domains affords ordered structures on the nanometer to micrometer size range. Significantly, protein polymers that are structurally polymorphic display tunable mechanical, chemical, and biological properties [1, 4, 5, 150].

We have recently synthesized a triblock copolymer, designated **B9**, that contains identical hydrophobic endblocks with $[(IPAVG)_4(VPAVG)]$ repeat sequences, separated by a central hydrophilic block with repeating units of $[(VPGVG)_2(VPGEG)(VPGVG)_2]$ [2].

Phase behavior and mechanical properties of elastin-mimetic polypeptides are critically dependent on the identity of the residues within the pentapeptide repeat unit Val/Ile-Pro-Xaa-Yaa-Gly. Yaa modulates the coacervation or inverse transition temperature (T_t) in water in a manner commensurate with the polarity of the amino acid side chain and polymer-solvent interactions. Substitution of Ala for Gly in the third position of the repeat results in a change in mechanical response from elastic to plastic [151]. Thus, the midblock of **B9** displays elastic-like behavior with spectroscopic features consistent with structural conformations of native elastin, including a highly mobile backbone, β-turns, and a loose helical β-spiral. The presence of glutamic acid in the midblock raises the inverse transition temperature, preventing coacervation of the midblock over a temperature range exceeding 75°C [152, 153]. Nonetheless, these protein polymers reversibly self-assemble from concentrated aqueous solution above the T_t of the hydrophobic endblocks (~18°C) to form a stable, water solvated, interlocking network. Two-dimensional Fourier transform infrared (FTIR) spectroscopy reveals that above the T_t, endblock secondary structure changes from helix to sheet with the assembly of physical crosslinks [84]. Due to the presence of Ala in the third position of the pentapeptide repeat, the hydrophobic endblocks form relatively rigid domains that display plastic-like behavior. Prior investigations from our group have confirmed robust viscoelastic and mechanical responses for this, as well as for other related elastin-mimetic triblock copolymers [1, 4-6].

In vivo studies have demonstrated excellent blood contacting properties in a primate arteriovenous shunt model when the triblock copolymer, **B9,** is coated as a thin film on the lumen of a small diameter vascular graft [7]. However, long-term biocompatibility and biostability for any of the members of this new class of physically crosslinked protein-based material has yet to be fully defined. Indeed, it is possible that amphiphilic protein hydrogels would display significant *in vivo* instability, given the

existence of naturally occurring amphiphiles in biological fluids, such as phospholipids, glycolipids, and lipoproteins [154]. Such amphiphiles could act as surfactants destabilizing the virtual crosslinks of protein-based material whose structural integrity is based on the association of hydrophobic domains [155, 156]. While structural instability may be acceptable for biodegradable systems, it has the potential to severely limit the longevity of biomaterials whose integrity is related to hydrophobic interactions. Many *non-covalently* crosslinked self-assembled systems, such as amphiphilic peptides, lipopeptides, or glycolipids that form thin films or fiber networks are useful for drug delivery where the half-life of the system is on the order of hours. In general, none of these approaches demonstrate stability beyond a few days [157-161].

We report herein that a virtually crosslinked elastin-mimetic triblock copolymer exhibits exceptional biocompatibility and long-term biostability over a period of at least seven months. In conducting these studies, we have employed magnetic resonance imaging (MRI) as a noninvasive tool to provide real-time structural information for both the implant and surrounding tissue, as well as insight into degradation behavior [162-164]. To our knowledge, this is the first evidence of a non-chemically or ionically crosslinked protein polymer system that exhibits long-term stability *in vivo*.

3.2 MATERIALS and METHODS

Synthesis and purification of the elastin-mimetic triblock copolymer B9.

The recombinant protein polymer **B9** was derived from concatemerization of elastin-mimetic peptide sequences, as previously described [2]. The structure consists of an ABA triblock where:

A block: $VPAVG[(IPAVG)_4(VPAVG)]_{16}IPAVG$

B block: $VPGVG[(VPGVG)_2VPGEG(VPGVG)_2]_{48}VPGVG$.

Individual colonies of **B9** in pET24-a in *E. coli* strain BL21 (DE3) were used to inoculate 30 mL of Circle Grow liquid media (Q-BIOgene) supplemented with the antibiotic kanamycin (50 µg/mL) and grown overnight at 37°C with shaking. A total of 5% vol/vol of the overnight culture was used to inoculate large expression flasks containing 500 mL Circle Grow media and antibiotic, followed by a 24 hour expression at 37°C with shaking.

Cells were harvested through centrifugation in sterile tubes at 1660 RCF for 20 minutes at 4°C. The supernatant was carefully decanted, cell pellets were resuspended in cold, sterile phosphate buffered saline (PBS) (20 mL per large culture flask pellet) and frozen at -80°C. Three freeze (-80°C) / thaw (25°C) cycles were employed for the initial cell fracture with equilibration back to cold temperatures following the cycles. Once cells were completely resuspended, six cycles of sonication, consisting of 20 second pulses with 20 seconds between each pulse in an ice bath, was employed to thoroughly break the cells. To recover any unbroken cells, a preparative centrifugation step was used at 1660 RCF for 10 minutes at 4°C. Unbroken cells, which pelleted out during the spin, were resuspended in cold, sterile PBS and re-sonicated, as described above.

The cold cell lysate was centrifuged at 20,000g for 40 minutes at 4°C. The supernatant was transferred to a cold, sterile tube and poly(ethyleneimine) (PEI) was added to a final concentration of 0.5%. This solution was centrifuged again at 20,000g for 40 minutes at 4°C to remove all nucleic acids and contaminating cellular material

precipitated by the PEI. The supernatant was transferred to new sterile 50 mL Falcon tubes and NaCl was added to a final concentration of 2M. The elastin-mimetic protein was salted out of solution at 25°C for 30-45 minutes. This solution was centrifuged at 9500g for 15 minutes at 25°C to recover the protein product ('hot-spin'). The supernatant was discarded and the protein pellet was resuspended in cold, sterile PBS on ice for up to 10-20 minutes to avoid solubilizing unwanted contaminates. The resuspended solution was then subjected to a 'cold spin' at 20,000g for 40 minutes at 4°C. The supernatant was transferred to sterile 50 mL tubes and salting precipitation repeated. The hot (25°C) / cold (4°C) spin cycles were repeated until a contaminating pellet was no longer observed after the cold spin. Typically, 6-10 cycles were required followed by a hot spin.

For *in vivo* studies, **B9** underwent a secondary treatment with sodium hydroxide The protein pellet was resuspended in cold, sterile PBS at approximately 50 mg per 20 mL. Sterile sodium hydroxide was added to a final concentration of 0.4N and mixed gently by hand. The mixture was incubated on ice for fifteen minutes, after which 5M sodium chloride was added to a final concentration of 2M. The protein was precipitated from solution at 25°C, centrifuged at 8500g for 20 minutes at 25°C, and resuspended in cold PBS. This treatment was repeated three times. Following the third treatment, the protein solution was adjusted to pH 6-8. A cold spin was performed at 20,000 rpm for 40 minutes at 4°C and the supernatant was desalted using a PD-10 desalting column (GE Healthcare Lifesciences) with molecular grade water (Cellgro). The end product was passed through 0.2 μm filter, eluted into autoclaved Lyoguard freeze drying trays (Gore), frozen at -80°C, and lyophilized. This procedure afforded **B9** as a white fibrous protein product with isolated yields of 50 mg/L of expression culture.

Lyophilized **B9** was resuspended in sterile molecular grade water at 1 mg/mL and endotoxin levels were assessed using the Limulus Amoebocyte Lysate (LAL) assay (Cambrex). Levels of endotoxin were typically 0.1 EU/mg (1 EU = 100 pg of endotoxin).

Structural characterization of the elastin-mimetic triblock copolymer B9.

Gel electrophoresis. Protein size and purity was assessed by sodium dodecyl sulfate-polyacrylamide gel electrophoresis (SDS-PAGE). A total of 10 μg of the elastin-mimetic polypeptide was run on a 7.5% gel along with Precision Plus Protein Kaleidoscope (Bio-Rad) molecular weight markers and negatively stained with Copper (Bio-Rad). MALDI-TOF mass spectrometry characterized a 165 kDa protein and the sequence was confirmed by amino acid compositional analysis [4].

*Rheological analysis of concentrated **B9** solutions.* Rheological data were acquired on an Advanced Rheological Expansion System III rheometer (ARES III, TA instrument, NJ) in parallel plate geometry with a plate diameter of 25 mm. The testing protocol for rheological analysis has been detailed elsewhere [1]. In brief, protein solutions were prepared at 100 mg/mL by adding distilled, deionized water to lyophilized protein at 4°C, shaking the solution for 48 h, and then allowing the solution to equilibrate for 72 h. The gap between parallel plates was adjusted between 0.2 - 0.35 mm and dynamic mechanical experiments were performed in shear deformation mode. The gelation temperature was determined by heating samples from 4°C to 37°C at a rate of 1°C per minute. Experiments were repeated on three samples and representative data presented.

In vivo biocompatibility of the elastin-mimetic triblock copolymer B9.

Subcutaneous injection. According to a protocol approved by Emory University Institutional Animal Care and Use Committee (IACUC), **B9** protein solutions were injected into the subcutaneous space of 8 week old inbred male C57BL/6 mice weighing

25–30 g obtained from Jackson Laboratory (Bar Harbor, ME). Mice were sedated using ketamine (95 mg/kg, IM) and xylazine (5 mg/kg, IM). A total of 200 µL of 100 mg/mL solution of endotoxin free **B9** was injected into the interstitial fascia where it immediately gelled. A set of three mice each received a single injection. All injections were conducted in the cold room using chilled syringes, needles, and solutions. Mice were immediately warmed following the injection. Three weeks post implantation, mice were sacrificed and the hydrogel explanted along with overlying skin.

Peritoneal injection. According to a protocol approved by Emory University Institutional Animal Care and Use Committee (IACUC), **B9** protein solutions were injected into the peritoneal cavity of 8 week old inbred male C57BL/6 mice weighing 25–30 g obtained from Jackson Laboratory (Bar Harbor, ME). Mice were sedated using ketamine (95 mg/kg, IM) and xylazine (5 mg/kg, IM) prior to protein injections. A total of 200 µL of 100mg/mL solution of endotoxin free **B9** was injected into the peritoneal cavity where it immediately gelled. A set of five mice each received a single injection. All injections were conducted in the cold room using chilled syringes, needles, and solutions. Mice were immediately warmed following the injection. One week post implantation, mice were sacrificed, and free cells in the peritoneal cavity were harvested by saline lavage, as detailed below, for FACS analysis prior harvesting the hydrogel for histological assessment.

Histological examination. Retrieved hydrogel samples were processed for histological and immunohistochemical evaluation to facilitate identification of cell types present. All samples were fixed overnight in 10% neutral buffered formalin and processed for parafin embedding. Sections were prepared at a thickness of 5 µm and stained with hematoxylin and eosin (H&E) or rat anti-mouse monoclonal F4/80 (CI:A3-1, Abcam) for infiltrating macrophages. In all cases, multiple sections for each of three to five samples were examined.

Fluorescent-activated cell sorting (FACS) of peritoneal lavage. Prior to harvesting implants, each peritoneal cavity was initially lavaged with 10 mL of cold Hank's Balanced Salt Solution containing 10 U/mL heparin and 1% BSA (Mediatech, Inc). Typically, 6 to 7 mL of lavage solution was retrieved and cells immunostained for flow cytometry with PE-conjugated rat monoclonal anti-mouse CD11b for macrophage, FITC-conjugated hamster anti-mouse CD3 for total T cells, FITC-conjugated rat monoclonal anti-mouse CD4 for helper T cells, FITC-conjugated rat monoclonal anti-mouse CD8 for cytotoxic T cells, FITC-conjugated rat monoclonal anti-mouse CD19 for B cells, and FITC-conjugated rat monoclonal anti-mouse Gr-1 for neutrophils (BD Biosciences Pharmingen). Antibodies were diluted in staining buffer (PBS pH 7.4 containing 1% BSA and 0.1% sodium azide) to 1 μg/50 μL/10^6 cells, incubated with cells for 30 minutes in the dark on ice, washed three times in staining buffer, and fixed in 1% paraformaldehyde. Analysis was performed on a FACScan using Cellquest (Becton Dickinson) and FlowJo software (Tree Star) [112]. Comparison between groups was analyzed via a Student's t-test and $p < 0.05$ were considered to be significant. Results are presented as mean ± SEM. The control group employed did not undergo surgery. At least five mice were enrolled in each experimental and control group.

Non-invasive assessment of protein polymer implants in vivo. *Fabrication of cylindrical protein polymer implants.* A cold solution of **B9 at** 100 mg/mL was drawn into a chilled 1 mL syringe (Becton Dickenson), equilibrated at 4°C for 30 minutes, and subsequently geled at 37°C. The tip of the syringe was removed with a sterile scalpel and the molded protein gel extruded into room temperature PBS, equilibrated overnight under a bio-hood, and then sectioned into 8 x 4.76 mm cylindrical test samples **(Figure 3-1)**.

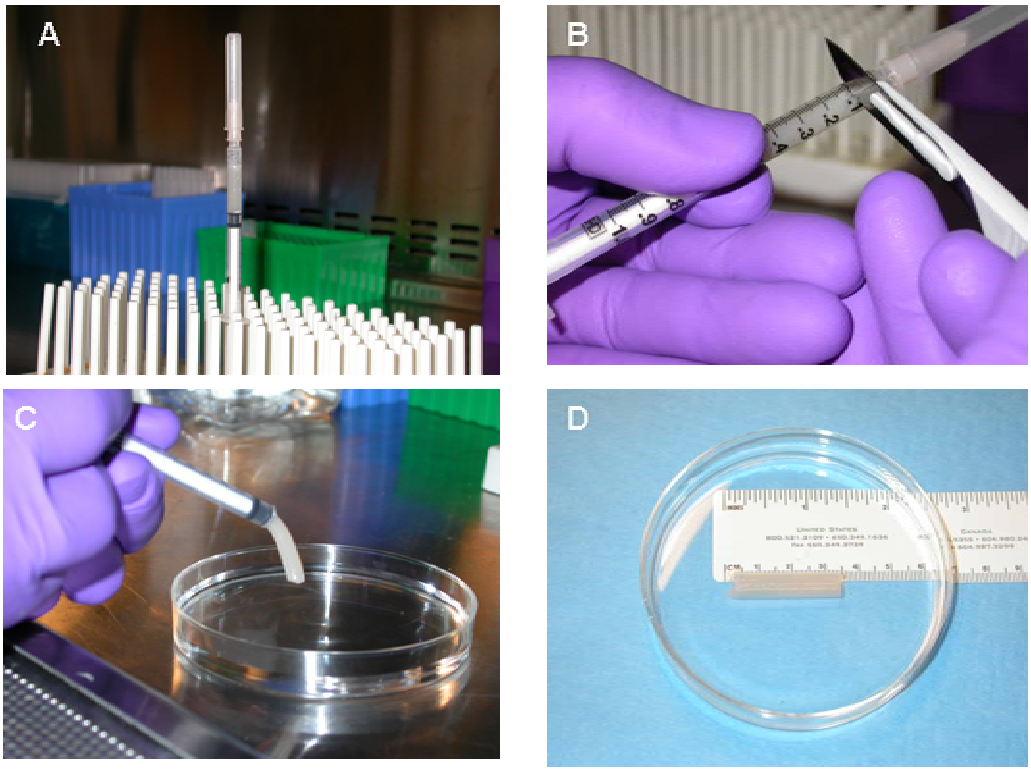

Figure 3-1. Syringe casting method for **B9** hydrogel implants. **(A)** 10wt% **B9** solution was drawn into syringe and allowed to gel at room temperature. **(B)** End of syringe was removed. **(C) B9** hydrogel was ejected from syringe into room temperature PBS. **(D)** Ejected sample equilibrated in PBS. This sample was sectioned into 8mm implants.

In vivo biostability. All animal experiments were approved by the Institutional Animal Care and Use Committee (IACUC) at Emory University. Eight-week-old inbred male C57BL/6 mice weighing 25–30 g were obtained from Jackson Laboratory (Bar Harbor, ME). Under ketamine (95 mg/kg, IM) and xylazine (5 mg/kg, IM) anesthesia, a 1 cm dorsal midline incision was performed and bilateral cylindrical gels implanted in the subcutaneous space, parallel to the spine. Eight mice were enrolled and serial MR imaging performed weekly for 6 weeks and every other week thereafter. During scanning, 2.5% isoflurane inhalation was utilized for induction followed by 1.8% isoflurane throughout the duration of imaging. Total scan time for each animal was less than one hour. At the termination of the study, all mice were sacrificed and samples with surrounding tissue harvested for immunohistochemical analysis.

^{1}H Magnetic Resonance Imaging. MR imaging was performed using a Varian/Inova 4.7T horizontal bore magnet operating at 200.56 MHz (Varian, Inc). The magnet was equipped with an 11.7 cm inner diameter shelf-shielded gradient system with a maximum gradient strength of 25 gauss/cm. Constructs implanted in mice were investigated using transmit/receive 16-element quadrature birdcage coil with an inner diameter of 3.8 cm. Each anesthetized mouse was secured in a home-built cradle and the implant centered within the magnetic field.

Exact positioning of the construct was determined using several fast-spin echo scout scans. A final high resolution fast-spin echo image (relaxation time, T_R = 2.0 sec, echo spacing, esp = 14 μs at number of averages, nt = 2) was collected to provide a more detailed image of the construct structure and surrounding microenvironment. A fast-spin echo sequence with an echo train length (ETL) of 8 was utilized, which afforded a field of view of 3.5 x 3.5 cm with a slice thickness of 0.5 mm **(Figure 3-2)**.

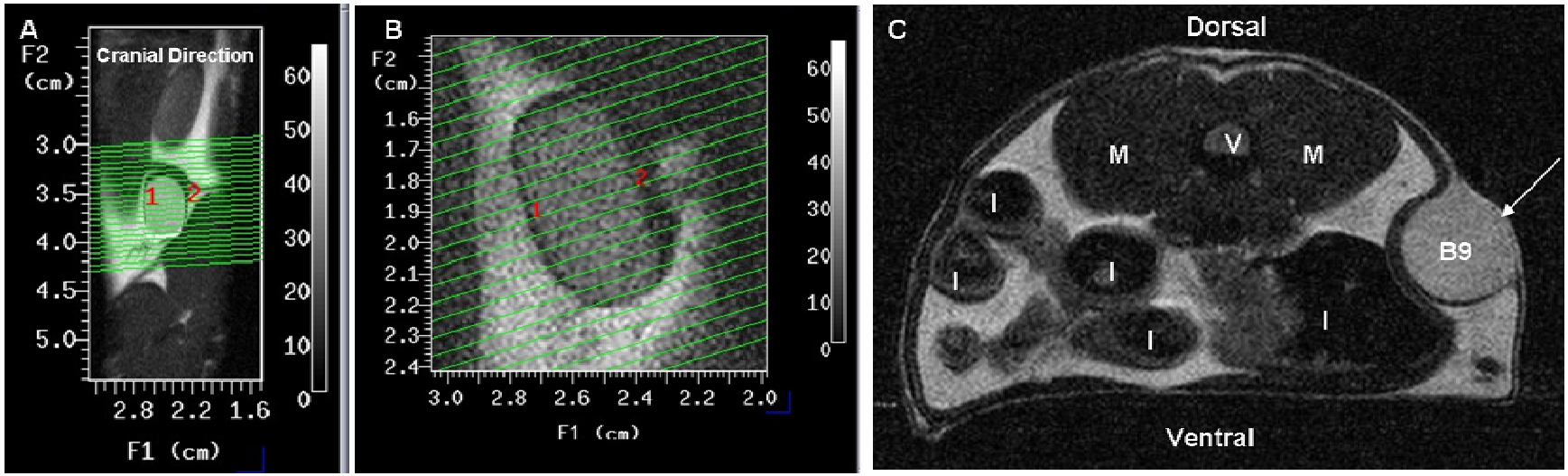

Figure 3-2. A. A coronal view through the C57BL/6 mouse showing the location of the implant. Image is oriented with the mouse vertical. The green lines shown are the planing of the 23 transverse-oblique slices through the implant. **B.** MR scan slices through implant. **C.** Transverse MR image of the subcutaneous **B9** implant. The light region on the outer surface is a cross section of the **B9** implant. Implant areas were assessed from individual images and summed to assess volume of the implant. Slice thickness of the scan is 500 µm. (V = verterbra, M = Psoas Major muscle, I = Intestine cross-sections, **B9** = cross-section of **B9** implant).

Characteristically, transverse images of each implant consisted of 23 slices at a thickness of 500 μm. The acquired data contained 256 x 256 points and was zero filled to 512 points in both the read and phase encoded directions. A 2-D Fourier transformation was performed, which provided a final in-plane resolution of 68 x 68 μm with a slice thickness of 500 μm **(Figure 3-3)**. Cross-sectiomal area and length measurements were made using the image processing program, Image J (NIH).

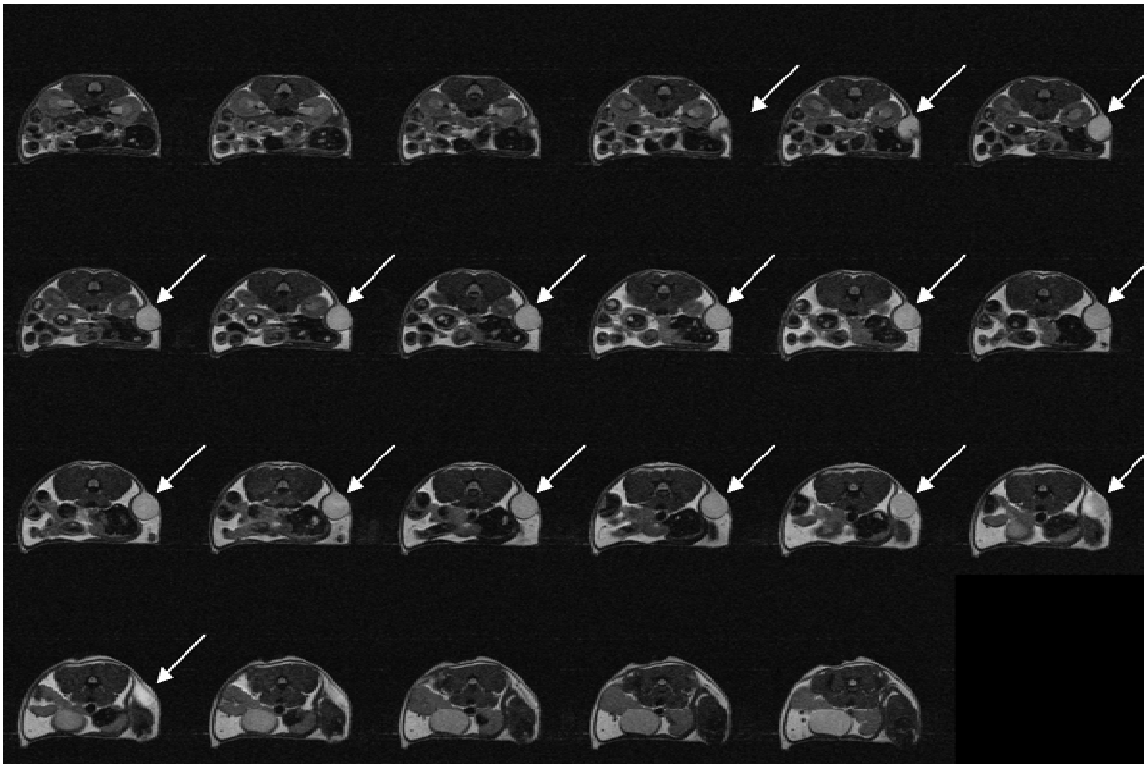

Figure 3-3. Transverse MR images of the subcutaneous **B9** implant. The light region on the outer surface is the cross section of **B9** implant. Slice thickness is 500 μm.

3.3 RESULTS

Characterization of B9. Gel electrophoresis of **B9** revealed a single band at 170 kDa consistent with prior studies from our laboratory **(Figure 3-4A)** [1, 4, 7]. Likewise, rheological behavior of aqueous solutions of **B9** was unchanged after NaOH treatment with an observed sol-gel transition at 18°C. The gel point of protein solutions can be detected by measurement of the shear storage (G') and loss (G") modulus as a function of temperature at a fixed frequency. Above 18°C, G' and G" increased while tan δ (G'/G") decreased, consistent with the formation of a viscoelastic gel **(Figure 3-4B)**.

Biocompatibility of injectable protein polymer gels. To assess *in vivo* responses to **B9** hydrogels, protein solutions were injected into either the subcutaneous space **(Figure 5)** or the peritoneal cavity in a mouse model. Peritoneal samples were retrieved one week after implantation and subcutaneous samples explanted at three weeks. Retrieved hydrogel samples were irregularly shaped, but optically transparent. Hematoxylin and eosin staining demonstrates the presence of a mild foreign body reaction for **B9** implants by the formation of a very thin fibrous capsule surrounding the implant. Observed capsule thickness was 35.75 ± 6.14 μm for subcutaneous specimens and 16.42 ± 2.85 μm for peritoneal samples without evident cellular infiltration into implants in either subcutaneous and peritoneal locations. Scattered macrophages were noted along the periphery of the fibrous capsule consistent with a mild foreign body response **(Figure 3-6 and 3-7)**. The magnitude and type of peritoneal cell response harvested, as determined by an analysis of saline lavage, did not reveal significant differences between those mice receiving **B9** and control non-treated mice **(Figure 3-8).**

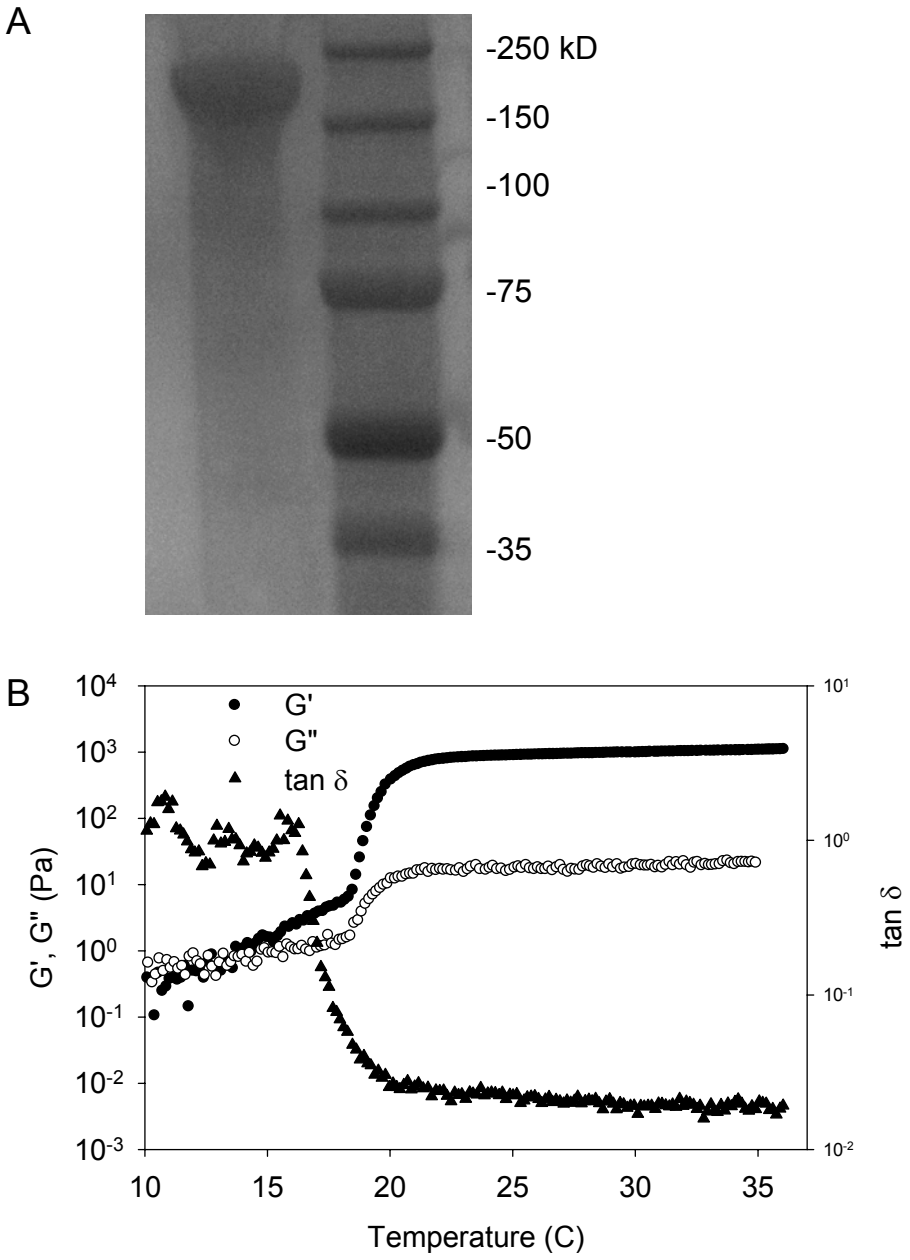

Figure 3-4. Structural Characterization of the B9 protein. A. Sodium dodecyl sulfate-polyacrylamide gel electrophoresis (SDS-PAGE) analysis revealed a single protein band at 170 KDa corresponding to **B9**. 10ug of the elastin-mimetic polypeptide was run on 7.5% gel and negatively stained with Copper stain (Bio-Rad). Molecular weight markers were Precision Plus Protein Kaleidoscope (Bio-Rad). **B.** Rheological behavior of 10 weight percent **B9** in water. Dynamic shear storage (G′) and loss modulus (G″) are plotted as a function of temperature (γ 2%, ω 1Hz). The gelation temperature was determined by heating samples from 4°C to 37°C at a rate of 1°C per minute. Experiments were repeated on 3 samples and representative data presented.

Figure 3-5. Subcutaneous injection mouse model. 200 uL of a 10 weight percent solution of **B9** was injected subcutaneously, which gelled instantly. A group of samples were retrieved three weeks for histology.

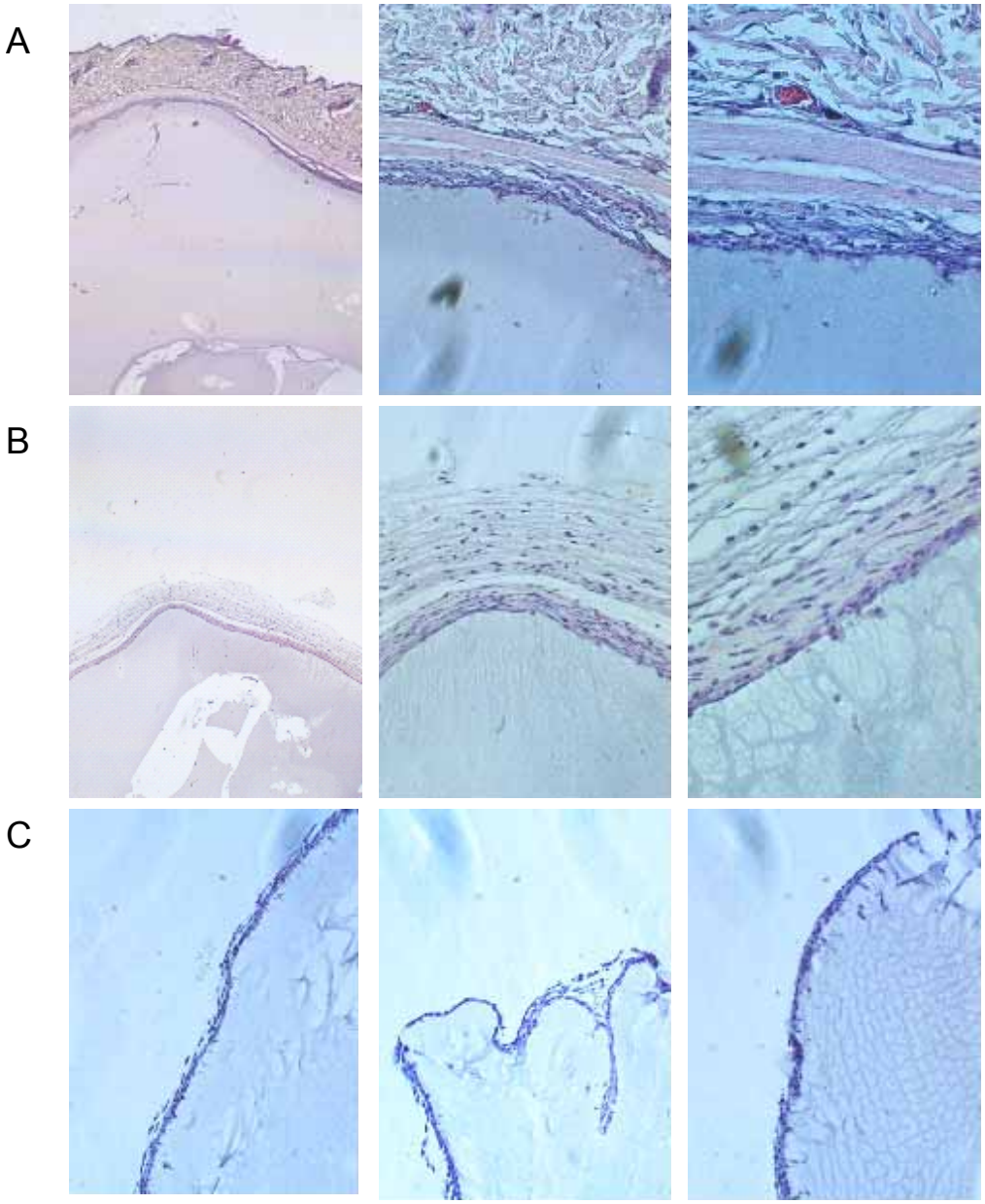

Figure 3-6. H&E staining of formalin fixed, paraffin embedded **B9** implants demonstrates the presence of a mild foreign body reaction along the periphery of the sample. Histological analysis of subcutaneous **B9** implants retrieved 3 weeks post-implant, skin side **(A)** and muscle side **(B)**. Histological analysis of peritoneal **B9** implants retrieved 1 week post-implant **(C)**. All images were obtained at 20X magnification and are oriented such that the **B9** hydrogel is located in the bottom right corner.

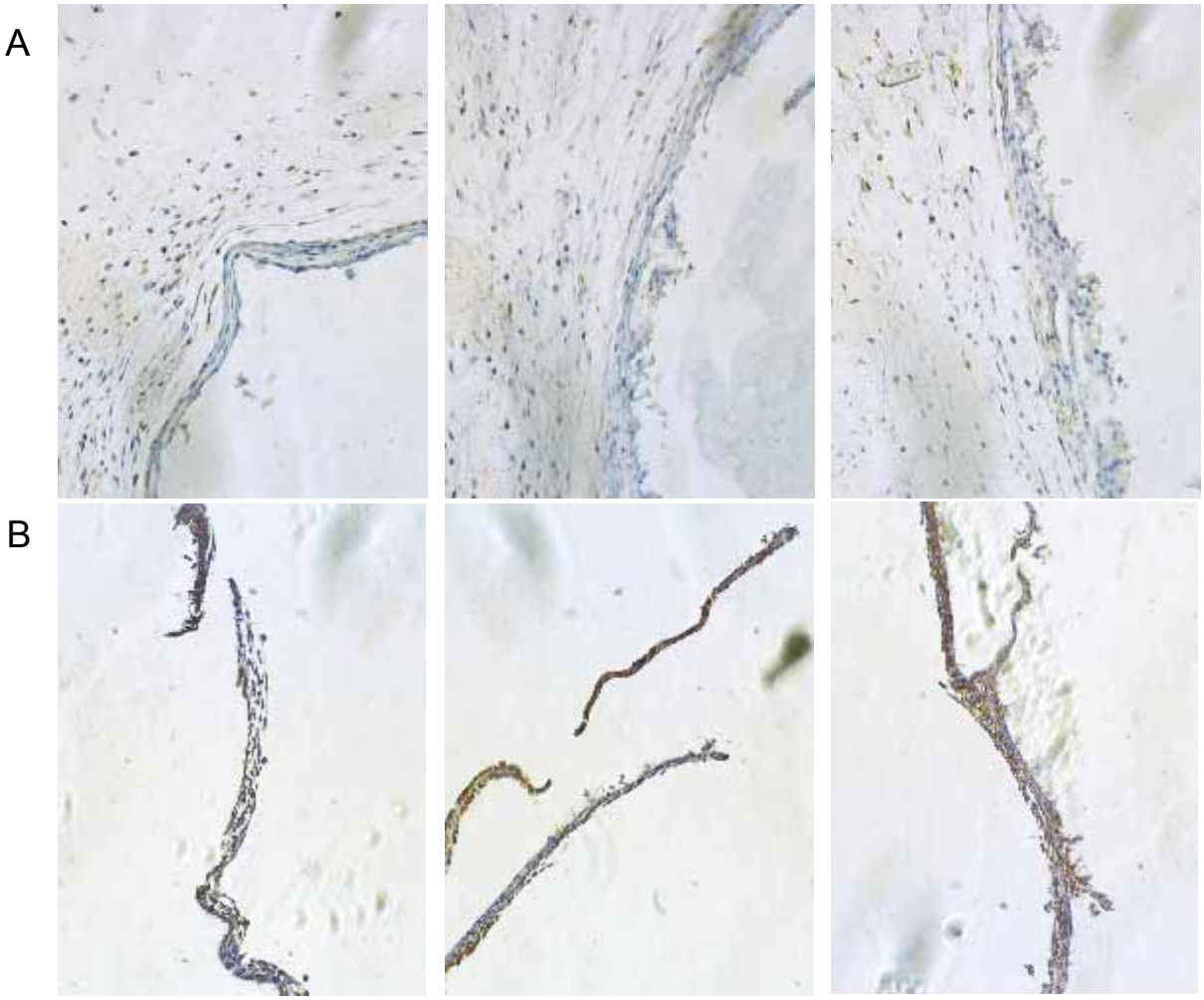

Figure 3-7. F4/80 staining of formalin fixed, paraffin embedded **B9** implants demonstrate the presence of macrophages along the periphery of the fibrous capsule but no infiltration into the **B9** implant. Histological analysis of subcutaneous **B9** implants retrieved 3 weeks post-implant **(A)** and peritoneal **B9** implants retrieved 1 week post-implant **(B)**. All images were obtained at 20X magnification and are oriented such that the **B9** hydrogel is located in the bottom right corner.

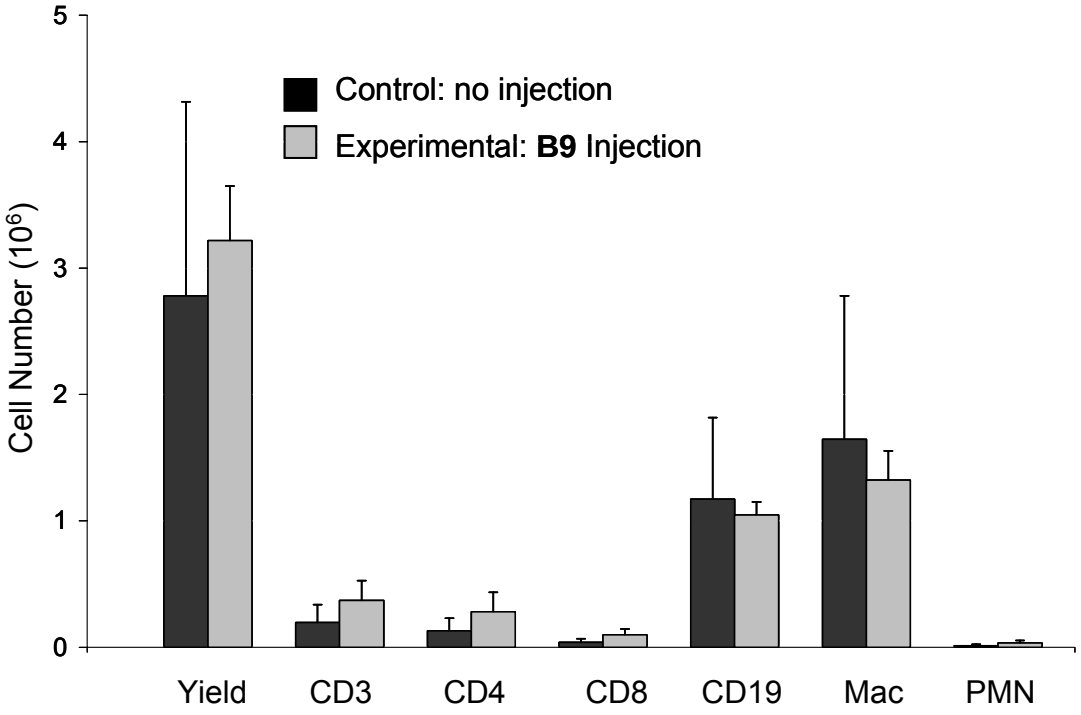

Figure 3-8. FACS analysis of peritoneal implanted **B9** 1 week post-implant (n=5). Experimental group showed no statistical difference in cell number from control group, $p < 0.05$. Cells were immunostained for flow cytometry with FITC-conjugated hamster anti-mouse CD3 for total T cells, FITC-conjugated rat monoclonal anti-mouse CD4 for helper T cells, FITC-conjugated rat monoclonal anti-mouse CD8 for cytotoxic T cells, FITC-conjugated rat monoclonal anti-mouse CD19 for B cells, PE-conjugated rat monoclonal anti-mouse CD11b for macrophage, and FITC-conjugated rat monoclonal anti-mouse Gr-1 for neutrophils (BD Biosciences Pharmingen).

Noninvasive in vivo monitoring of implanted protein gels. MR imaging provides a useful means for *in situ* characterization of implanted biomaterials. Adequate contrast was achieved between the implant and surrounding tissue, which reflected the high water content of the protein gel **(Figure 3-2 and 3-3)**. Implant cross sectional areas and lengths were assessed through analysis image analysis over 7 months and data is currently being compiled **(Figure 3-9)**. No evidence of calcification was observed.

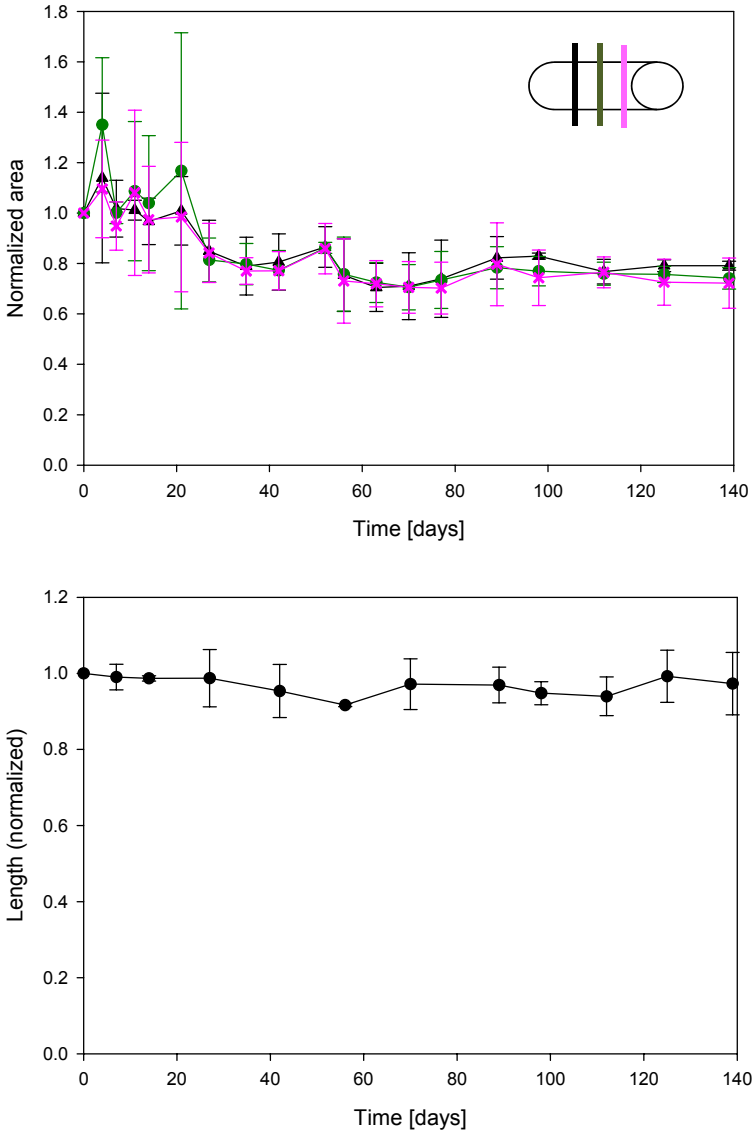

Figure 3-9. Biostability of B9 implants assessed by MRI. Implant cross-sectional areas and lenths were obtained through image analysis over 7 months and data is currently being compiled. Four month biostability data is presented in this figure.

3.4 DISCUSSION

Molecular self-assembly is ubiquitous in nature and has recently been exploited for biomaterial design. Self-assembly is mediated by a number of weak, noncovalent bonds, including hydrogen bonding, as well as electrostatic, hydrophobic, and van der Waals interactions ultimately forming higher order structures. One such example of natural molecular self-assembly is tropoelastin which coacervates to align tropoelastin molecules in preparation for intermolecular crosslinking [63-65]. At ambient temperatures, tropoelastin is soluble in aqueous solutions, however, as the temperature is raised, molecular aggregation occurs through hydrophobic interactions. Coacervation is a lower critical solution temperature (LCST) phenomenon in which the protein forms a more ordered system upon increasing temperature. The same phenomena has been observed with recombinant elastin proteins where precise control over the temperature at which coacervation occurs has been correlated with amino acid sequence [66, 67] and exploited for tunable control over the assembly process.

Tissue-material responses, including the rate and extent of biodegradation, are integral to assessing the suitability of elastin-like biopolymers for implant related applications. To date, reports documenting *in vivo* responses to elastin-mimetic protein implants have been limited; largely confined to several studies performed 15 to 20 years ago on proteins synthesized chemically and subject to radiation crosslinking [82, 121] In these investigations, homopolymers or copolymers composed of VPGVG, VPGKG, VPGEG, IPAVG, and VPAVG reportedly did not induce significant inflammatory or allergic reactions [82, 121-123]. The most thoroughly characterized variant, chemically synthesized poly(GVGVP), underwent *in vitro* toxicity and mutagenicity assays and was administered via intravenous, intraocular, intramuscular, intraperitoneal, and subcutaneous routes without toxic effect [82, 121]. A fibrous capsule was noted three weeks after intramuscular implantation of a radiation crosslinked sample [82]. In a more

recent report, elastin microparticles prepared from chemically synthesized poly(VPAVG) were evaluated following subcutaneous and intravitreal injections. No inflammatory response observed after 28 days. However, tractional retinal detachment noted [122]. The failure to detect an immune mediated reaction to these polymers is consistent with other studies that have sought to identify potentially immunogenic epitopes on native elastin. While polyclonal and monoclonal antibodies can be raised against peptides derived from the hydrolysis of native elastin, neither VPGVG nor VPAVG peptides were among the recognized sequences [124]. Moreover, VPGVG peptides were unable to competitively inhibit the binding of any of the antibodies raised against native elastin, which further supports the notion that this pentapeptide is not present among antigenic elastin epitopes [124].

Recently, genetically engineered elastin-mimetic protein polymers have been investigated *in vivo* as non-thrombogenic coatings [7, 125], targeted drug delivery vehicles [126-128], and as an implantable material [129]. In the latter instance, after a 13 week implant period in the subcutaneous space, recombinant human tropoelastin 'sponges', chemically crosslinked with with bis(sulfosuccinimidyl) suberate were surrounded by a fibrous capsule with a minimal to moderate inflammatory response [129]. Non-chemically crosslinked recombinant elastin-like proteins have also been administered within the intra-articular space as a 650 μM protein solution. Although the biological response was not evaluated, this study revealed a three hour half-life for non-aggregating VPGVG proteins and a three day half-life for aggregating VPG**X**G proteins, where **X** = V:G:A at a ratio of 1:7:8 [128]. As a related material, a 47 kDa recombinant silk-elastin-like protein (SELP), comprised of GAGAS silk-like [S] and GVGVP elastin-like [E] amino acid sequences ($[S]_4[E]_4[EK][E]_3$) has been studied after injection into the subcutaneous space. Histological analysis revealed minimal fibrous encapsulation after four weeks with a mild degree of inflammation that included the presence of

macrophages in the surrounding tissue [130]. SELPs have also been used for adenoviral gene delivery and demonstrate prolonged and localized expression of adenoviruses for up to 15 days, suggesting the potential for cancer gene therapy [131, 132]. A summary of *in vivo* biocompatibility studies conducted on elastin- mimetic proteins is presented in **Table 3-1**.

The evaluation of *in vivo* biocompatibility has largely been based on characterizing local tissue responses to subcutaneously implanted materials where the intensity and duration of the inflammation and wound healing, including capsule formation, is evaluated histologically [133, 134]. Although histological studies of biopolymers containing elastin-mimetic sequences have previously noted the presence of 'mild inflammation' [121, 122] and 'a reaction that was limited to a typical cell mediated response to the presence of a foreign body' [129], the extent of fibrous capsule thickness has not been reported. Fibrous capsule thickness has been investigated for a variety of polymeric and ceramic implants designed for tissue repair, cell encapsulation, or as drug delivery systems [135-138, 165]. Capsule thicknesses are dependent on implant site and material type and typically varies between 2 and 150 μm over implantation periods of one to three months. For example, greater capsule thickness has been observed for materials within intraperitoneal sites compared to those in subcutaneous sites over identical implant durations [136]. Ceramic materials, aluminum calcium phosphate, hydroxyapatite, and tricalcium phosphate, appeared to invoke the mildest inflammatory response with the thinnest fibrous capsule, approximately 2.5 μm and 6 μm, after 90 day implant periods in the subcutanteous and peritoneal cavities, respectively [136]. As an illustration of the effects of surface chemistry, implants comprised of poly(alkyl methacrylate) (PAMA) with short alkyl side chains exhibited a thicker fibrous capsule than those with long side chains (140 μm vs 120 μm) [135]. Additionally, self-assembled monolayers of alkanethiols on gold with different terminal

functional groups displayed surface dependent inflammatory responses after one week in subcutaneous tissue. Hydrophobic methyl terminated surfaces induced thick fibrous capsules (130 μm) and greater recruitment of inflammatory cells, as compared to hydrophilic COOH- (80 μm) and OH- (70 μm) terminated surfaces [139]. Likewise, polypropylene implants whose surfaces were modified with –OH groups triggered formation of a thicker capsule (~100 μm) that when modified with –COOH moeities (37 μm) [140]. In contrast, surface topography does not appear to have a significant effect on capsule thickness, although it may influence local inflammatory responses [141]. Relatively inert synthetic polymers, such as, silicone, and organic biopolymers, such as cellulose also elicit a foreign body reaction after subcutaneous implantation with an observed fibrous capsule thickness of approximately 90 μm and 80 μm, respectively, at four weeks. [165]. In this report, FACS analysis of peritoneal lavage fluid harvested one week after injection of **B9** demonstrated no apparent difference in either the number or type of inflammatory cells when compared to those mice not exposed to the polymer gel **(Figure 3-8)**. Significantly, as a subcutaneous implant, **B9** protein polymer gels initiated only a limited local inflammatory response. Remarkably, the resultant fibrous capsule is among the thinnest observed to date for non-ceramic implants in comparable implant sites and over similar periods of implantation. This effect may be related to the presence of glutamic acid residues in the hydrophilic midblock that segregate to the surface with an enriched concentration of –COOH groups at material-tissue interface.

Table 3-1. Biocompatibility evaluation of elastin-mimetic polypeptides

Recombinant Elastin-Mimetic	Assay	Reported Results	Testing Comments
Chemically synthesized Poly (VPGVG)	Ames mutagenicity test	Non-mutagenic	Test samples were determined as innocuous as negative controls [121]
Chemically synthesized Poly (VPGVG)	Cytotoxicity-agarose overlay	Non-toxic	No evidence of fibroblast cell death or lysis following incubation for 24 hours [121]
Chemically synthesized Poly (VPGVG)	Acute systemic toxicity	Non-toxic	No difference in IV injections of 24 hour extracts of gamma irradiated sheets of poly(VPGVG) and control extracts [121]
Chemically synthesized Poly (VPGVG)	Intracutaneous toxicity	Non-toxic	No erythema or edema was observed at injection site after 24, 48, and 72 hours [121]
Chemically synthesized Poly (VPGVG)	Muscle implantation	Favorable at 7 days	Needle injection of film fragments, material was a ‘slight irritant’ as compared to the negative control [121]
Chemically synthesized Poly (VPGVG)	Acute intraperitoneal toxicity	Non-toxic at 4 weeks	Recovered implants were reported as ‘very similar to pre-implant condition’ [121]
Chemically synthesized Poly (VPGVG)	Systemic antigenicity study	Non-antigenic	No anaphylactic signs from IP injections three times a week, every other day, for 14 and 21 days [121]
Chemically synthesized Poly (VPGVG)	Dermal sensitation	Non-sensitizing at 7 days	Intradermal injections were challenged with solutions to provoke a mild acute inflammation at injection site, but ‘showed no significant evidence of causing dermal sensitization [121]
Chemically synthesized Poly (VPGVG)	Pyrogenicity	Non-pyrogenic	IV injection into rabbit ear vein and temperature of the animals were monitored [121]

Recombinant Elastin-Mimetic	Assay	Reported Results	Testing Comments
Chemically synthesized Poly (VPGVG)	Lee White Clotting Study	Normal clotting time	Used canine blood, all clotting times were within normal ranges for dog [121]
Chemically synthesized Poly (VPGVG)	*In vitro* hemolysis test	Non-hemolytic	0% hemolysis reported for rabbit blood determined spectrophotometrically [121]
Chemically synthesized Poly (VPGVG)	Bone implantation	No calcification or ossification	Fibrous granulation tissue, no calcification or ossification at 3 weeks [82]
Chemically synthesized Poly (VPGVG)	IM implantation	No calcification or ossification	Fibrous tissue capsule with a medium range of active phagocytic cell infiltration at muscle site with no evidence of calcification or ossification, reported as ‘passive tissue reaction similar to those found for biodegradable suture materials at three weeks [82]
Microbially expressed triblock	Baboon arteriovenous shunt model	Non-thrombogenic	Minimal fibrin and platelet deposition over a 1 hour time period of elastin-mimetic impregnated PTFE graft [7]
Chemically synthesized Poly (VPAVG)	Subcutaneous injection	Non-inflammatory	Oedema was measured after microparticle injection at 24 hours in a hind paw injection model [122]
Chemically synthesized Poly (VPAVG)	Intraocular injection	Non-inflammatory	28 days post-injection displayed minimal signs of inflammation, though tractional retinal detachment was observed with fibroblastic activity [122]
Microbially expressed poly VPGVG (aggregating) and VPGAG (non-aggregating)	Intra-articular injection	Biodegradable	Protein remained in joint for 2 (non-aggregated protein) to 30 days (aggregated protein) [128]
Microbially expressed human tropoelastin	Subcutaneous implant	Well tolerated	Uniform encapsulation with minimal to moderate inflammation at 13 weeks [129]

Elastin-mimetic proteins such as **B9** and other multiblock systems afford the ability to form physical or virtual crosslinked networks through the self-association of chemically similar domains. In the case of elastin-mimetic proteins [1-5, 84], repeat peptide sequences of self-associating blocks are chosen, such that coacervation or phase separation of these domains occurs in water under physiologically relevant conditions (pH 7.4, 37°C), which maximizes hydrophobic interactions that drive self-assembly. In turn, the sequence of the non-crosslinking domain is selected in a manner that precludes coacervation. This typically has required the incorporation of hydrophilic residues in the fourth position of the pentapeptide repeat sequence (Val-Pro-Gly-Xaa-Gly), such as glutamic acid, which limits the tendency for block aggregation. Physically crosslinked protein-based materials possess a number of advantages over their chemically crosslinked counterparts, including ease of processability, the ability to avoid the addition or removal of reagents or unreacted intermediates needed for chemical crosslinking, and the capacity to incorporate biologically or chemically active agents or cells that might otherwise be sensitive to covalent crosslinking schemes. Moreover, if blocks are of sufficient size and chemical diversity the potential to access diverse polymer morphologies exists. This provides the capacity to tune a wide range of functional responses, such as mechanical behavior, permeability or drug elution characteristics, as well as the potential to design templated materials [74, 86, 91].

Most biomaterials whose integrity is based on self-association of hydrophobic constituents display short-lived stability *in vivo* and have been utilized for drug delivery or wound healing applications. The instability of these systems can be attributed to natural surfactants, other amphiphilic molecules, or enzymes that promote lysis and solubulize specific lipids and proteins. **Table 3-2** summarizes the *in vitro* and *in vivo* stability of a number of physically crosslinked amphiphilic systems. Phospholipids, lipopeptides, and glycolipids have been extensively employed as drug carriers when formulated as

vesicles, liposomes, or micelles, all of which have relatively short half-lives even when directly injected within tissues [166]. Similarly, amphiphilic graft copolymers, such as alkylated carrageenan [167], poly(2-hydroxyethyl methacrylate)-g-oligolactide, or poly(ethylene glycol)-g-poly(DL-lactic acid-*co*-glycolic acid) all degrade rapidly [168, 169]. Recently, amphiphilic peptides that self-assemble as fibrous networks have been described as vehicles for cell and drug delivery [160, 170]. These systems display relatively rapid dissociative responses, as well. In contrast, structures that self-associate through electrostatic interactions, including calcium or barium crosslinked alginate gels or alginate-polylysine thin films [171, 172], generally exhibit greater biostability.

A number of materials that self-assembly also require additional crosslinking for biomedical applications. Collagen has been used as a scaffold for tendon, cartilage, and bone regeneration [173-175], as well as for drug delivery [176] and skin substitutes [177]. However, most collagen systems are crosslinked by a variety of chemical [178-181] or physical [182, 183] means. In fact, non-crosslinked collagen displays a limited lifetime *in vivo*, with significant degradation observed within three to four weeks [129, 184]. Natural silk is also degradable, but over longer durations with a >50% loss of strength at 6-12 weeks [185-187]. Likewise, recombinant tropoelastin has been fabricated into a chemically crosslinked ‘sponge’. Degradation was evident 13 weeks after implantation when formulated with an open porous surface enabling cells to penetrate the implant, but limited when produced with a smooth surface [129]. Similarly, crosslinking and chemical modification has been employed to reduce degradation rates of hyaluronic acid hydrogels [188].

Significantly, this study demonstrates the long-term durability of a self-assembled elastin-mimetic protein polymer hydrogel, even in the absence of covalent crosslinks. MRI has been previously used to monitor biomaterial degradation and swelling behavior of a number of polymeric materials [162-164, 189-191], including hydrogels [189-194].

To our knowledge, these *in vivo* studies are the first to demonstrate that self-assembled protein-based materials of any form can be designed with structural stability approaching that displayed by many electrostatically or covalently crosslinked biopolymers.

Table 3-2. Biostability in physically crosslinked systems

	Application	Biostability
Crosslinked by hydrophobic interactions		
Hydrophobized polysaccharides, (eg, Dextran and Pullan)	Drug delivery	Dextran-4 hours-7 days [195, 196] Pullan-*in vitro*, 1 week [197]
Leucine zipper motifs	N/A	*In vitro* chemical denaturation studies indicated incorporation of fluorinated amino acids improved stability [198]
Silk Elastin-Like Proteins	Drug delivery	Stability controlled by the length of silk block, fewer silk blocks resorbed by 1 week, more repeats (8 blocks) demonstrated no evidence of resorption at 7 weeks [199] Hydrogels investigated for drug release stable for >30 days [130]
Natural Silk	Sutures	6-12 weeks, with a >50% loss of strength [185, 186]
Crosslinked by ionic interactions		
Alginate crosslinked with calcium ions	Drug delivery and encapsulation	2-12 weeks [172]
Chitosan crosslinked with glycerol-phosphate disodium salt and heat	Drug delivery	Days-weeks dependent upon deacylation, with longer residence times observed with higher degree of deacylation [200]
Carrageenan crosslinked with potassium ion or metallic ions	Drug delivery	1-2 days [167]
Alginate-PLL multilayers	Coatings for implantable devices	Stable as a film at 4 weeks with no observed cellular adhesion or defects [171]
Crosslinked by crystallization		
PVA homopolymer	Drug delivery	stable at 37C *in vitro* for 6 months [201]
poly (HEMA-g-(L)oligolactate) and poly (HEMA-g-(D)oligolactate)	Drug delivery	Stable for <70 days *in vitro* [168]
PEG-PL(G)A-PEG triblock copolymers	Drug delivery	Partial degradation observed (PLGA backbone and PEG grafts) and complete degradation (PEG backbone with PLGA grafts) after 7 days [169]

3.5 CONCLUSIONS

Elastin-based protein polymers are a promising class of material characterized by high degree of biocompatibility and a tunable range of mechanical properties from plastic to elastic. A variety of options facilitate the processing of these biopolymers into gels, films, or nanofibers for any of a number of implant applications in orthopedics, as well as in plastics, cardiovascular, and general surgery. Additionally, the potential exists for incorporating bioactive compounds onto the polymer backbone or within the protein matrix. Likewise, such materials provide a prospective vehicle for cell delivery. In this report we have characterized local tissue response and long-term *in vivo* biostability of a physically crosslinked recombinant elastin-mimetic copolymer. We predict elastin-mimetic triblock copolymers will find utility as structural components of artificial organs and engineered living tissues, as carriers for controlled drug release, or as biocompatible surface coatings.

CHAPTER 4

Recombinant Elastin Protein Expression in *Pichia pastoris*

4.1 INTRODUCTION

Over the past decade a number of reports have described the design of synthetic genes, which encode elastin-like proteins (ELP) for bacterial expression in *Escherichia coli*. Although advantages exist, significant limitations associated with E. coli expression systems have been noted. The lack of eukaryotic post-translational systems, the insolubility of over-expressed mammalian proteins by sequestering into inclusion bodies, difficult purification from a pool of cytoplasmic proteins and cellular contaminants, and endotoxin contamination have encouraged the use of other expression systems including yeast, plant, insect, and mammalian cells. Endotoxin has been a specific concern for ELP expression as it becomes associated with the protein product upon cell lysis. Endotoxin, an amphiphillic lipopolysaccharide, is a toxic constituent found in the outer cell wall of gram-negative bacteria and known to induce pyrogenic pathologies [202]. A number of approaches have been utilized to reduce endotoxin contamination including sodium hydroxide digestion [203, 204], centrifugal ultrafiltration, phase separations with detergents [205-208] or solvents [209], neutralizing agents [210], and endotoxin selective absorber matrices [211] and membranes [212]. Removal of endotoxin from ELPs has often required one of these secondary purification treatments in addition to traditional purification through temperature induced precipitation, thereby, reducing overall protein yields.

Recently, yeast and plant expression systems have been explored for the expression of ELPs and related matrix proteins. For example, recombinant silk-elastin

proteins have been successfully expressed in tobacco and potato plants [213]. Additionally, the expression of a variety of target proteins in transgenic tobacco has been enhanced by an order of magnitude when fused to elastin-like polypeptides [214-216]. Nonetheless, while transgenic plants offer the potential for scalability, reduced costs [217], and inherent biosafety through a reduced risk of viral or prion contamination [215], high yields have largely been limited to selected antibodies, enzymes, and vaccines [218]. The majority of recombinant proteins accumulate in only small amounts.

As an alternate approach, yeast expression systems have become an increasingly attractive host for the expression of heterologous proteins [219, 220], due to their capacity to be incorporated into industrial-scale fermentation schemes characterized by high cell densities in relatively inexpensive media. In addition, heterologous proteins have been efficiently secreted into the expression medium, resulting in low-cost recovery of the protein. Significantly, endotoxin is not produced by yeast, thereby simplifying purification and sterilization strategies. However, overall protein expression is influenced by two variables, culture cell density and the amount of recombinant protein per cell [221] and as a consequence of the more complex process of protein production in a eukaryotic organism, yields are often low as compared to *E. coli* expression systems. Nonetheless, tropoelastin, collagen, and silk-like proteins have all been expressed in yeast with varying degrees of success [222-225].

In this report, a novel strategy was devised to construct a gene with enhanced sequence diversity that encodes a highly repetitive elastin-like protein polymer for expression in *P. pastoris*. Traditionally, large repetitive genes that comprise most protein polymers have been created using a concatemerization strategy where a pentapeptide repeat cassette (monomer repeat unit) is self-ligated in a head-to-tail fashion [2, 98]. While this strategy has proven suitable for expression of elastin-like proteins in *E. coli*, the translation of repetitive gene sequence, especially in other host

systems, is often associated with reduced levels of protein expression. Moreover, repetitive sequences are often prone to mutational events. Given these potential limitations, we designed a modified concatemerization strategy in which seven dissimilar monomer repeat units, encoding identical pentapeptide repeat sequences, served as a monomer library for the concatemerization reaction. In this manner, a protein polymer gene was generated through random incorporation of distinct monomer repeat units. DNA monomers encoding identical amino acid sequences were synthesized in a manner that accounted for the preferred codon usage of *P. pastoris,* but in which the third nucleotide for proline, glycine and valine codons was degenerate. Thus, concatamerization of the monomer library produced a genetically nonrepetitive DNA sequence for the pentapeptide repeat [$(VPGVG)_2VPGEG(VPGVG)_2$]. By limiting genetic repetition, the risk of genetic deletions, rearrangements, or premature termination errors during protein synthesis was minimized [220, 226, 227].

4.2 MATERIALS and METHODS

Synthetic gene construction of Yeast ELP monomer library. A collection of distinct single-stranded oligonucleotides corresponding to a monomer repeat unit was chemically synthesized (Sigma Genosys, Inc). This was accomplished through use of degenerate bases incorporated into the design of the **Yeast ELP** coding sequence. Specifically, W encoded for A or T in proline and glycine and H for A, T, or C in valine. When chemically synthesized, equal molar amounts of the assigned nucleotides were used when synthesizing the degenerate position affording random incorporation of bases at those designated positions **(Table 4-1B)**. The lyophilized sequences were resuspended in elution buffer (10mM tris-HCl, pH 8.5) to a final concentration of 0.5 µg/uL. DNA Polymerase I Klenow fragment (New England Biolabs) was utilized in a primed extension of the oligonucleotide template for the second strand synthesis yielding the double stranded cassette of the monomer repeat unit. An aliquot of the reaction mixture was analyzed via gel electrophoresis (4% GTG NuSieve, 1 X TBE buffer) to verify a single band corresponding to the size of the monomer repeat unit (~75bp). Subsequently, a preparative gel was used to isolate DNA and the corresponding band was purified via Amicon Ultrafree Centrifugal Filter Units (Millipore) and isolated via ethanol precipitation. A total of 20 µg of the DNA cassette was digested with *Bam*H I (10U/µg) and *Hin*D III (10U/µg) restriction enzymes, extracted with phenol/chloroform, and isolated via ethanol precipitation.

Table 4-1. Amino acid sequence and related nucleic acid coding sequence for the **Yeast ELP** gene in *E. coli* **(A)** and *P. pastoris* **(B)** expression systems.

A

Val	Pro	Gly	Val	Gly	Val	**Pro**	Gly	Val	Gly	Val	Pro	Gly
GTA	CCT	GGT	GTT	GGC	GTT	**CCG**	GGT	GTT	GGT	GTA	CCA	GGC
Glu	Gly	Val	**Pro**	Gly	Val	Gly	Val	Pro	Gly	Val	Gly	
GAA	GGT	GTA	**CCG**	GGT	GTT	GGC	GTA	CCA	GGC	GTA	GGC	

B

Val	Pro	Gly	Val	Gly	Val	Pro	Gly	Val	Gly	Val	Pro	Gly
GTT	CCA	GG**W**	GT**H**	GG**W**	GT**H**	CC**W**	GG**W**	GT**H**	GG**W**	GT**H**	CC**W**	GG**W**
Glu	Gly	Val	Pro	Gly	Val	Gly	Val	Pro	Gly	Val	Gly	
GAA	GG**W**	GT**H**	CC**W**	GG**W**	GT**H**	GG**W**	GT**H**	CC**W**	GG**W**	GT**H**	GG**W**	

A. CCG is a high usage codon encoding proline in *E. coli* (24.5%), but extremely low in *P. pastoris* (3.9%)
B. Degenerate base **W** encodes for A or T while **H** encodes for A, T, or C (Sigma Genosys)

The pZErO-1 (Invitrogen) acceptor plasmid (1 µg) was prepared via *Bam*H I and *Hin*D III double digestion, followed by heat inactivation of the enzymes at 65°C and a dilution of the digested plasmid to 10ng/µL. **Yeast ELP** monomers were designed with *Bam*H I and *Hin*D III overhangs to enable cloning into pZErO-1 at these restriction sites.

The DNA cassettes and respective acceptor plasmids were ligated together in the presence of T4 DNA ligase (New England Biolabs) at 16°C for 30 minutes. A 2 µL aliquot of the ligation reaction mixture was used to transform 40 µL of electrocompetent TOP10F' *E. coli* cells (Invitrogen). A total of 100 µL of the transformation mixture was spread onto low salt Luria Broth (LSLB) agar (5 g tryptone, 2.5 g yeast extract, 2.5 g NaCl, 7.5 g agar, 200 mL ddH_2O, pH 7.5) supplemented with Zeocin (50 µg/µL). The plates were incubated for 12 hours at 37°C. Twenty transformants were selected from each plate to inoculate individual 7mL cultures of LSLB/Zeocin media. Cultures were rotary incubated for 12 hours at 37°C. Plasmid DNA was isolated following a Qiagen Spin Miniprep protocol (Quiagen, Inc.). Miniprepped DNA was initially screened by a *Bam*H I and *Hin*D III double digestion. Positive transformants were verified by agarose gel electrophoresis (4% GTG NuSieve agarose, 1X TBE buffer). Automated DNA sequencing utilizing the M13 forward and M13 reverse primers confirmed correct and unique DNA products for seven separate monomer repeat unit cassettes, yielding the **Yeast ELP** monomer library **(Table 4-2).**

Table 4-2. Monomer Library.

A

	Val	Pro	Gly	Val	Gly	Val	Pro	Gly	Val	Gly	Val	Pro	Gly	Glu	Gly	Val	Pro	Gly	Val	Gly	Val	Pro	Gly	Val	Gly
M1:	GTT	CCA	GGA	GTC	GGA	GTT	CCT	GGT	GTT	GGA	GTA	CCA	GGT	GAA	GGT	GTT	CCT	GGT	GTA	GGA	GTC	CCT	GGT	GTA	GGT
M2:	GTT	CCA	GGT	GTC	GGA	GTA	CCA	GGT	GTT	GGA	GTC	CCT	GGA	GAA	GGT	GTA	CCT	GGT	GTT	GGT	GTT	CCT	GGA	GTA	GGT
M3:	GTT	CCA	GGT	GTC	GGT	GTA	CCT	GGT	GTA	GGT	GTT	CCT	GGT	GAA	GGT	GTA	CCA	GGT	GTC	GGT	GTA	CCT	GGT	GTA	GGA
M4:	GTT	CCA	GGT	GTC	GGA	GTA	CCT	GGA	GTT	GGT	GTC	CCT	GGT	GAA	GGT	GTT	CCA	GGA	GTT	GGA	GTC	CCA	GGT	GTA	GGA
M5:	GTT	CCA	GGT	GTT	GGA	GTT	CCT	GGA	GTT	GGT	GTC	CCT	GGA	GAA	GGA	GTT	CCT	GGT	GTT	GGA	GTA	CCT	GGA	GTC	GGT
M6:	GTT	CCA	GGT	GTT	GGT	GTT	CCT	GGT	GTT	GGT	GTT	CCC	GGA	GAA	GGA	GTC	CCT	GGA	GTC	GGA	GTT	CCT	GGT	GTA	GGT
M7:	GTT	CCA	GGT	GTT	GGA	GTT	CCT	GGA	GTA	GGT	GTT	CCT	GGA	GAA	GGA	GTA	CCT	GGT	GTT	GGT	GTA	CCA	GGT	GTT	GGT

B

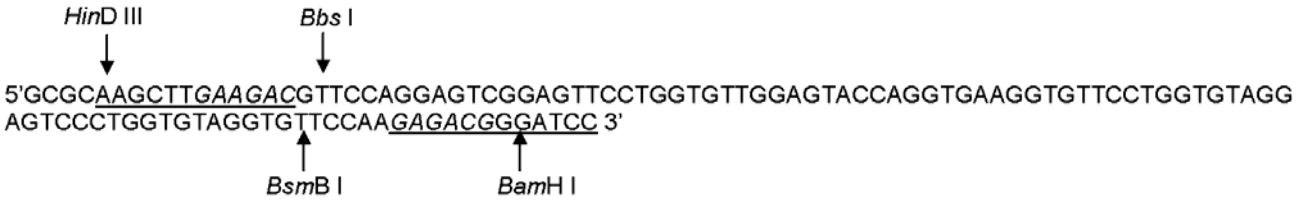

C

5-'TCCAGGAGTCGGAGTTCCTGGTGTTGGAGTACCAGGTGAAGGTGTTCCTGGTGTAGGAGTCCCTGGTGTAGGTGT
CCTCAGCCTCAAGGACCACAACCTCATGGTCCACTTCCACAAGGACCACATCCTCAGGGACCACATCCACAAGGT-3'

A. Nucleic acid sequence of the seven unique **Yeast ELP** monomer units created using the wobble base system and employed in multimerization of the **Yeast ELP** gene.

B. Recognition (underlined) and cleavage sites (arrows) for restriction enzymes within the representative monomer, **M1**, repeat unit.

C. Monomer repeat unit, **M1**, with cohesive ends generated from a *Bbs* I / *Bsm*B I sequential digestion and used in the multimerization reaction. Note that *Bbs* I / *Bsm*B I are type II restriction enzymes and cleave the DNA downstream of their recognition sites.

Concatamerization of the Yeast ELP monomer library. Concatamerization reactions utilized a total of 3.2 µg (0.4 µg of each monomer) of the *Bbs* I / *Bsm*B I digested DNA. Monomers were then ligated randomly end-to-end via T4 DNA ligase. The multimerization mixture was separated by size using agarose gel electrophoresis (1% agarose, 1 X TBE buffer) **(Figure 4-2A).** Concatemers were excised in blocks, <500 bp, 500-1000 bp, 1000-3000 bp and purified using Zymoclean Gel DNA Recovery protocol (Zymo Research, Inc). Concatamers of 1000-3000bp in size were ligated into the acceptor plasmid at the *Bbs* I site at 16°C for 16 hours. The acceptor plasmid was prepared from the pZErO-1 plasmid containing a single monomer repeat unit, digested with *Bbs* I, and dephosphorylated with SAP (Shrimp Alkaline Phosphatase, Roache) to prevent self ligation. Ligation mixtures were used to transform competent TOP10F' cells and 100 µL of the transformation mixture was plated on LSLB/Zeocin agar plates. DNA from positive clones were isolated via MacConnell automated miniprep and screened through double digestion using *Bam*H I and *Hin*D III restriction enzymes. Clones of predetermined size (approximately 1.5 kB) were isolated and sequences confirmed with automated DNA sequencing.

Construction of the modified pPICZα-A expression plasmid. Single stranded oligonucleotides encoding the sense and anti-sense strands of the **Yeast ELP** adaptor were chemically synthesized (Sigma Genosys, Inc.) **(Table 4-3).** The **Yeast ELP** adaptor is a ~50 bp DNA cassette designed to contain restriction enzyme cut sites midway through the cassette to allow for insertion of the **Yeast ELP** concatamer and allow for facile cloning into the pET24-a expression vector within the multiple cloning region. This ensures correct insertion of the gene in frame with the N-terminal α-factor secretion signal sequence and the C-terminal polyhistidine tag and *c-myc* epitope. The DNA was suspended in 10mM Tris buffer (pH 8) to a final concentration of 0.5 µg/µL. A

solution of 10 µg of each corresponding oligonucleotide, 4 µL 5M NaCl, 4 µL 1M $MgCl_2$, 152 µL of sterile ddH2O was subjected to an annealing procedure initiated at a reaction temperature of 99°C with incremental temperature decrements of 1°C every 5 minutes to a final reaction temperature of 30°C. The resultant double stranded DNA cassette was analyzed by agarose gel electrophoresis (4% GTG NuSieve agarose, 1X TBE buffer).

Double stranded synthetic DNA was phosphorylated through a 2 hour incubation with T4 poynucleotide kinase (New England Biolabs) in the presence of T4 DNA ligase buffer with 10mM ATPs (New England Biolabs). The enzymes were removed with phenol/chloroform/isoamyl alcohol (25:24:1) and the dsDNA was recovered through an ethanol precipitation.

The pPICZα-A plasmid (1 µg, Invitrogen) was doubly digested with *Xho* I and *Xba* I, followed by heat inactivation of the enzymes at 65°C, and dilution to 10ng/µL. The adaptor was designed with *Xho* I and *Xba* I overhangs to enable its cloning into pPICZα-A. Adaptor and plasmid were ligated together in the presence of T4 DNA ligase at 16°C for 30 minutes. A 2 µL aliquot of the ligation reaction mixture was used to transform 40 µL of electrocompetent TOP10F' *E. coli* cells. A total of 100 µL of the transformation mixture was spread onto low salt LB (LSLB) agar supplemented with Zeocin (50 µg/µL). The plates were incubated for 12 hours at 37°C. Five transformants were selected from each plate to inoculate individual 7mL cultures of LSLB/Zeocin media. Cultures were rotary incubated for 12 hours at 37°C. Plasmid DNA was isolated following a Qiagen Spin Miniprep protocol. DNA was initially screened by a *Xho* I and *Xba* I double digestion. Positive transformants were verified by agarose gel electrophoresis (4% GTG NuSieve agarose, 1X TBE buffer). Automated DNA sequencing utilizing the AOX1 5' and AOX1 3' primers confirmed the correct DNA product.

Table 4-3. Nucleic acid sequence of **Yeast ELP** adaptor with related amino acid coding sequence and restriction enzyme cut sites.

	Val	Pro	Ala	Val	Gly	Val	Pro				Pro	Ala	Val	Gly
CTCGAGAAAAGAGAGGCTGAAGCT	GTT	CCA	GCT	GTT	GGT	GTT	CCA	AGAGACGGTACCCGTCTCTT			CCA	GCT	GTT	GGT CTAGA
Xho I								*Bsm*BI	*Bsm*BI					*Xba* I

Adaptor was inserted at *Xho*I and *Xba* I sites within the pPICZα-A expression vector. The **Yeast ELP** gene was inserted within the adaptor at the double *Bsm*B I sites.

Cloning the Yeast ELP gene into the modified pPICZα-A expression plasmid.

The modified pPICZα-A plasmid was digested with restriction enzyme *Bsm*B I and SAP dephosphorylated. The **Yeast ELP** gene was excised from the pZErO-1 plasmid via sequential digestion using restriction enzymes *Bbs* I and *Bsm*B I and purified from an agarose gel. A ligation reaction was performed to relocate the **Yeast ELP** gene from pZErO-1 to pPICZα-A. The ligation mixture was transformed into electrocompetent TOP10F' cells and plated on LB media under Zeocin antibiotic selection. Isolated DNA from transformants was screened via agarose gel electrophoresis using *Xho* I and *Xba* I double digestion. A product of 1575bp was observed **(Figure 4-2B).** Automated DNA sequence analysis using AOX1 5' and AOX1 3' primers confirmed correct insertion of the **Yeast ELP** gene in frame with the N-terminal α–factor secretion signal and the C-terminal peptide containing the *c-myc* epitope and the polyhistidine tag.

Preparation of P. pastoris for chemical transformation. The preparation of chemically competent *X-33 P. pastoris* cells was performed following the EasyComp Transformation (Invitrogen) protocol. Briefly, a YPD (Yeast Extract Peptone Dextrose) agar plate was streaked with the *X-33* strain of *P. pastoris* such that isolated individual colonies grew after an incubation at 30°C for 2 days. A total of 10mL of YPD media was inoculated with a single colony and grown overnight at 30°C in a shaking incubator (250 rpm). The cells were diluted from the overnight culture to an OD_{600} of 0.1 in 10mL of YPD. Cells were pelleted by centrifugation at 500g for 5 minutes at 25°C and resuspended in 1mL Solution 1 (EasyComp), yielding competent *X-33* cells. A total of 50 µL of competent cells were aliquoted into 1.5mL sterile screw-cap tubes and stored at -80°C.

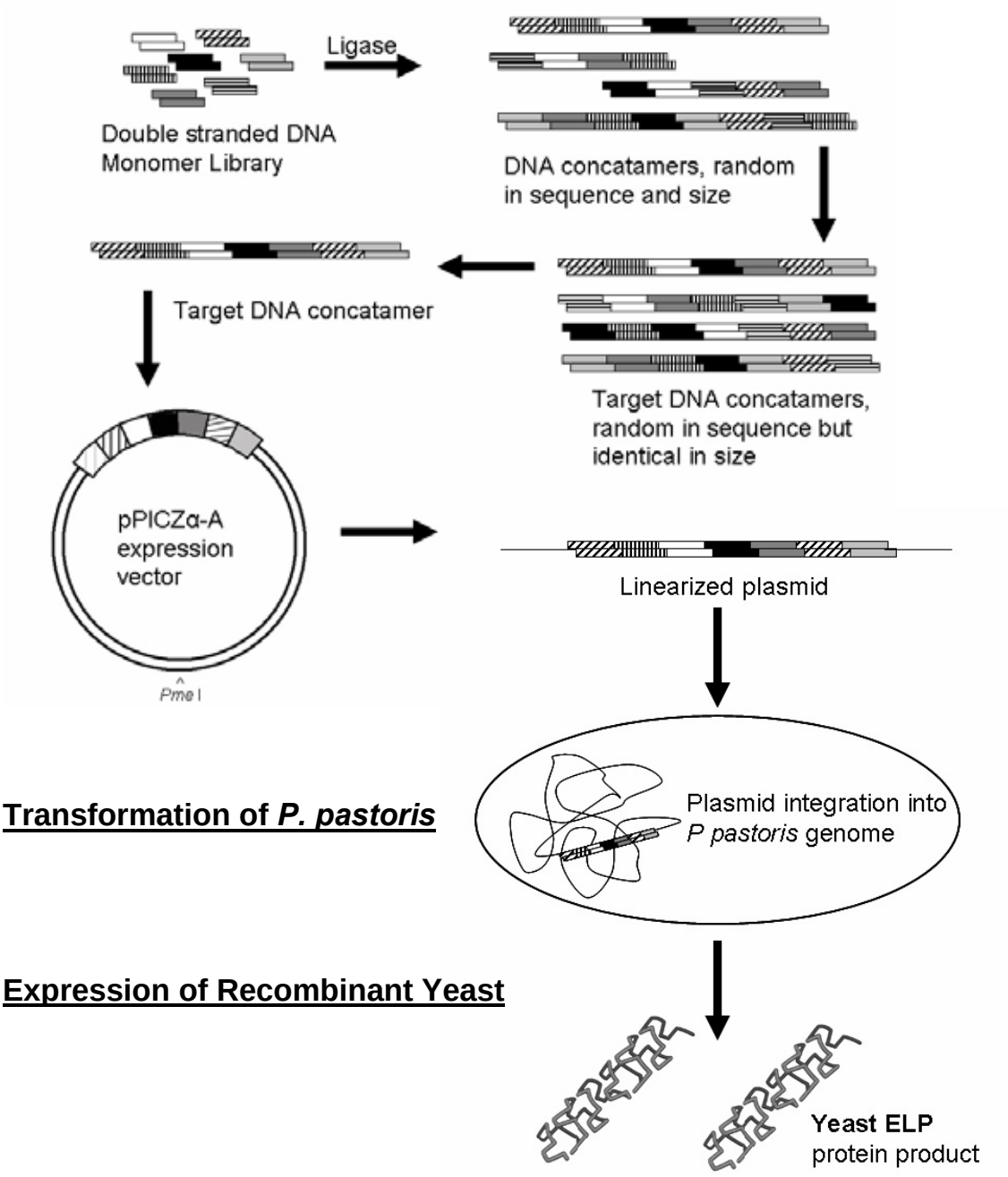

Scheme 4-1. Cloning strategy in the construction of the **Yeast ELP** gene. The seven unique double stranded DNA monomer cassettes were ligated together to form concatamer of random sequence. A target multimer of 1575bp was selected, cloned into the recombinant plasmid, pPICZα-A and integrated into the *P. pastoris* host DNA.

Transformation of the Yeast ELP gene into P. pastoris. *E. coli* was utilized to propagate the plasmid containing the **Yeast ELP** gene. A total of 5 to 10 µg of plasmid carrying the **Yeast ELP** gene was isolated and was linearized within the 5' AOX1 region through digestion with restriction enzyme *Pme* I to promote integration into the *P. pastoris* host. A vector linearized within the 5' AOX1 region will integrate by gene insertion into the host's 5' AOX1 region. The linearized plasmid was isolated via preparative gel electrophoresis (1% agarose, 0.5X TAE) and purified using Zymoclean Gel Recovery.

Transformation was performed following the EasyComp transformation protocol. One tube of competent *X-33* cells was thawed at room temperature. A total of 3 µg of linearized **Yeast ELP** DNA was added to the thawed cells. A total of 1mL of Solution II (EasyComp) was added to the DNA-cell mixture, vortexed, and incubated for 1 hour at 30°C in a water bath. The mixture was mixed every 15 minutes to increase transformation efficiency. Following the incubation, cells were heat shocked at 42°C for 10 minutes. Cells were split into two centrifuge tubes with 1mL of YPD medium added to each tube and incubated at 30°C for 1 hour to allow for expression of Zeocin resistance. Cells were pelleted by centrifugation at 3000g for 5 minutes at 25°C and the pellet resuspended in 150 µL of Solution III (EasyComp). The entire transformation was spread on YPDS (Yeast Extract Peptone Dextrose with Sorbitol)/Zeocin agar plates and incubated at 30°C for 4 days.

PCR screening for correct gene insertion into the P. pastoris host. All polymerase chain reaction (PCR) screening was performed using the Qiagen Taq PCR, which includes the Q-solution to assist in the amplification of difficult to amplify G-C rich DNA. According to the manufacturer's instruction, a 50 µL reaction mixture using the AOX1 5' and AOX1 3' primers (5 µM) and Q-solution was subjected to a PCR cycle that

employed 25 cycles of a one minute fifteen second denaturation at 94°C, one minute fifteen second primer anneal at 57°C, and a three minute primer extension at 72°C.

Expression of Yeast ELP in P. pastoris. A single colony of the transformants was used to inoculate 25mL of BMGY, a buffered glycerol complex medium, in a 250mL baffled flask, grown at 30°C with shaking until and OD_{600} of 2 was reached. Cells were harvested by centrifugation at 3000g for 5 minutes at 25°C and resuspended in 100mL BMMY, a buffered methanol complex medium, for induction of expression in a 1L flask. To maintain induction, 100% methanol was added to a final concentration of 0.5% methanol every 24 hours for 4 days. After 4 days, cells were harvested and supernatant collected. Both the cellular fraction and supernatant was analyzed for protein expression.

Purification of Yeast ELP from P. pastoris. Prior to protein purification, the supernatant was concentrated using an Amicon Ultra centrifugal filter with a molecular weight cut off of 30,000 kDa. Metal affinity chromatography was used for purification of **Yeast ELP**, which isolated the protein by the polyhistidine tag, according to manufacturer instructions. Briefly, a cobalt based TALON metal affinity resin (Clontech) was equilibrated with equilibration buffer (50mM sodium phosphate, 300mM NaCl, pH 7.0). The concentrated supernatant was run through the column by gravity flow followed by extensive washes with equilibration buffer. The bound protein was eluted with Elution buffer (50 mM sodium phosphate, 300mM NaCl, 250mM imidizole, pH 7.0) and desalted using PD-10 desalting columns (GE Healthcare Life Sciences). Lyophilization afforded protein **Yeast ELP** as fibrous solid in an isolated yield of 2.5 mg/L. Efforts to optimize yields are underway [228].

Additionally, as observed with other structural protein expression, some protein was isolated from both the cytosolic and membrane fractions, though most of the protein was found to be secreted into the media. It has been noted that some higher eukaryotic

proteins are not compatible with the yeast secretory apparatus and these proteins remain trapped at some point along the secretory pathway [228, 229]. To isolate this protein, the harvested cells were resuspended in breaking buffer (20mM Tris-Cl, pH 7.5, 1 mM EDTA, 5% glycerol) and then disrupted through vortexing cycles. An analytical spin was used to assess breaking efficiency. Cell lysates were centrifuged at 40,000g for 40 minutes at 4°C and the cytosolic fraction was collected and His-purified. The membrane fraction was detergent extracted with 0.5% Triton X-100 overnight at 4°C. The lysate was centrifuged at 40,000g for 40 minutes at 4°C and the soluble membrane fraction collected and His-purified. Isolated yields of less than 1 µg were obtained from both cytosolic and membrane fractions, which confirmed that the ELP was not trapped in the secretory pathway.

Identification of the recombinant elastin protein, Yeast ELP. *Sodium dodecyl sulfate (SDS) polyacrylamide gel electrophoresis* was performed. Samples were separated on a 4-20% gradient acrylamide-SDS gel and total protein was visualized with Coomassie G250 (BioRad). Western blot analysis was performed by transfer to an Immobilon PSQ (Polyvinylidene fluoride) (PVDF) membrane (Millipore) and probed with either mouse His-tag monoclonal antibodies (Novagen) or anti-*c-myc* mouse monoclonal antibodies followed by a goat-anti-mouse HRP (horseradish peroxidase) secondary antibody. Bands were visualized by using the ECL Western blotting detection kit (Amersham Biosciences). Both antibodies stained a band at 65 kDa, corresponding to the **Yeast ELP** protein.

Edman degradation was used to identify the repeat unit of **Yeast ELP** to confirm expression. Briefly, the protein was electroblotted on a PVDF membrane and stained with Amido Black (BioRad). The **Yeast ELP** protein negatively stained using this stain. Approximately 0.5 to 2.0 pmol of protein obtained from the membrane was used for N-

terminal sequence analysis using automated sequencers at the Microchemical and Proteomics Facility at Emory University.

4.3 RESULTS and DISCUSSION

Conceptual framework for the design of Yeast-expressed ELP. The elastin-like protein, **Yeast ELP**, was employed as a test substrate for assessing the efficacy of monomer library concatamerization in the design of a nonrepetitive ELP gene for expression in yeast. The **Yeast ELP** protein comprises a concatenated series of pentapeptide repeat units yielding 21 repeats of the pentapeptide monomer sequence $[(VPGVG)_2VPGEG(VPGVG)_2]$. Our group has investigated this repeat sequence as a constituent of multiblock protein copolymers expressed by *E.coli*. As a consequence of its high transition temperature (>> 37°C), this sequence affords a conformationally flexible protein segment under physiologically relevant conditions [1-4].

In order to express a highly repetitive elastin-like protein in *P. pastoris,* a novel strategy was employed to reduce primary DNA sequence repetition without altering the recurring 21-mer peptide sequence. This was accomplished through the design of a DNA monomer library. Protein engineering has frequently used protein libraries that include defined amino acid mixtures at certain positions of interest [230, 231]. Two of the most commonly used methods for library generation are random mutagenesis and cassette mutagenesis. Random mutagenesis introduces random point mutations throughout the entire protein. The most common method for creating such a library is PCR. This method has been utilized in studies, for example, aimed to identify amino acids integral to enzymatic function and protein-protein interactions [232]. Cassette mutagenesis is a method of library creation where a region of interest is targeted for

mutagenesis through the use of degenerate oligonucleotides. We have used degenerate oligonucleotides in the design of our DNA monomer repeat unit to create a library of monomers, which were subsequently ligated together to create our target ELP gene.

The genetic code is degenerate in that the protein biosyntheic machinery utilizes 61 sense codons to encode the 20 amino acids. Due to this degeneracy, different nucleotide sequences code for the same amino acid. These coding differences are restricted to usually one position in the codon triplet and allow for multiple nucleotides to encode the same amino acid, thereby increasing variability of the primary DNA sequence of the protein. For example, the third position of the glycine codons (GGA, GGG, GGC, GGT) is a fourfold degenerate site because all nucleotide substitutions at this site are synonymous, in that the coded amino acid is unchanged. Degenerate bases allow for the incorporation of multiple nucleotides into the specified site within a codon. As detailed in **Table 4-1B**, the monomer repeat unit for the **Yeast ELP** gene was designed through chemical synthesis based on the degenerate bases, W, encoding for either A or T, and H, encoding for A, T or C. While the primary genetic sequence for the **Yeast ELP** was based on the midblock sequence of a previously reported triblock protein expressed in *E. coli* [1, 2], the sequence was modified in accordance with the preferred codon usage of *P. pastoris* **(Figure 4-1).** The codon triplet encoding proline residues was determined to be critically important in the successful expression of this protein. CCG, a high usage codon in *E.coli* and used extensively for encoding proline in the pentapeptide repeat is not adequately translated in *P. pastoris*. Therefore, in the design of the **Yeast ELP** gene, only CCA and CCT codons were employed to code for proline residues **(Table 4-1).**

Pichia pastoris [gbpln]: 66 CDS's (38158 codons)

fields: [triplet] [frequency: per thousand] ([number])

UUU 23.6 (901)	UCU 23.9 (911)	UAU 14.7 (561)	UGU 8.3 (318)
UUC 18.9 (721)	UCC 16.3 (621)	UAC 18.3 (698)	UGC 4.4 (168)
UUA 14.5 (553)	UCA 15.4 (587)	UAA 0.9 (35)	UGA 0.3 (13)
UUG 31.9 (1218)	UCG 6.8 (258)	UAG 0.5 (18)	UGG 9.8 (375)
CUU 16.1 (614)	CCU 15.3 (584)	CAU 10.4 (395)	CGU 6.7 (256)
CUC 7.6 (291)	CCC 6.5 (249)	CAC 9.1 (346)	CGC 2.3 (87)
CUA 11.4 (435)	CCA 17.5 (668)	CAA 24.1 (918)	CGA 4.3 (163)
CUG 15.5 (591)	CCG 3.9 (150)	CAG 14.5 (554)	CGG 1.8 (70)
AUU 31.0 (1184)	ACU 23.7 (903)	AAU 22.9 (875)	AGU 12.2 (464)
AUC 19.0 (725)	ACC 14.0 (533)	AAC 25.5 (974)	AGC 7.3 (279)
AUA 11.3 (432)	ACA 14.2 (541)	AAA 30.0 (1145)	AGA 19.9 (760)
AUG 19.2 (734)	ACG 6.0 (230)	AAG 34.8 (1328)	AGG 6.7 (254)
GUU 27.0 (1032)	GCU 29.9 (1141)	GAU 36.8 (1405)	GGU 27.1 (1035)
GUC 14.7 (561)	GCC 17.0 (649)	GAC 26.5 (1012)	GGC 8.5 (326)
GUA 10.0 (381)	GCA 16.4 (624)	GAA 40.6 (1550)	GGA 20.0 (762)
GUG 12.8 (487)	GCG 3.5 (134)	GAG 29.9 (1141)	GGG 6.0 (230)

Figure 4-1. Codon Usage Table for *P. pastoris* (Codon Usage Database, NCBI GenBank)

Design of a library of nonrepetitive DNA monomers. Chemically synthesized, single-stranded oligonucleotides designed with degenerate bases at the specified locations, were obtained from SigmaGenosys. At each degenerative base location, equal molar amounts of each base were introduced. For example, at a W site, equal amounts of A and T were available during synthesis. Through primed extension, double stranded cassettes of the monomer repeat units were generated. The cassettes were digested with restriction enzymes *Bam*H I and *Hin*D III to enable cloning into the pZErO-1 cloning plasmid at the complementary sites within the multiple cloning region. Multiple transformants were screened and automated DNA sequencing confirmed correct and unique DNA products for seven separate monomer cassettes, comprising the **Yeast ELP** monomer library **(Table 4-2A).**

The literature reports that gene locations enriched in repetitive sequences are 'hot spots' for mutational events such as insertions, deletions, and frame shifts [233, 234]. DNA sequences with GC and CA/GT repeats have been reported to undergo spontaneous deletions [235, 236], while regions rich in AT have been reported as 'hot spots' for frame shifts and deletions [237]. Additionally, long repetitive sequences have been found to be less stable than shorter ones [238]. Specifically, in *P. pastoris*, the expression of foreign genes with high A and T content can be affected by premature transcription termination [239, 240], therefore, care was taken in the genetic design to limit such 'hot spot' motifs.

Concatamerization and identification of the Yeast ELP gene. Since automated DNA synthesis is currently limited to the production of oligonucleotides of lengths corresponding to approximately 100 bases, sequences encoding larger proteins cannot be directly synthesized. DNA cassette concatamerization is a commonly employed method for assembling genes encoding large, repetitive proteins **(Scheme 4-**

1) [2, 98]. The genes composing the monomer library were designed with non-palindromic cohesive ends. This was accomplished through the use of type II restriction enzymes, *Bbs* I and *Bsm*B I, which recognize and cleave non-palindromic sequences as detailed in **Table 4-2B**, creating the digested cassette in **Table 4-2C**. Consequently, random ligation of the seven DNA monomers proceeds in a head-to-tail fashion to generate concatamers of varying lengths by increments of a monomer repeat unit. Concatamers were separated by size, or degree of concatamerization, on an agarose gel **(Figure 4-2A)** and concatamers of 1000 to 3000bp in size were isolated and ligated back into the acceptor plasmid. A clone of 1575bp was identified and was denoted as **Yeast ELP (Figure 4-2B).**

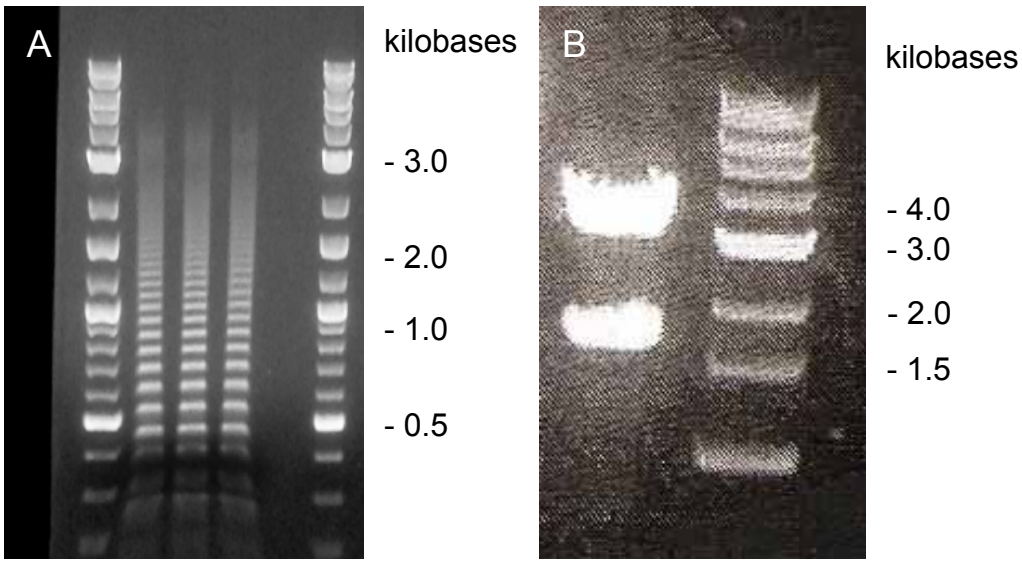

Figure 4-2. A. 1% TAE (Tris-acetate-EDTA) agarose gel. Ladder of concatamerization products, each band indicates different sized concatamers, differing by 75 bp (addition of one monomer cassette). Seven unique monomer units were pooled in equal amounts in the concatamerization reaction for random incorporation of the monomer units in the concatamerization of the **Yeast ELP** gene. **B.** 1% TAE (Tris-acetate-EDTA) agarose gel. *Xho* I / *Xba* I digested **Yeast ELP** (1575bp), pPICZα-A (3.6 kb). DNA standard used was a 1Kb DNA ladder (NEB).

Expression system employed for Yeast ELP. Recombinant elastin proteins have traditionally been expressed through microbial expression in *E. coli [241].* Nonetheless, recognized drawbacks exist. In particular, purification of the expressed protein products is labor intensive as isolation from a pool of cytoplasmic proteins and cellular contaminants is required. Additionally, endotoxin, an amphiphillic lipopolysaccharide found in the wall of gram-negative bacteria, is released upon cell lysis and can become associated with the target protein [202]. As an alternative, the methylotropic yeast, *P. pastoris* was investigated for elastin expression and secretion. Notably, *P. pastoris* secretes very low levels of native proteins, which simplifies purification protocols [1, 242]. Moreover, endotoxin is not present as a potential contaminant.

Recent reports have described the expression of structural proteins in yeast. Spider dragline silk-like proteins have been expressed in both *E. coli* and *P. pastoris* at high levels [223, 243]. Likewise, full length tropoelastin has been expressed in *Saccharomyces cerevisiae* using a fusion peptide for targeted secretion into the endoplasmic reticulum with enhanced biostability [222]. *P. pastoris* has also been employed for co-expression of Type-I, -II or -III collagen with prolyl 4-hydroxylase yielding collagen fibrils that display D-periodic banding [224, 225]. However, issues related to gene rearrangement have been observed with these highly repetitive proteins. For example, a 101 amino acid spider dragline silk-like protein, derived from the major dragline protein of *Nephila clavipes* [244], produced multiple sized protein products, each an integral number of repeats of the 101 amino acid sequence encoded by the gene. It was speculated that different sized products were the result of expansion or deletion of the DNA repeat sequence [223]. Additionally, the importance of genetic sequence diversity is noted among patients with trinucleotide repeat associated disease where sequence divergence between repeated sequences reduce the severity of the

disease and likelihood of inheritance [245, 246]. In fact, studies examining spontaneous deletions demonstrate that alteration of a single base pair within homology regions reduces the deletion incidence by an order of magnitude [247].

In this report, *P. pastoris* was employed as the host for expression of the recombinant protein **Yeast ELP**. The methylotrophic yeast strain *X-33* was selected. Without glucose present, *P. pastoris* uses methanol as a carbon source. The alcohol oxidase promoter (AOX 1) controls the expression of alcohol oxidase, which is integral to the initial step in methanol metabolism [228, 248]. The expression vector pPICZα-A **(Figure 4-3 and 4-4),** takes advantage of the AOX 1 promoter and uses methanol to induce protein expression of the **Yeast ELP** protein.

The 5' AOX1 gene within the pPICZα-A vector allows for targeted integration of the expression construct through homologous recombination into the *P. pastoris* genome, creating a stable host able to generate high levels of protein expression (**Figure 4-5**). The pPICZα-A vector also contains a Zeocin resistance gene that allows for antibiotic screening of transformed cells. Additionally, this vector includes the C-terminal fusion tags, c-myc epitope and polyhistidine (6xHis) sequences, that facilitate purification and analysis of expressed proteins. Finally, pPICZα-A contains an α-factor secretion signal, which targets the protein product for secretion into the growth media.

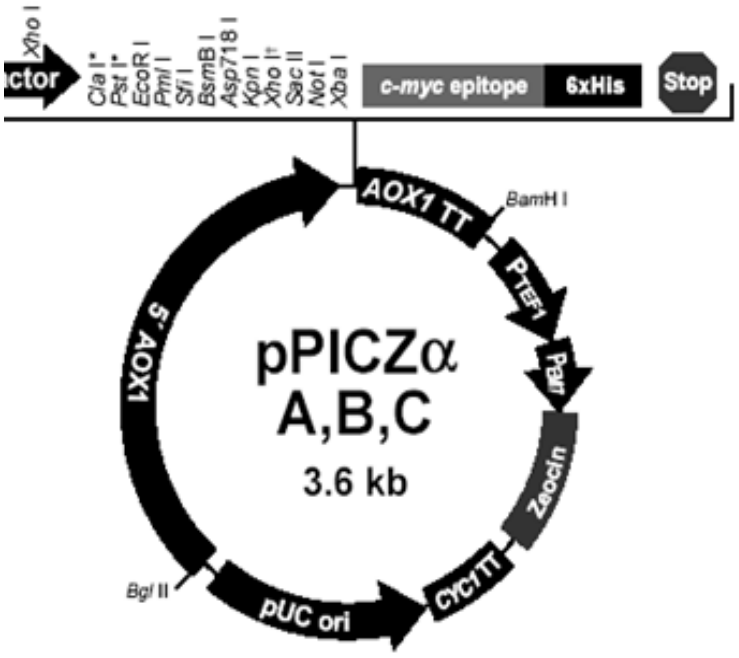

Figure 4-3. pPICZα-A expression vector (Invitrogen). The **Yeast ELP** gene was cloned into the vector at the *Xho* I and *Xba* I restriction sites within the multiple cloning region. Vector was linearized with *Pme* I digestion for integration into the *P. pastoris* genome at the AOX1 crossover sites. The expressed elastin product has an α-factor signal sequence for secretion which is subsequently cleaved. Additionally, the protein retains a 5' *c-myc* epitope and 5' 6XHis-tag which can be used for purification or identification via Western blotting.

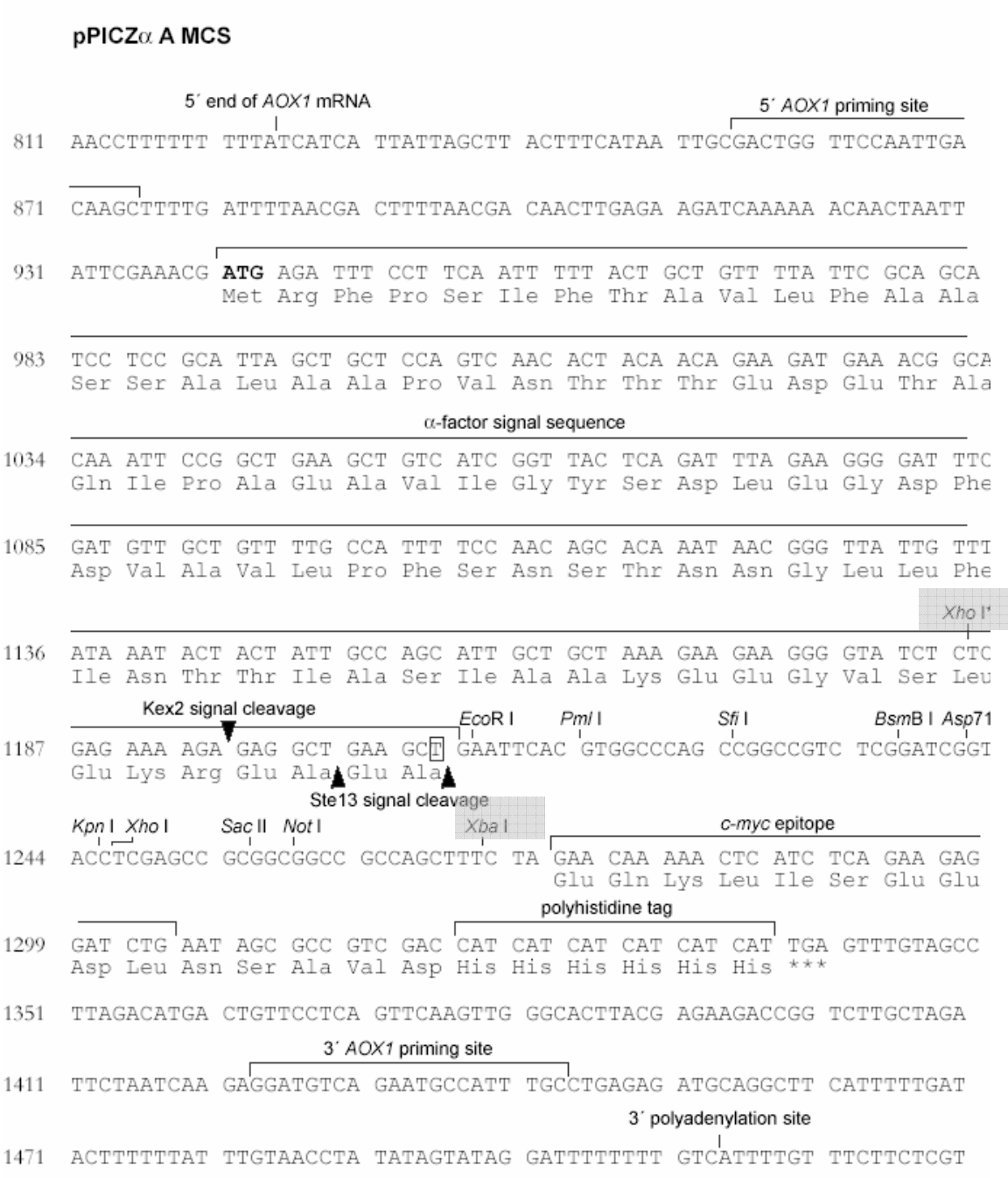

Figure 4-4. pPICZα-A expression vector multiple cloning region (MCR) (Invitrogen). The **Yeast ELP** gene was cloned into the vector at the *Xho* I and *Xba* I restriction sites ( ) within the multiple cloning region. Verification of gene insertion through PCR amplification employed the 5' and 3' AOX1 primers.

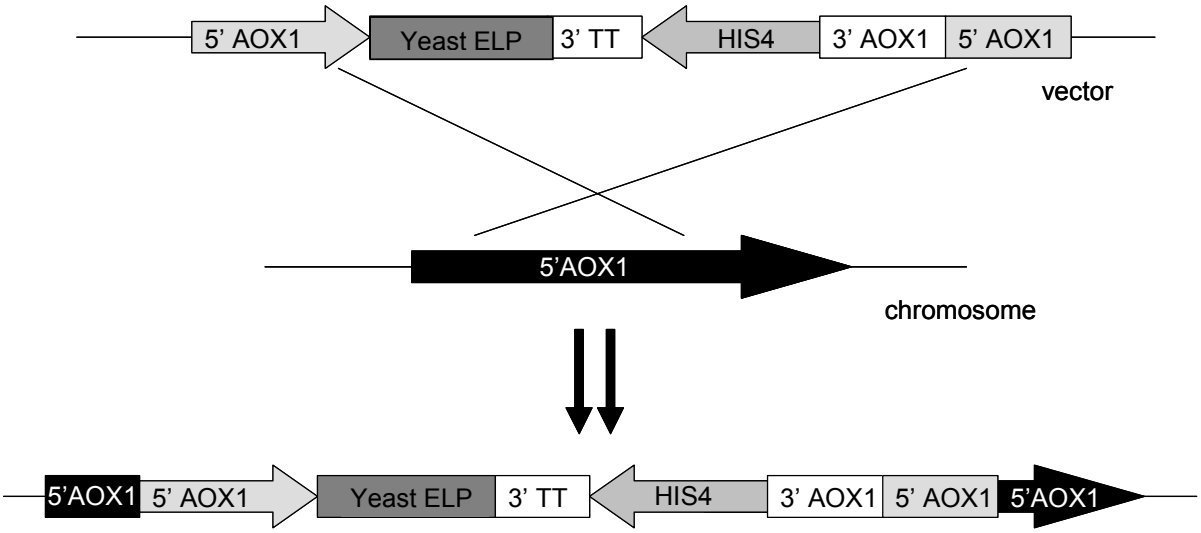

Figure 4-5. Plasmid integration in *P. Pastoris*. pPICZα-A vector containing the **Yeast ELP** gene of interest was linearized within the 5' AOX1 region through digestion with restriction enzyme *Pme* I. Linearized plasmid was integrated by gene insertion into the host AOX1 region.

The 1575 bp **Yeast ELP** concatamer was inserted into a specially designed adaptor at the double *Bsm*B I sites **(Table 4-3)** for cloning into the pPICZα-A expression vector at *Xho* I and *Xba* I restriction sites within the multiple cloning region. This allowed for correct in frame insertion of the gene with the N-terminal α-factor secretion signal and the C-terminal *c-myc* epitope and polyhistidine tag.

Confirming Integration by PCR. Polymerase Chain Reaction (PCR) was used to analyze *P. pastoris* integrants to determine successful introduction of the expression cassette into the yeast chromosome. The **Yeast ELP** gene was amplified using the AOX1 5' (5´-GACTGGTTCCAATTGACAAGC-3´) primer paired with the AOX1 3' (5´-GCAAATGGCATT-CTGACATCC-3´) primer. Using this method, two bands were expected in positive transformants, one corresponding to the **Yeast ELP** gene (1575bp gene + 588bp from the pPICZα-A parent plasmid) and the other to the *AOX1* gene within the chromosome (approximately 2.2 kb). All PCR screening was performed using the Qiagen Taq PCR, which includes Q-solution to assist in the amplification of G-C rich DNA. The PCR product obtained was suggestive of incomplete amplification as multiple product bands were observed **(Figure 4-6A)**, most likely as a result of both its repetitive nature and its G-C rich DNA. PCR products were run on a preparative agarose gel. Amplification of the positive control, **Yeast ELP** miniprep DNA from *E. coli* propagation, appeared as a smear and ladder product **(Figure 4-6A, Lane 1).** Empty *X-33* cells were analyzed as a negative control and amplification of only the AOX1 gene from the yeast chromosome at 2.2 kb was evident **(Figure 4-6A, Lane 2).** A screen of colonies indicated a possible transformant where a smear and ladder product was observed **(Figure 4-6A, Lane 3).**

Confirmation of **Yeast ELP** gene integration was accomplished through amplification using Yeast ELP 3'-2 (5'-CTCCGACTCCTGGAACAC-3') primer paired with

the AOX1 5' (5´-GACTGGTTCCAATTGACAAGC-3´) primer. The Yeast ELP 3'-2 primer was designed to amplify only a 400bp product between the regions of the AOX1 5' priming site within the pPICZα-A vector and into the 5' terminus of the **Yeast ELP** gene. This product was present in the positive control and the putative transformant, but not observed in the negative control (**Figure 4-6B, Lane 1, 2, and 3,** respectively). DNA sequencing verified the identity of the 400bp PCR product as the expected region from the AOX1 5' priming site into the 5' segment of the **Yeast ELP** gene; confirming insertion of **Yeast ELP** into the *P. pastoris* chromosome.

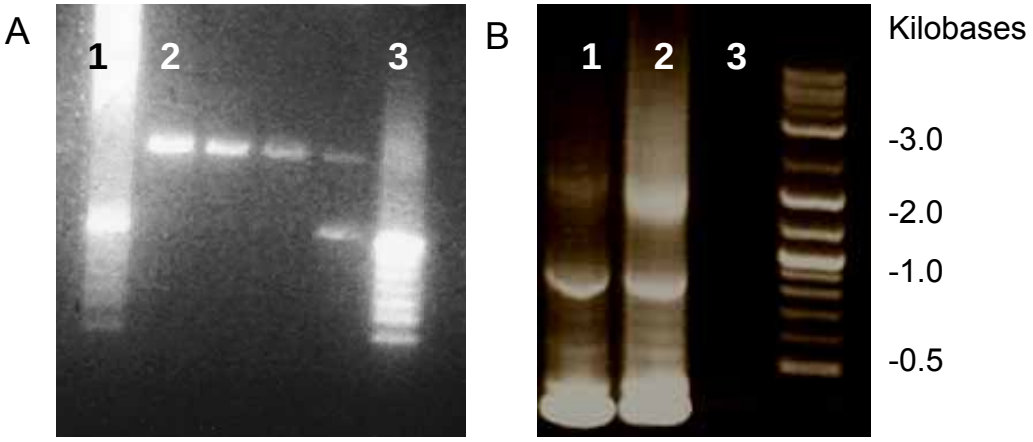

Figure 4-6. **A.** 1% TAE (Tris-acetate-EDTA) agarose gel of PCR products using AOX1 5' and AOX1 3' primers. Note incomplete amplification of the **Yeast ELP** gene as observed with the smear and ladder product (Lane 1). Lane 1: Positive Control, Yeast ELP miniprep DNA. Lane 2: Negative Control, empty X-33 colony stab, note the yeast chromosome has PCR product of 2.2 kb. Lane 3: Colony PCR product of X-33 transformed cells containing **Yeast ELP**, note that the smear and ladder product is also observed. **B.** 1.5% TAE (Tris-acetate-EDTA) agarose gel of PCR products utilizing the Yeast ELP 3'-2 primer and AOX1 5' primer. Target product, approximately 400bp in size, was excised from the gel, purified, and correct sequence verified through DNA sequence analysis using the AOX1 5' primer. Lane 1: Positive control, **Yeast ELP** miniprep DNA, 400bp PCR product observed. Lane 2: Colony PCR product of X-33 transformed cells containing **Yeast ELP**, 400bp product observed. Lane 3: Negative Control, empty X-33 colony stab, no 400bp product observed.

Western blot analysis. **Yeast ELP** was isolated and affinity purified from the growth media with non-optimized yields of 2 mg/L. Small amounts of the protein were

identified in the membrane and soluble cytosolic fractions, but in low amounts and were not utilized in protein analysis. The expected molecular mass for the **Yeast ELP** protein was approximately 56 kDa. As the expressed protein product did not stain with Coomassie, Western blot analysis was utilized to confirm the identity. An anti-His primary antibody revealed the protein band migrating at approximately 65 kDa and was confirmed as the band corresponding to **Yeast ELP** using the anti-*myc* antibody **(Figure 4-7 A and B).** Elastin proteins tend to migrate approximately 20% higher than the theoretical molecular weight in a PAGE gel [75, 97]. To confirm the product was not migrating at a higher mass due to glycosylation, the purified protein was treated with N-glycosidase F (Prozyme), an enzyme which catalyzes the release of all N-linked oligosaccharides added by yeast during secretion. A 65 kDa product was observed before and after treatment with the enzyme [229, 249] **(Figure 4-7C).**

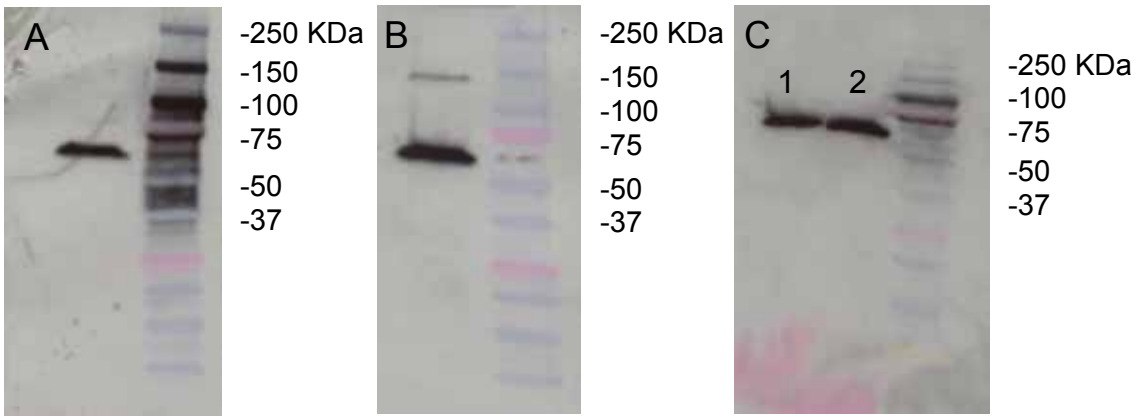

Figure 4-7. Western blotting of elastin-mimetic protein **Yeast ELP** run on a 4-20% SDS-PAGE gel. **A**. c-myc primary antibody, goat-anti-mouse secondary antibody. **B**. anti-His primary antibody, goat-anti-mouse secondary antibody. **C.** Deglycosylation of **Yeast ELP**. Western blotting of elastin-mimetic protein **Yeast ELP** run on a 4-20% SDS-PAGE gel, anti-His primary antibody, goat-anti-mouse secondary antibody. Marker lane: Precision Plus Protein Kaleidoscope (Bio-Rad). Lane 1: Purified Yeast ELP, Lane 2: Purified and deglycosylated **Yeast ELP**. Analysis indicates no deglycosylation of the **Yeast ELP** protein.

4.4 CONCLUSION

In this report, we have demonstrated the expression of a 56 kDa elastin-like protein from *P. pastoris*. We have employed a new strategy, monomer library multimerization, in designing non-repetitive ELP genes for highly repetitive protein sequences. This was accomplished through the synthesis of seven unique monomer cassettes utilizing degenerate bases. The monomer cassettes were randomly ligated in a concatamerization reaction, thereby creating the target gene with varying genetic sequences throughout, which, nonetheless, encode identical repetitive amino acid sequences. We anticipate that this strategy will be useful for creating large, repetitive genes for a variety of expression systems; in order to more closely approach the genetic diversity inherent to native DNA sequences. Additionally, the potential exists to generate glycosylated ELPs through incorporating appropriate glycosylation sites. Indeed, several approaches such as genomics, combinatorial libraries, and synthetic chemistry have been employed for sugar chain remodeling of human proteins in *P. pastoris* and other expression systems [250-252].

CHAPTER 5

CONCLUSIONS and FUTURE DIRECTIONS

With over 500,000 coronary bypass surgeries being performed each year, the need for an adequate vessel replacement material is apparent [8]. The generation of protein polymers that mimic native structural proteins offers a replacement strategy to develop a vascular graft with clinical performance results that match or exceed those of a native vessel. The elastin protein component, which is responsible for distensibility and elastic recovery, appears to be critical in the development of mechanical properties that match the native blood vessel [48-52]. The work presented in this dissertation describes the design of novel protein polymers composed of repetitive amino acid sequences based on the primary sequence of native elastin. These studies are the first evaluation of *in vivo* biocompatibility and long-term biostability of these protein polymers. Additionally, these studies are the first to report the monomer library concatamerization strategy in the synthesis of recombinant elastin-mimetic genes for protein expression in *Pichia pastoris*. The methodologies established can serve as a framework for the design, evaluation, and characterization of the next generation of recombinant elastin-mimetic protein polymers.

As these studies provide the foundation work for the long-term goal of creating a vascular graft substitute which mechanically matches native vasculature, several recommendations for future investigations are proposed for each of the previous chapters.

Chapter 2. Elastin-Mimetic Protein Polymers Capable of Physical and Chemical Crosslinking. We have employed genetic engineering in the design of novel

protein polymers composed of repetitive amino acid sequences or peptide blocks whose structural complexity imparts distinct mechanical, chemical or biological properties. Previously, our group has reported the synthesis of elastin-mimetic multiblock copolymer composed of identical endblocks derived from self-associating, hydrophobic sequences that display plastic-like mechanical responses (Ile-Pro-Ala-Val-Gly), separated by a central block that is both hydrophilic and elastomeric (Val-Pro-Gly-Glu-Gly) [1, 2]. Significantly, these multiblock systems afford the ability to form physical or virtual crosslinked networks through the self-association of chemically similar domains under physiologically relevant conditions (pH 7.4, 37°C).

Although, physically crosslinked protein-based materials possess a number of advantages over their chemically crosslinked counterparts, physical crosslinks and the related domains so formed may be deformed or damaged at applied stresses lower than those required to disrupt covalent crosslinks. In the present study, we have synthesized a new class of recombinant elastin-mimetic triblock copolymer capable of both physical and chemical crosslinking. We have demonstrated that chemical crosslinking provides an independent mechanism for control of protein mechanical responses. Specifically, elastic modulus and tensile strength were enhanced and creep strain reduced through the addition of chemical crosslinking sites. Additionally, we have demonstrated exceptional biocompatibility of gluteraldehyde crosslinked multiblock systems.

Although the incorporation of chemical crosslinking sites improved the elastic modulus, ultimate tensile strength, and creep responses of these protein polymers, a moderate decrease in resilience was observed. The targeted resilience criterion for crosslinked systems was greater than 80% at a 35-40% strain. We suggest that crosslinking stabilizes the semi-rigid endblocks beyond the effects of physically crosslinking alone. Since crosslinking was performed prior to preconditioning, the capacity of the chain entanglements between the midblock and the endblock domains to

structurally rearrange in resonse to the conditioning protocol may have been restricted, in particular, limiting the response of the elastomeric midlbock. Future experiments could explore the effect of preconditioning prior to crosslinking and its subsequent effects on resilience.

These protein polymers were designed for acellular as well as cell based technologies. Gluteraldehyde was employed as a model crosslinking system but because of the cytotoxicity associated with this crosslinker, it is not adequate for crosslinking cell containing systems. In this regard, other groups have investigated crosslinking agents which are non-toxic to cells, including THPP [101, 102] and a natural crosslinker, genipin [65, 92]. Future experiments could explore the efficiency of these crosslinkers for the **LysB10** and **R4**. Presently, a research thrust in our laboratory is to modify the **LysB10** protein to include cell binding domains. In such systems, it might be advantageous to crosslink proteins in the presence of cells, therefore biocompatible crosslinking systems will have to be investigated.

The versatility of these materials has been displayed through the capacity to process triblock protein polymers into a variety of forms, including films, gels, and fiber networks [1, 5, 7, 253, 254]. The fabrication of artificial organs and engineered living tissues is dependent on the ability to generate and assemble novel materials into appropriate 2-D or 3-D structures and to precisely tailor material-related properties to achieve a desired clinical response [10]. It is likely that the design of artificial matrices will require the emulation of many, if not all, of the morphological and physiologic features of native tissues, thus reformulation of recombinant proteins into fiber networks has been investigated. In this regard, electrospinning technology has been employed in the fabrication of elastin-mimetic fiber networks. Specifically, in the late 1990s, our group was the first to demonstrate that electrospinning could be used to fabricate native and recombinant collagen and elastins into non-woven fiber networks comprised of

nanometer scale fibers that more closely mimic native scaffolds [41, 103, 255-257]. Future experiments could explore using **LysB10** and **R4** in the generation of nonwoven fiber networks. The ability to chemically crosslink **LysB10** and **R4** fibers has the potential to enhance mechanical responses. A complete description of the science of electrospinning and the current pursuits of electrospinning elastin and recombinant elastin proteins can be found in **Appendix B**.

As an example, electrospinning of the **B9** protein polymer demonstrated promising results in the development of a protein scaffold for tissue engineering with mechanical behaviors approaching those of the elastin fiber network component of a blood vessel (unpublished data). It is likely that mechanical behaviors and biostability of electrospun fiber networks can be enhanced with chemical crosslinking, thus **LysB10** and **R4** afford the potential to create superior scaffolding materials.

Alternative methods to modulate mechanical behaviors of fiber networks, specifically thermal annealing, have been investigated. Thermal annealing takes place in the hydrated state well above the protein's inverse transition temperature (60°C). Thermal annealing has been employed as a processing strategy to alter the microstructure of polymeric materials, most often to increase the crystallinity or to modulate microphase separation in order to improve material or application dependent properties, including strength or stiffness [258-260], hardness [259], viscoelastic properties [261, 262], water absorptive properties [261, 263], or photoluminescence [263].

Thermal annealing of **B9** fiber networks showed encouraging results for improving network mechanical responses. This treatment appears to induce a temperature triggered phase mixing of midblock and endblock regions over this thermal transition as determined from solid-state NMR, which has substantial impact on the hydration levels of fiber networks. Significantly, a ~50% decrease in equilibrium swelling

ratio was assocated with thermal annealing. Thermally induced enhancement to mechanical properties was observed as an increase in ultimate tensile strength and elastic modulus, and likely is a consequence of both thermally induced interpenetration of hydrophobic and hydrophilic domains and the resultant decrease in water content (unpublished data). It is likely that we can exploit tunable control over these properties through thermal annealing in both fiber networks and film based systems therefore serving as a potential method of modulating mechanical responses of **LysB10** and **R4** proteins processed as films, gels or fiber networks.

Chapter 3. Biocompatibility of Recombinant Elastin-Mimetic Proteins. The triblock copolymer, designated **B9**, contains identical hydrophobic endblocks with $[(IPAVG)_4(VPAVG)]$ repeat sequences, separated by a central hydrophilic block with repeating units of $[(VPGVG)_2(VPGEG)(VPGVG)_2]$ [2] and reversibly self-assembles from concentrated aqueous solution above the T_t of the hydrophobic endblocks (~18°C) to form a stable, water solvated, interlocking network. *In vivo* studies have demonstrated excellent blood contacting properties in a primate arteriovenous shunt model when the triblock copolymer, **B9,** is coated as a thin film on the lumen of a small diameter vascular graft [7]. However, long-term biocompatibility and biostability for any physically crosslinked protein-based materials has yet to be fully defined.

Specific reports documenting *in vivo* responses to elastin-mimetic protein implants have been limited; largely confined to several studies performed 15 to 20 years ago on proteins synthesized chemically and subject to radiation crosslinking [82, 121] In these investigations, homopolymers or copolymers composed of VPGVG, VPGKG, VPGEG, IPAVG, and VPAVG reportedly did not induce significant inflammatory or immune mediated reactions [82, 121-123].

The evaluation of *in vivo* biocompatibility has largely been based on characterizing local tissue responses to subcutaneously implanted materials where the

intensity and duration of the inflammation and wound healing, including capsule formation, is evaluated histologically [133, 134]. In this report, **B9** implants initiated limited local inflammatory activity and displayed among the thinnest fibrous capsule observed for comparable implant sites and period of implantation [135-141]. FACS analysis of peritoneal lavage fluid harvested one week after injection confirms biocompatibility with no apparent difference in either the number or type of inflammatory cells observed in control non-injected mice and those implanted with a **B9** gel. These data suggest that this biopolymer does not induce a significant inflammatory reaction.

To assess biostability of **B9** hydrogels, we have employed magnetic resonance imaging (MRI) to monitor implant volume changes for the duration of the experiment [162-164]. To date, **B9** hydrogel implants have been surprisingly stable, retaining greater than 60% of their original volume at seven months. Most biomaterials whose integrity is based on self-association of hydrophobic constituents display short-lived stability *in vivo* and have been utilized for drug delivery or in wound healing applications. To our knowledge, these *in vivo* studies are the first to demonstrate that self-assembled protein-based materials of any form can be designed with structural stability approaching that displayed by many electrostatically or covalently crosslinked biopolymers. This study is ongoing. When significant biodegradation is observed, the implant and surrounding tissue will be excised and examined histologically.

The work presented in Chapter 3 serves as a preliminary study to define protocols necessary for *in vivo* evaluation of these materials, including, endotoxin removal from amphiphilic recombinant elastin-mimetic proteins, fabrication of uniform hydrogel implants, histological evaluations of those hydrogels, and *in vivo* evaluation using the MRI, in addition to establishing methodologies for data analysis.

Given the biostability of physically crosslinked systems, it would be interesting to evaluate the biostability of physically and chemically crosslinked systems and thus, the

impact that crosslinking has on the stability of these proteins *in vivo*. Chemically crosslinked **LysB10** and **R4** hydrogels can be employed for these studies. It is likely these proteins will exhibit enhanced biostability characteristics when crosslinked with gluteraldehyde or other chemical agents as compared to physically crosslinked **B9** proteins. Given the longevity of these materials in vivo and their hemocompatibility, it is likely they will find utility as structural components of artificial organs and engineered living tissues, as carriers for controlled drug release, or as biocompatible surface coatings.

Chapter 4. Recombinant Elastin Protein Expression in *Pichia pastoris.*

Recombinant elastin proteins have traditionally been expressed through microbial expression in *E.coli* [241]. Nonetheless, recognized drawbacks exist, specifically, difficult target protein purification and endotoxin contamination during protein extraction. As an alternative, the methylotropic yeast, *P. pastoris* was investigated for elastin expression and secretion. Notably, *P. pastoris* secretes very low levels of native proteins, which simplifies purification protocols [1, 242]. Moreover, endotoxin is not present as a potential contaminant. Tropoelastin, collagen, and silk-like protein have all been expressed in yeast with varying degrees of success [222-225].

In the present study, we have demonstrated the expression of a 56 kDa elastin-like protein, **Yeast ELP,** from *P. pastoris* based on the pentapeptide repeat $(VPGVG_2)VPGEG(VPGVG)_2$. A novel strategy was devised to construct a gene with enhanced sequence diversity that encodes a highly repetitive elastin-like protein polymer for expression in *P. pastoris*. Traditionally, large repetitive genes that comprise most protein polymers have been created using a concatemerization strategy where a pentapeptide repeat cassette (monomer repeat unit) is self-ligated in a head-to-tail fashion [2, 98]. While this strategy has proven suitable for expression of elastin-like proteins in *E. coli*, the translation of repetitive gene sequence, especially in other host

systems, is often associated with reduced levels of protein expression. Moreover, repetitive sequences are often prone to mutational events. Given these potential limitations, we designed a modified concatemerization strategy in which seven dissimilar monomer repeat units, encoding identical pentapeptide repeat sequences, served as a monomer library for the concatemerization reaction. We anticipate that this strategy will be useful for creating large, repetitive genes for a variety of expression systems; in order to more closely approach the genetic diversity inherent to native DNA sequences.

The expression of **Yeast ELP** served as a model system evaluating the efficacy of the monomer library concatamerization strategy in the synthesis of repetitive elastin genes for expression in *P. pastoris*. The ultimate goal of this work is to create an alternative expression system for multiblock elastin-mimetic protein polymers. **Yeast ELP** was a model protein based upon the sequence of the elastomeric midblock domain (E) of the **B9** protein [2, 4]. In order to construct a triblock (P-E-P), plastic-like domains (P) encoding the pentapeptide repeat, IPAVG, were constructed in an analogous manner using the modified concatamerization strategy described in Chapter 4. This work has been conducted in collaboration with the laboratory of Vincent Conticello, PhD at Emory University. Future work for this project includes assembling these elastic-like and plastic-like genes into a gene encoding the P-E-P triblock. This assembly strategy for such triblock copolymers has been extensively detailed in Chapter 2.

Yeast expression systems have become an increasingly attractive host for the expression of heterologous proteins [219, 220], due to their capacity to be incorporated into industrial-scale fermentation schemes characterized by high cell densities in relatively inexpensive media. In addition, heterologous proteins have been efficiently secreted into the expression medium, resulting in low-cost recovery of the protein. Significantly, endotoxin is not produced by yeast, thereby simplifying purification and sterilization strategies. However, **Yeast ELP** yields must be optimized for large-scale

expression. There are a variety of variables which can be modulated to improve expression. Fermentation will likely improve expression levels as higher cell densities can be achieved [228]. Additionally, it has been noted that induction levels increase three to five times in cells which are fed methanol at growth-limiting rates relative to growing cells in excess methanol. A fermenter would allow for the controlled feeding of methanol and enable monitoring of methanol feed rate and dissolved oxygen levels within the culture [228]. Other alternatives which can be explored for optimizing protein expression including switching expression vector, employing alternative signal sequence, or utilizing a different *P. pastoris* expression strain.

Additionally, the potential exists to generate glycosylated ELPs through incorporating appropriate glycosylation sites. The synthetic strategy we employ in the genetic design allows for incorporation of glycosylation recognition sequences to be incorporated into the elastin gene, for example, Asn-X-Ser/Thr, the recognition sequence for N-glycosylation in *P. pastoris*. Indeed, several approaches such as genomics, combinatorial libraries, and synthetic chemistry have been employed for sugar chain remodeling of human proteins in *P. pastoris* and other expression systems [250-252]. Glycoengineering recombinant elastin molecules with strategically placed carbohydrates has the potential to increase molecular stability, solubility, and reduce immunogenicity [264].

APPENDIX A

DNA Coding Sequences

A.1 Coding sequences for DNA monomer repeat units of individual blocks of **LysB10**……122

A.2 Coding sequences for DNA monomer repeat units of individual blocks of **R4**….. 123

Table A-1. Coding sequences for DNA monomer repeat units of individual blocks of **Lys B10**

Elastin Monomer (E_1)

Val Pro Gly Ala Gly Val Pro Gly Ala Gly Val Pro
AGCTTGAAGAC GTT CCA GGT GCA GGC GTA CCG GGT GCT GGC GTT CCG
*Hin*D III *Bbs* I

Gly Ala Gly Val Pro Gly Ala Gly Val Pro Gly Ala Gly Val Pro
GGT GAA GGT GTT CCA GGC GCA GGT GTA CCG GGT GCG GGT GTT CCA AGAGACGG
*Bsm*B I *Bam*H I

Plastin Monomer (P_1)

Ile Pro Ala Val Gly Ile Pro Ala Val Gly Ile Pro Ala Val Gly
AGCTTGAAGAC ATT CCA GCT GTT GGT ATC CCG GCT GTT GGT ATC CCA GCT GTT GGC
*Hin*D III *Bbs* I

Ile Pro Ala Val Gly Ile Pro Ala Val Gly Ile Pro
ATT CCG GCT GTA GGT ATC CCG GCT GTT GGT ATT CCA AGAGACGG
*Bsm*B I *Bam*H I

Lysine Insert (I)

Ile Pro Ala Val Gly Lys Ala Ala Lys Val Pro Gly Ala Gly Val Pro
AGCTTGAAGAC ATT CCA GCT GTT GGT AAG GCG GCC AAG GTT CCA GGT GCA GGC GTT CCA AGAGACG
*Hin*D III *Bbs* I *Bsm*B I *Bam*H I

Lysine Adaptor

Val Pro Ala Val Gly Lys Val Pro Pro
GATCC GTT CCA GCT GTT GGT AAG GTT CCA AGAGACGGTACCCGTCT CTT CCA
*Bam*H I *Bsm*B I *Bsm*B I
Ala Val Gly Lys Ala Ala Lys Ala Stop
GCT GTT GGT AAG GCG GCC AAG GCG TAA
*Hin*D III

Table A-2. Coding sequences for DNA monomer repeat units of individual blocks of **R4**

Elastin Monomer (E_2)

```
                    Val  Pro  Gly  Ile  Gly  Val  Pro  Gly  Ile  Gly  Val  Pro
AGCTTGAAGAC GTT CCA GGT ATT GGC GTT CCG GGT ATC GGT GTG CCA
HinD III          Bbs I
Gly  Ile  Gly  Val  Pro  Gly  Ile  Gly  Val  Pro  Gly  Ile  Gly  Val  Pro
GGC ATC GGT GTA CCG GGT ATT GGC GTT CCA GGC ATT GGC GTT CCA AGAGACGG
                                    BsmB I          BamH I
```

Plastin Monomer (P_2)

```
                    Ile  Pro  Ala  Val  Gly  Ile  Pro  Ala  Val  Gly  Ile  Pro  Ala  Val  Gly
AGCTTGAAGAC ATT CCA GCT GTT GGT ATC CCA GCT GTT GGT ATC CCA GCT GTT GGC
HinD III          Bbs I

Ile  Pro  Ala  Val  Gly  Ile  Pro  Ala  Val  Gly  Ile  Pro
ATT CCG GCT GTA GGT ATC CCG GCA GTG GGC ATT CCA AGAGACGG
BsmB I          BamH I
```

Lysine Insert (I)

```
                    Ile  Pro  Ala  Val  Gly  Lys  Ala  Ala  Lys  Val  Pro  Gly  Ala  Gly  Val  Pro
AGCTTGAAGAC ATT CCA GCT GTT GGT AAG GCG GCC AAG GTT CCA GGT GCA GGC GTT CCA AGAGACG
HinD III          Bbs I                                                          BsmB I          BamH I
```

Lysine Adaptor

```
          Val  Pro  Ala  Val  Gly  Lys  Val  Pro                                   Pro
GATCC GTT CCA GCT GTT GGT AAG GTT CCA AGAGACGGTACCCGTCT CTT CCA
BamH I                              BsmB I                                  BsmB I
Ala  Val  Gly  Lys  Ala  Ala  Lys  Ala  Stop
GCT GTT GGT AAG GCG GCC AAG GCG TAA
                                    HinD III
```

Appendix B

Electrospun Elastin and Collagen Nano-Fibers

B.1 Introduction 133

B.2 Electrospinning as a biomedical fabrication technology 134

B.2.1 The science of electrospinning 134

B.2.2 Generation of nanofibers with controlled structures and morphology 136

B.3 Generation of collagen and elastin small diameter fibers and fiber networks 137

B.3.1 Native collagen and biological function 138

B.3.2 Collagen as a biomaterial 139

B.3.3 Electrospun collagen nanofibers 139

B.3.4 Biological role of elastin 142

B.3.5 Elastin as a biomaterial 143

B.3.6 Recombinant elastin technologies 144

B.3.7 Generation of elastin and elastin-mimetic small diameter fibers and networks 145

B.4 Generation of crosslinked fibers and fiber networks 148

B.4.1 Crosslinking collagen networks 149

B.4.2 Crosslinking elastin networks 149

B.5 Multicomponent electrospun assemblies 151

B.6 Elecrospun nanofiber networks and the potential for the incorporation of living cells 152

B.7 Future Trends: Biomedical applications for electrospun collagen and elastin nanofiber networks 153

Electrospun Elastin and Collagen Nano-Fibers

** Modified from Sallach RS and Chaikof EL. Electrospun Elastin and Collagen Nano-Fibers. Submitted as a Chapter to Handbook of Natural-based Polymers for Biomedical Applications*

B.1 Introduction

Current pursuits in the discipline of biomedicine, including artificial organs and engineered living tissues, are dependent on the ability to generate novel materials, fabricate or assemble materials into appropriate 2-D or 3-D structures, and to precisely tailor material-related properties in order to achieve a desired clinical response [10]. To that end, of profound importance is the development of artificial extracellular matrices (ECM). These structures are integral to the fashioning of microenvironments that are engineered for ideal mechanical and biological performance. It is likely this design will require the mimicry of many, if not all, morphological or physiologic features of native tissues. Decades of research have indeed demonstrated that as our ability to control the physical and biological properties of scaffolding materials improves, the quality of the tissues thus formed is enhanced.

More specifically, molecular and supramolecular organization of type I collagen and elastin fiber assemblies establishes and important paradigm for the design in the development of novel scaffolds. In the body, both tissues and organs are organized into 3-D structures, each having specific architectures, directly dependent upon its biological function. This architecture is believed to foster cellular ingrowth and proliferation by providing appropriate channels for mass transport and spatial cellular organization, thus directing new tissue formation. The use of electrospinning technology in the arena of biomedicine has expanded the capacity of native and recombinant proteins to be fabricated into artificial extracellular matrices that more closely mimic native scaffolds. This chapter will review efforts in the development of novel structural protein materials,

fabrication of nanofiber networks using electrospinning technology, and applications of subsequent structures in biomedicine.

B.2 Electrospinning as a biomedical fabrication technology

Tissue and organ systems can be considered in general terms as a fiber-reinforced composite material with associated mechanical properties largely a consequence of protein fiber networks. Electrospinning has been applied in this regard as a mechanism for generating protein nanofibers and nanofiber networks.

B.2.1 The science of electrospinning

Electrospinning is a technique which relies on electrostatic forces to produce nanometer to micrometer sized fibers from polymer solutions or melts. The generation of fibers by electrospinning was first patented in 1934 by Anton Formhals for textile and polymer science [265]. It was not until 1977 that a revived interest in electrospinning technology emerged within the field of biomedicine for applications of wound dressings [266]. Traditionally, engineering plastics and conducting polymers have been electrospun, but recently, with emphasis on tissue engineering and microelectronics, electrospinning protein polymers and carbon precursors have been explored.

Electrospinning is essentially a drawing process utilizing electrostatic interactions in the creation of exceptionally long fibers with uniform diameters. This process is different from traditional methods of fiber formation as it is based on elongation of a viscoelastic jet of polymer solution or melt. Since elongation is achieved without contact, as with other drawing processes, this method is optimal for the development of delicate nanofibers.

Electrospinning is a variant of the electrospraying technique. Both involve the use of voltage to create a jet of polymer solution. Electrospray involves the development of small droplets of low concentration solutions, a result of varicose break-up, and has been employed in areas such as mass spectrometry and ink jet printing. Alternatively, electrospinning results in the development of a small diameter fiber from highly viscous solutions. Fibers with large surface to volume ratios are produced through stretching as a consequence of the repulsion of surface charge and evaporation of the solvent [267].

There are three basic components to an electrospinning apparatus; a voltage supply, a spinneret connected to a syringe containing the polymer solution or melt, and a grounded collector. A high voltage is applied to the spinneret while the polymer solution is slowly being extruded. This induces evenly dispersed charges in a pendent drop at the tip of the spinneret, relaxing the fluid surface. This surface charge and the external Columbic forces from the electric field combine to form a tangential stress [268]. This causes the drop to become distorted into a shape known as a Taylor cone. At a critical threshold value, the electric field strength will overcome that of surface tension and the polymer solution will be ejected as a charged jet from the spinneret tip. As the jet travels to the grounded collector it undergoes a stretching and whipping phenomena which substantially reduces the diameter of this fiber. It is then collected on the grounded collecting apparatus creating a randomly oriented nonwoven fiber network [267].

It was initially considered that the nanometer sized fibers created by electrospinning were the result of splitting and splaying of the jet due to the repulsion of surface charges [269]. However, with high-speed photography the ability to capture images of jet instabilities revealed that it was rapid oscillations within the jet that were responsible for stretching the fibers [268]. The jet was seen to travel only a few centimeters in a straight path thereupon it entered into a conical envelope and was continuously bent and whipped into a spiraling loop. As the perimeter of the loops

increased, the diameter of the jet decreased [270]. Thinning of fiber diameters as much as 3 orders of magnitude have been noted [271].

B.2.2 Generation of nanofibers with controlled structures and morphology

Fiber morphology and diameter of fibers generated using the electrospinning technique is controlled by the experimental design and dependent on both formulation and operation parameters. Critical formulation parameters include solvent selection and protein concentration while operation parameters comprise applied voltage, gap distance, and flow rate. Through the modulation of these parameters, distinct fiber morphologies are observed. Many groups have investigated and optimized spinning conditions to produce desirable electrospun fibers. The formation of beaded fibers has been a concern and as a result of investigations by Reneker and others options for eliminating beads have been characterized [41, 272]. Most fibers produced by optimized electrospinning conditions have circular cross-sections while some exhibit a ribbon-like morphology, a physical difference dependent on solution concentration. For example, reports describing electrospinning of recombinant elastin proteins reveal solution concentration and flow rate to be most critical in controlling fiber morphology, as determined by high resolution microscopy. At low concentrations of recombinant elastin protein, Lys-25, (5 wt %) short, fragmented fibers were formed with a triangle- or spindle-shaped beaded morphology. At higher concentrations (10 wt %) uniform fibers were generated with diameters ranging between 300-400 nm with little variation in morphology with infrequent exception of fiber splitting at triangle-shaped bifurcation points. At 20 wt % a new morphological pattern was noted, defined by the emergence of flat or ribbon-shaped fibers, which appeared twisted during deposition [41].

Controlling the diameter of circular fibers has been widely discussed in literature. It has been determined that certain parameters are critical in influencing the diameter,

including polymer concentration, electric field strength, and flow rate. The following plots summarize the experimental evidence of the relationship of electrospinning parameters to fiber morphology **(Figure B-1)** [271, 273, 274].

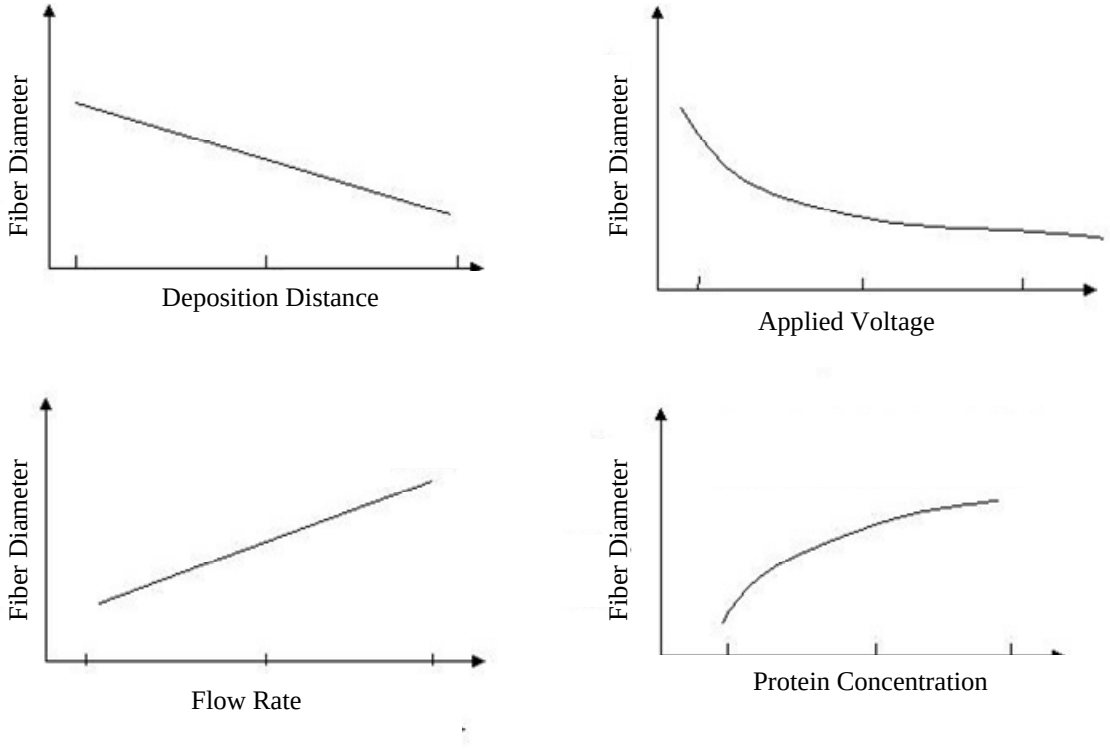

Figure B-1. Experimental evidence summary plots of the relationship of electrospinning parameters to fiber morphology. **(A)** Fiber diameter as a function of deposition distance at constant applied voltage, flow rate and protein concentration, **(B)** Fiber diameter as a function of applied voltage at constant flow rate, depositon distance, and protein concentration**, (C)** fiber diameter as a function of flow rate at constant applied voltage, deposition distance, and protein concentration**, (D)** Fiber diameter as a function of protein concentration at constant applied voltage, deposition distance, and flow rate. (adapted from Bowlin, VCU, http://www.egr.vcu.edu/bme/faculty/bme-bowlin.html)

B.3 Generation of collagen and elastin small diameter fibers and fiber networks

It is as integrated fiber networks that collagen and elastin constitute the fundamental structural elements of tissue. Thus, whether matrix proteins are produced

synthetically or extracted from native tissue, it is likely that their versatility as scaffolds for tissue engineering applications will be significantly enhanced when reformulated into fiber networks.

B.3.1 Native collagen and biological function

As a principle constituent of the extracellular matrix, collagen is ubiquitously present in all connective tissues. The most abundant form of collagen isolated from adult connective tissues, such as skin, tendon, and bone, is type I collagen. Characteristically, it is composed of two α 1(I) chains and one α 2(I) chain, each slightly more than 1000 amino acids long, and organized as a triple helix and stabilized primarily by hydrogen bonds [275]. A single molecule of type I collagen has a molecular mass of 285 kDa, a width of ~14 Å, and a length of ~3000 Å. In native connective tissues, type I collagen molecules form fibrillar elements twenty to several hundred nanometers in diameter that are organized into protein networks of varying architecture. Functionally, collagen fiber networks act to resist high strain deformation and in the process transmit forces, dissipate energy, and prevent premature tissue mechanical failure [276].

Collagen's tensile strength, its stability in a biological environment, and its capacity to present specific ligands for cell surface receptors are properties that are in large measure dependent on the integrity of collagen's characteristic triple-helical conformation [275, 277-279]. For example, the energy requirement for collagen degradation by collagenase I (MMP-1) is reduced by a factor of *two* if native fibrillar (multimeric) collagen is in a monomeric form, but by a factor of ten if the triple helix is denatured [280]. Thus, while the self-assembly of monomeric collagen into an ordered supramolecular system is an important physiologic mechanism for fibril formation, the uniquely coiled-coil triple helix is the dominant structural feature. This structure dictates collagen stability and defines its mechanical properties. Consequently, the generation of

a robust load-bearing fiber network with appropriate mechanical integrity and biological function mandates maximal preservation of the collagen triple helix during the process of fiber formation.

B.3.2 Collagen as a biomaterial

Collagen is a biodegradable, biocompatible, and non-immunogenic structural protein, which makes it a suitable component for a variety of biomedical applications. As a biomaterial, collagen has been predominantly used after processing into a dry powder or slurry, a hydrogel after solution phase cross-linking, or as a porous matrix with or without the addition of other components after freeze-drying [281]. For example, collagen has been used in cosmetic and urological surgery as an injectable compound for tissue augmentation [282]; in orthopedic surgery as an implantable matrix to promote bone growth [283-285]; and in plastic and general surgery as a topical agent for the treatment of both chronic non-healing wounds and burn injuries or as a template for tissue regeneration [286, 287]. However, it is as a native protein network that the versatility of collagen as scaffolding material could have the most profound impact in the area of tissue engineering. Notably, collagen fiber networks constitute the principle structural elements of a variety of acellular bioprosthetic tissue substitutes, such as porcine heart valves and bovine artery heterografts, as well as other tissue derived matrices, including porcine subintestinal submucosa and bovine pericardium.

B.3.3 Electrospun collagen nanofibers

The production of collagen fibers has been reported, and has traditionally relied upon wet spinning processes that involve the extrusion of a protein solution through a spinneret into an acid-salt coagulating bath, which usually contains aqueous ammonium sulfate, acetic acid, isopropanol, or acetone. Further treatments in ethanol and acetone

solutions are often required for fiber dehydration. For example, Hirano et al. [288] described the production of chitosan-collagen fibers (d > 30 μm) produced by wet spinning from an aqueous acetic acid-methanol solution into an ammonia solution containing 40-43% ammonium sulfate. Likewise, Fofonoff and Bell [289] have reported a method for forming collagen fibers (d > 100 μm) by wet spinning from an aqueous acetic acid solution into a heated coagulating bath containing alkaline alginic or boric acid. The collagen fiber is formed by polymerization when the acid in the collagen is neutralized upon contact with the neutralizing solution and the fibers are subsequently dehydrated in acetone and ethanol baths. An additional example is provided by Furukawa et al. [290] in which solubilized collagen is spun into a coagulating bath containing an inorganic salt, such as sodium, aluminum, or ammonium sulfate. Nonetheless, limitations of these approaches are recognized, including: (i) the use of conditions which likely induce significant conformational changes in native protein structure, including protein denaturation; (ii) the generation of fibers that range from tens to hundreds of microns in diameter and are much larger than those observed in native tissues [291-293]; and (iii) a reliance on biologically toxic solvent systems. Although research in the area of wet spinning collagen has advanced and significant improvements have been achieved, an alternate approach for submicron collagen fiber formation, electrospinning, has recently been investigated [42, 45, 256, 294-297]. The architecture generated from this process is similar to that found in most native extracellular matrices, thus underscoring the electrospinning technique for design of novel scaffolds.

The first report of electrospun collagen fibers employed a weak acid solution to electrospin type I collagen-polyethylene oxide (PEO) blends at ambient temperature and pressure. High resolution microscopy was employed to resolve the influence of critical electrospinning parameters, specifically, solution viscosity, conductivity, and flow rate on subsequent fiber ultrastructure and size. A variety of fiber microstructures were

observed: beaded, round, and ribbon-like filaments. Ultimately, fibers of uniform morphology and ultrastructure, with average diameters of 100-150 nm, were generated. Significantly, this procedure outlined a non-toxic and non-denaturing approach for the generation of collagen containing nanofibers and nonwoven fiber networks **(Figure B-2)** [256].

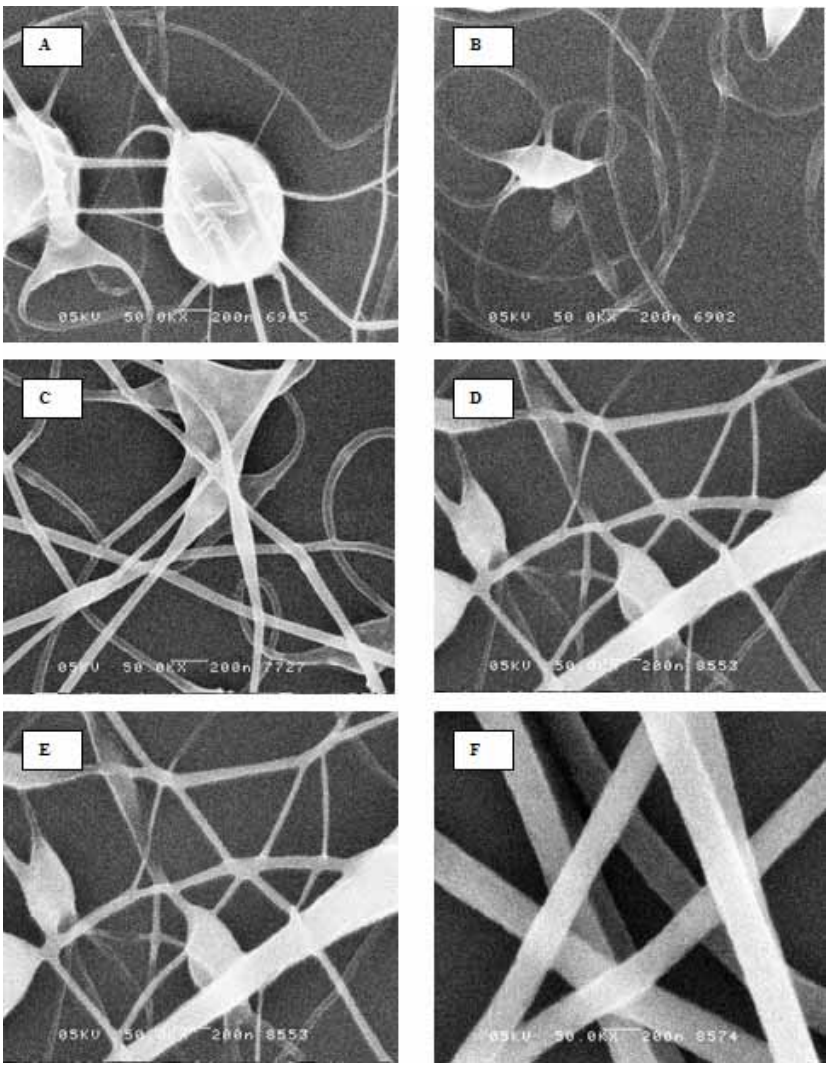

Figure B-2. SEM micrographs of PEO-collagen blended fibers spun from 2 wt% acid solution (34 mM NaCl) at a flow rate of 100 µl min^{-1} and at different collagen–PEO weight ratios: **(A)** 30 : 1, 50 000x magnification, **(B)** 10 : 1, 50 000x magnification **(C)** 5 : 1, 50 000x magnification, **(D)** 2: 1, 50 000x magnification, **(E)** 1 : 1, 20 000x magnification, **(F)** 1 : 2, 50 000x magnification. Fibers of uniform morphology and ultrastructure, with average diameters of 100-150 nm, were generated (adapted from [256]).

Similarly, other approaches have investigated various collagen sources and isotypes in the production of collagen nanofibers. Typically, acid soluble type I collagen from rat tail tendons or calf skin have been utilized. Type I and Type III collagen from human placenta has also been investigated [294]. Results indicate that identity and source of collagen are significant to the morphological, mechanical, and biological properties of the electrospun collagen networks. Additionally, solvent such as HFIP (1,1,1,3,3,3 hexafluoro-2-propanol) have been used for electrospinning of collagen. While some investigators have claimed preservation of native collagen structure, studies in our own laboratory demonstrate complete loss of triple helical structure when examined by circular dichroism spectroscopy, differential scanning calorimetry, or x-ray diffraction [256, 297, 298].

B.3.4 Biological role of elastin

Native elastin is a highly insoluble matrix protein which functions to provide extensibility and resilience to most tissues of the body. Elastin networks are responsible for maximizing the durability of tissues that are loaded by repetitive forces by minimizing the conversion of mechanical energy to heat which ultimately results in tissue damage [52]. In addition to the structural role, elastin creates an environment, which promotes proper cell function and modulates cellular attachment, growth, and responses to mechanical stimuli.

Elastin fibers appear to exist as two morphologically different components, a highly isotropic amorphous elastin constituent within an organized microfibrilar scaffold [69]. Understanding of the mechanism of fiber assembly in native elastin is limited; however, it appears to take place in proximity to the cell membrane where microfibrils emerge as fiber bundles. Amorphous elastin is synthesized by smooth muscle cells as a soluble monomer, the 72 kDa precursor tropoelastin, and is secreted within each fiber

bundle. Reminiscent of natural rubber, it is organized into insoluble networks reminiscent through enzymatic crosslinking via oxidation by lysyl oxidase [71].

The distinctive composition of tropoelastin affords unique physical properties of this structural protein. Tropoelastin is rich in glycine (33%), proline (10-13%), and other hydrophobic residues (44%) rendering elastin an extremely hydrophobic protein [61]. Tropoelastin contains distinct crosslinking and hydrophobic domains. Crosslinking domains are alanine rich, containing pairs of lysine residues thereby facilitating intermolecular crosslinking. Alternatively, the hydrophobic domains within tropoelastin are composed of three-quarters valine, glycine, proline, and alanine. Investigations have elucidated that the precise sequence and size of this region are not critical for appropriate function; however, the total size of the protein polymer, 750-800 residues, is highly conserved among species [62].

B.3.5 Elastin as a Biomaterial

A failure of current acellular bioprostheses is the inability to exhibit mechanical properties that match those of native tissues, primarily a result of the loss or degradation of the elastin protein networks, thereby reinforcing the importance of elastin fiber networks is bioprosthetic design. Isolated elastin matrices from acellular allo- and xenogenic tissues have been investigated as scaffolding materials with these studies confirming that native protein fiber networks can be used to fabricate an artificial scaffold. However, these scaffolds often require the addition of structural proteins or must be seeded with cells to demonstrate proper biochemical and biomechanical function [40, 299]. Despite successes, recognized drawbacks, including tissue heterogeneity, incomplete cell extraction, the generation of ill-defined chemical crosslinks, progressive biodegradation, and the potential risk of viral transmission from animal tissue, continue to dampen enthusiasm for this approach. As a promising

alternative in the generation of biomimetic scaffolds, soluble elastin, derived either as fragmented elastin, in the form of alpha- or kappa-elastin, or as the natural monomer tropoelastin [42], have been successfully electrospun. Additionally, through genetic engineering of synthetic polypeptides, novel elastin proteins have been created for such applications. Utilizing these strategies affords the ability to tailor matrix composition and content, fiber size and architecture, or other features that may influence 3-D hierarchical tissue structure, thus enabling the ability to design a scaffold with precisely defined mechanical and biological properties.

B.3.6 Recombinant elastin technologies

It has been postulated that the generation of protein polymers that mimic native structural proteins and the assembly of these recombinant proteins either alone or in combination with naturally occurring matrix proteins provides an opportunity to optimize the mechanical properties of artificial tissues. In this way, recombinant technologies have been pursued in the generation of elastin-mimetic protein polymers. Through the structural characterization of the hydrophobic domains, the ability to base synthetic protein polymers on native elastin sequences is feasible. The pioneering work of Urry elucidated the elastomeric pentapeptide repeat, VPGVG, from human elastin, which now serves as the fundamental sequence extensively investigated by both chemical methodologies and recombinant technology [79, 80]. VPGVG is a common repeat unit within the hydrophobic domain of human elastin and is responsible for resultant elastic properties. Additionally, this domain is responsible for facilitating fiber formation through coacervation phenomena, behaviors consistent with native elastin. Spectroscopic analysis has revealed that native elastin, and likewise, protein polymers containing this repeat, exhibit β-turns and helical β- spiral conformations and display an inverse temperature transition defined by the generation of a more ordered system upon

increasing temperature. This loss of entropy is a consequence of protein folding into β - spiral conformation and the subsequent reorientation of water from the elastin chain [81]. Studies have elucidated the amino acid in the fourth (X) position (VPGXG) modulates the coacervation temperature with more polar amino acids increasing transition temperature [66, 67, 83]. Preservation of the glycine and proline residues maintain the structure and function of elastin analogs [83]. This discovery has led to the generation of recombinant elastin analogs designed for biomedical applications. For instance, this technology has been employed in the design of amphiphilic elastin protein polymers consisting of hydrophobic and hydrophilic domains. Through precise sequence design and control of processing conditions, these elastin analogs exhibit a wide range of properties advantageous for biomedical applications, as micelles, physically crosslinked hydrogels, or nanofiber networks [1-3, 5, 83]. Additionally, groups have incorporated cell binding domains, RGD or REDV, into elastin sequences to functionalize elastin matrix components for endothelial cell attachment [85, 86]. Genetic engineering strategies afford the ability to modulate macroscopic properties on the molecular level. Therefore the potential exists to generate synthetic polypeptides that mimic native proteins. In this regard, there is an inherent opportunity to precisely engineer recombinant sequences to targeted design criteria such as tensile strength, elastic modulus, viscoelasticity, and in vivo stability, as well as the optimization of a desired host response.

B.3.7 Generation of elastin and elastin-mimetic small diameter fibers and fiber networks

As material for tissue engineering applications, elastin is intended to provide both mechanical support and potentially act as a scaffold for cellular repopulation. As such, it is likely when reformulated into fiber networks that the versatility of elastin as a scaffolding material will be significantly improved. In this regard, electrospinning has

been investigated as a mechanism for generating fibers with diameters < 1 μm. When proteins are reformulated as fiber systems desired mechanical and biological properties can be achieved for biomedical applications. For instance, flexibility of a fibrous system can be controlled by either a decrease in fiber diameter or an increase in fiber number [300]. Thus, reformulating elastin proteins into fiber networks provides an additional level of control over the properties of the artificial matrix designed. Specifically, studies have indicated electrospun fabrics composed of small diameter fibers (<1μm) were found to have decreased porosity, increased fiber density, increased mechanical strength, as well as an optimized biological environment for promoting cell adhesion as compared to larger diameter fibers (7μm) [42, 47]

Previous reports have demonstrated the feasibility of electrospinning soluble elastin as a single component system as well as in collagen-elastin blends. Concentrated solutions of soluble elastin produced fibers with average diameters from ranging from 100 nm to 3 μm have been generated with fiber diameter being highly dependent upon solvent systems utilized [42, 45, 46, 297]. Additionally, collagen-elastin blends produced fibers with diameters ranging from nanometers to micrometers [297, 301]. Subsequent work has endeavored to improve the mechanical properties, specifically the compliance and mechanical strength of these elastin based matrices, through the addition of synthetic polymeric materials such as PLGA, poly (D,L-lactide-co-glycolide). Notably, compliance testing of collagen-elastin-PLGA electrospun scaffolds demonstrated behavior consistent with in vivo mechanical behavior of bovine arteries. Specifically, controlling the ratio of collagen, elastin, and PLGA facilitated the modulation of electrospinning characteristics as well as the strength and stability of the electrospun scaffold, as a burst pressure of nearly 12 times normal systolic pressure was observed [295].

Recently, attempts to electrospun human tropoelastin have been undertaken. Interestingly, electrospinning of these materials produced ribbon-shaped fibers, several microns in diameter, which appeared to retain a unique periodicity, controlled by modulating the solution flow rate. Morphology of these fibers is reminiscent of the topology of elastin in native tissues, for instance, the architecture of the elastic lamina within blood vessels [42].

Notwithstanding reports with promising results, important limitations remain associated with native elastin electrospinning strategies. In consideration, significant investigation in the design of recombinant elastin proteins, microbial expression of these proteins, and reformulation into protein fiber networks by means of electrospinning has been explored. The first report of fiber formation from an elastin-like analog was described utilizing a 81 kDa recombinant elastin peptide polymer, Lys-25, comprised of the repeat sequence (Val-Pro-Gly-Val-Gly)4(Val-Pro-Gly-Lys-Gly). Electrospinning of a 15-wt% solution afforded a fabric with a unimodal distribution of fiber diameters **(Figure B-3).** Moreover, in the absence of high rotational or translational speeds on a collecting mandrel, fiber orientation was random. Interestingly, pulsed field gradient NMR spectroscopy was utilized to access network porosity and pore size distribution in 3-D fabrics and revealed Lys-25 electrospun matrices as physiologically ideal for cellular seeding in that regard (Fig 4) [41, 103]. While a number of elastin-mimetic protein polymers can be fabricated as fibers and covalently crosslinked, a family of recombinant elastin triblock copolymers containing chemically distinct midblocks have been investigated in the generation of virtually crosslinked fibers and fiber networks. Specifically, these studies demonstrate that self-assembling triblock elastin analogues have the capacity to form stable fibers, but without a requirement for chemical crosslinking [1]. As an example, electrospinning was used to produce tubular conduits from a triblock copolymer. Mechanical properties were assessed in PBS at 37°C.

Hydrated samples displayed an elastic modulus of 0.29 ± 0.03 MPa, a strain to failure of 151 ± 29%; values comparable to the elastin component of the arterial wall (Young's modulus ~ 0.3 MPa) [30, 302].

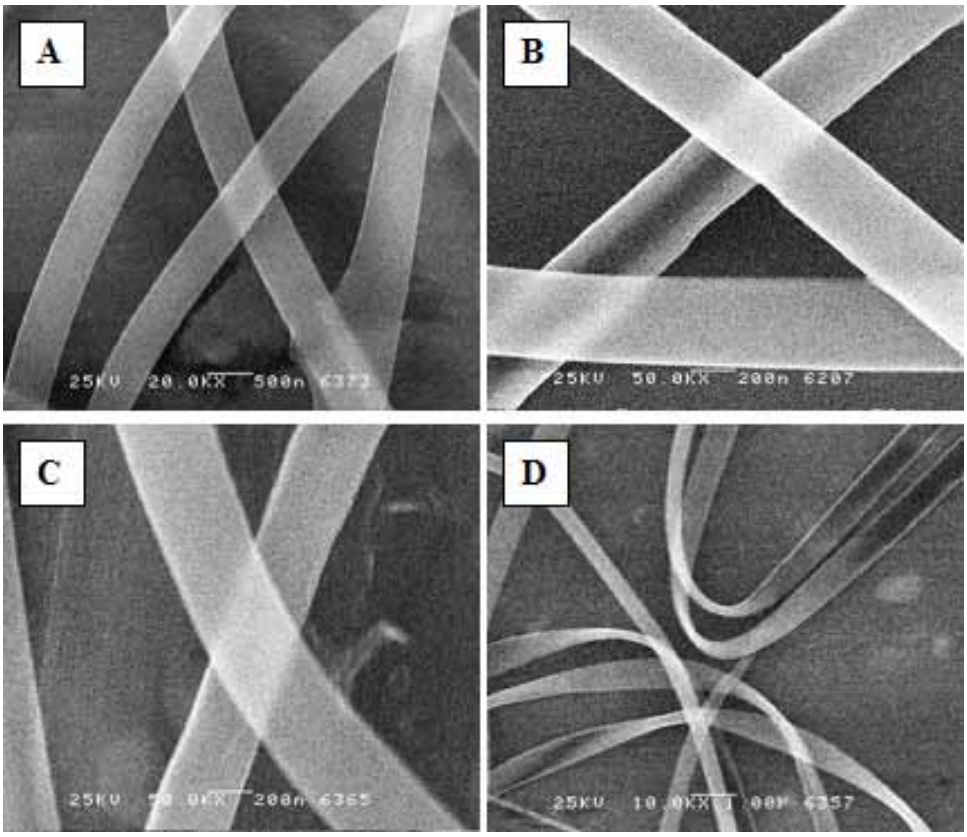

Figure B-3. First reported fiber formation from an elastin-like analog utilizing a 81 kDa recombinant elastin peptide polymer. SEM micrographs of elastin-mimetic peptide fibers spun from 15 wt % solution at 50 **(A),** 100 **(B),** 150 **(C),** and 200 µl min^{-1} **(D)** flow rate. Electrospinning of a 15-wt% solution afforded a fabric with a unimodal distribution of fiber diameters (adapted from [41]).

B.4 Generation of crosslinked fibers and fiber networks

It is generally understood that crosslinking is necessary for the maintenance of biostability in engineered collagen and elastin scaffolds. In native tissues, lysyl oxidase, a specific amine oxidase, catalyzes the formation of aldehyde cross-link intermediates in

the solid state providing intermolecular crosslinking within collagen and elastin networks. Presumably, the incorporation of various degrees of crosslinking can be used to further tailor and control the material properties of the scaffold to specific applications.

B.4.1 Crosslinking collagen networks

Glutaraldehyde is the traditional crosslinking agent for bioartificial devices. While it has been shown to enhance stability and further reduce immunogenicity, it does exhibit potential cytotoxicity and late induction of collagen calcification. Therefore, alternative crosslinking approaches have been reported, including chemical (carboiimide, diisocyanates, and polypoxy compounds) and solid state photocrosslinking. For example, Chaikof and colleagues described the derivitization of type I collagen with methacrylate groups [103, 303] and cinnamate groups for photocrosslinking [304] while preserving collagen's triple helical structure.

B.4.2 Crosslinking elastin networks

Crosslinking of native elastin, as well as synthetic elastin-mimetic protein polymers has most often been investigated using solution phase systems; either gamma irradiation [88, 90], chemical [95-97, 103], or enzymatic based approaches [305], as well as solid state photocrosslinking [303]. Nevertheless, for most biomedical applications of synthetic scaffolds, vapor phase glutaraldehyde crosslinking is currently the system utilized, with successful in vitro and in vivo biocompatibility results. Directed efforts in alternative chemical crosslinking strategies, in which no additional chemical entities are introduced and stable amide linkages are formed, have also been investigated. For example, mixed solutions of EDC (N-(3-dimethylaminopropyl)-N'-ethylcarboiimide hydrochloride) and NHS (N-hydroxysuccinimide) were employed to crosslink electrospun collagen-elastin scaffolds with no apparent alteration to fiber morphology as determined

my microscopy analysis. Scaffold stability and biocompatibility was assessed in vitro through cell seeding of smooth muscle cells with promising results [297].

Alternatively, incorporation of reactive lysine residues into recombinant elastin design provides the ε-amino moiety of lysine for crosslinking using a variety of approaches. This strategy affords the ability to achieve precise control over the nature and degree of crosslinking, and facilitates spatial and temporal control over the reaction process. Specific investigations into reactive group spacing as well as crosslinking strategies on the modulation of important biological behaviors of elastin analogs has been conducted with the general conclusion that the placement of well defined crosslinks enhance the biostability of elastin and improve biologically relevant properties. For example, methacrylate groups were incorporated into the protein polymer backbone in order to facilitate site-specific solid-state photocrosslinking using either UV or visible light activated photoinitiators [103]. Mechanical analysis confirmed superior biologically relevant behaviors comparable to the elastic behavior comparable to native elastin.

Significantly, in response to deleterious effects of chemical crosslinking reagents, a new class of recombinant proteins have been investigated, self-assembling triblock elastin copolymers, which have the capacity to form stable fibers, but without a requirement for chemical crosslinking [1-3]. Due to the nature of the copolymer design, they form physically or virtually crosslinked systems. Notably, nanofiber formation was influenced by solvent conditions with nanofibers in the diameter range of 100-400 nm generated utilizing a solvent which identically solvates both blocks of the copolymer while nanofibers with diameter ranging from 800 nm^{-3} μm generated from an aqueous solution which preferentially solvates only the midblock. Subsequent mechanical evaluation indicates that modulation of elastic and plastic behavior of the triblock protein is directly dependent on the solvent systems used in fabrication. In particular, mechanical evaluation of the triblock elastin protein fibers under physiological conditions

revealed elastic modulus and ultimate tensile strength comparable to that of native tissues such as the elastin component of the arterial wall (Young's modulus ~ 0.3 MPa) [30, 302].

B.5 Multicomponent electrospun assemblies

It is likely that the molecular structure and supramolecular organization of collagen and elastin fiber assemblies within native tissues establishes an important paradigm for the design of a biomimetic scaffold. Therefore, the hierarchal assembly of these protein fiber networks is essential for generating constructs with both enhanced biostability and blood contactability, as well as mechanical properties that closely match those of the native tissue. As such, the potential of electrospinning multicomponent systems in the design of biomimetic scaffolds is substantial since it affords an additional level of control in vitro to recreate native architectures.

In this regard, two electrospinning techniques have been employed to create nanofibrous bicomposites, multilayering electrospinning and multicomponent (mixing) electrospinning [306]. Multilayering electrospinning requires sequential deposition of two unique materials onto the same collector, such that a hierarchal ordered structure is obtained. This method has been employed to fabricate constructs composed of synthetic polymers lined with biocompatible native proteins such as collagen, fibrin and laminin.

As an alternate technique, mixing electrospinning, in which two unique materials are simultaneously electrospun from different syringes, ultimately yields a fiber network of mixed identity. This method is of particular interest in creating tubular constructs for tissue engineering of blood vessels. For instance, a bilayered construct can be engineered with an outer layer of circumferentially oriented fibers mimicking the tunica media and an inner layer of randomly oriented fibers acting as the elastic lamina of the

blood vessel [307]. This method has also been employed to modulate porosity and microvoid spaces within an electrospun scaffold through fiber-leaching. Several such studies involving simultaneous spinning of PEO and other synthetic or natural polymers, followed by dissolution of the PEO component in water have been investigated in the modulation of scaffold architecture [256, 306].

Additionally, blended solutions have been investigated, specifically collagen-elastin blends, which yield a fiber matrix in which singular components are indistinguishable. These types of matrices have exhibited enhanced mechanical and biological behaviors compared to matrices composed of the individual components [45, 46]. Collagen-glycosaminoglycan scaffolds have also been electrospun from blended solutions with a pore structure (mean diameter of 260 nm) similar to that found in native matrices. Upon vapor phase crosslinking, these scaffolds exhibited biostability and resistance to collagenases along with increased cellular proliferation when seeded with cells [295].

B.6 Electrospun nanofiber networks and the potential for the incorporation of living cells

Both collagen and elastin matrix proteins provide a useful physiological starting point for the creation of a biochemical and biomechanical environment that is optimized for enhanced cell adhesion, migration, proliferation, and differentiation. Fabrication of these proteins into nanofiber networks provide the potential to incorporate various cell types; endothelial cells, SMC, fibroblasts, stem cells, chondrocytes, osteoblasts, human or animal cells which have been genetically engineered to produce a protein of interest (eg, growth factor, peptide hormone, antiangiogenic protein).

In vitro investigations indicate the architecture of electrospun networks supports mass transport and spatial cellular organization. Specifically, as a consequence of the

fiber nano-dimensions, the surface-to-volume ratio, and the unique three-dimensional architecture within these electrospun matrices, movement of signaling molecules, nutrients, and metabolic waste is likely enhanced and cell-cell and cell-matrix interactions are facilitated [308]. Specifically, collagen and elastin scaffolds have been shown to promote cell adhesion, migration and proliferation of a variety of cell types in vitro, with promising results concerning biocompatibility and biostability.

B.7 Future Trends: Biomedical applications for electrospun collagen and elastin nanofiber networks

There is a long felt need for durable materials for medical and veterinary use in organ and tissue substitutes. Such materials must be compatible with human and animal physiologies such that thromboses, inflammation and other harmful physiological reactions are not induced. Furthermore, durable and biologically compatible materials which do not require lengthy preconditioning periods prior to implantation are required. Over the past decade, considerable effort has been directed towards developing scaffolds using both synthetic and natural polymers. As the majority of human tissues and organs originate from hierarchically organized fibrous structures, electrospinning fiber networks is of particular interest in the development of these unique matrices. Importantly, scaffold geometry can be modulated for a variety of tissue engineering applications, simply by the shape of the collector, such that seamless and complex scaffold geometries can be fabricated. Additionally, from a commercial distribution perspective, the electrospinning technique is a rapid and efficient technology which can easily be conducted utilizing a sterile technique to generate a material which will likely have a long shelf life.

The many diverse areas of research in which electrospinning is being employed within biomedicine underscores the range of applications for which this technology can

be utilized. These matrices not only mimic native ECM architecture, which ultimately reproduce native mechanical and biological performance, but also provide the opportunity to further tailor biological responses. Additionally, the electrospinning technique provides enormous flexibility to tissue engineering of biocompatible matrices for a variety of applications. These matrices have potential in drug delivery [304], vascular bioengineering of blood vessels and heart valves [44, 309], hard and soft tissue reconstruction, load bearing prosthetic materials, materials to facilitate wound closing and/or healing and stem cell delivery [310].

REFERENCES

1. Nagapudi K, Brinkman WT, Thomas BS, Park JO, Srinivasarao M, Wright E, et al. Viscoelastic and mechanical behavior of recombinant protein elastomers. Biomaterials 2005;26(23):4695-4706.

2. Wright ER, Conticello VP. Self-assembly of block copolymers derived from elastin-mimetic polypeptide sequences. Adv Drug Deliv Rev 2002;54:1057-1073.

3. Wright ER, McMillan RA, Cooper A, Apkarian RP, Conticello VP. Thermoplastic elastomer hydrogels via self-assembly of an elastin-mimetic triblock polypeptide. Advanced Functional Materials 2002; 12(2):1-6.

4. Nagapudi K, Brinkman WT, Thomas BS, Wright ER, Conticello VP, Chaikof EL. Protein-based thermoplastic elastomers. Macromolecules 2005;38:345-354.

5. Wu X, Sallach R, Haller CA, Caves JA, Nagapudi K, Conticello VP, et al. Alterations in physical cross-linking modulate mechanical properties of two-phase protein polymer networks. Biomacromolecules 2005;6(6):3037-3044.

6. Wu X, Sallach RE, Caves JM, Conticello VP, Chaikof EL. Mechanical stability and deformation responses of physically crosslinked protein-based materials. Biomacromolecules In Review.

7. Jordan SW, Haller CA, Sallach RE, Apkarian RP, Hanson SR, Chaikof EL. The effect of a recombinant elastin-mimetic coating of an ePTFE prosthesis on acute thrombogenicity in a baboon arteriovenous shunt. Biomaterials 2007;28(6):1191-1197.

8. AHA. American Heart Association Heart Disease and Stroke Statistics-2008 Update: American Heart Association; 2008.

9. Baim DS. Percutaneous treatment of saphenous vein graft disease. Journal of the American College of Cardiology 2003;42(8):1370-1387.

10. Chaikof EL, Matthew H, Kohn J, Mikos AG, Prestwich GD, Yip CM. Biomaterials and scaffolds in reparative medicine. Ann N Y Acad Sci 2002;961:96-105.

11. Conte MS. The ideal small arterial substitute: A search for the holy grail? FASEB J 1998;12:43-35.

12. Ballyk PD, Walsh C, Butany J, Ojha M. Compliance mismatch may promote graft-artery intimal hyperplasia by altering suture-line stresses. Journal of Biomechanics 1998;31:229-237.

13. Bos GW, Poot AA, Beugeling T, van Aken WG, Feijen J. Small diameter vascular graft prosthesis: Current status. Archives of Physiology and Biochemistry 1998;106(2):100-115.

14. Kannan RY, Salacinski HJ, Butler PE, Hamilton G, Seifalian AM. Current status of prosthetic bypass grafts: A review. J Biomed Mater Res Part B: Appl Biomater 2005;74B:570-581.

15. Tai NR, Salacinski HJ, Edwards A, Hamilton G, Seifalian AM. Compliance properties of conduits used in vascular reconstruction. British Journal of Surgery 2000;87:1516-1524.

16. Esquivel CO, Blaisdell FW. Why small caliber vascular grafts fail: A reivew of clinical and experimental experience and the significance of the interaction of blood at the interface. Journal of Surgical Research 1983;41:1-15.

17. Greisler HP, Gosselin C, Ren D, Kang SS, Kim DU. Biointeractive polymers and tissue engineered blood vessels. Biomaterials 1996;17:329-336.

18. Meinhart JG, Deutsch M, Fischlein T, Howanietz N, Froschl A, Zilla P. Clinical autologous in vitro endothelialization of 153 infrainguinal ePTFE grafts. Ann Thorac Surg 2001;71:S327-331.

19. Hedeman Joosten PP, Verhagen HJ, Heijnen-Snyder GJ, van Vroonhoven TJ, Sixma JJ, de Groot PG, et al. Thrombogenesis of different cell types seeded on vascular grafts and studied under blood-flow conditions. J Vasc Surg 1998;28(6):1094-1103.

20. Pasic M, Muller-Glauser W, von Segesser L, Odermatt B, Lachat M, Turina M. Endothelial cell seeding improves patency of synthetic vascular grafts: Manual versus automatized method. Eur J Cardiothorac Surg 1996;10(5):372-379.

21. Weinberg CB, Bell E. A blood vessel model constructed from collagen and cultured vascular cells. Science 1986;231(4736):397-400.

22. Nerem RM, Ensley AE. The tissue engineering of blood vessels and the heart. American Journal of Transplantation 2004;4(supp 6):36-42.

23. Nerem RM, Seliktar D. Vascular tissue engineering. Annu Rev Biomed Eng 2001;3:225-243.

24. Barocas VH, Girton TS, Tranquillo RT. Engineered alignment in media equivalents: Magnetic prealignment and mandrel compaction. J Biomech Eng 1998;120(5):660-666.

25. Seliktar D, Black RA, Vito RP, Nerem RM. Dynamic mechanical conditioning of collagen-gel blood vessel constructs induces remodeling in vitro. Annals of Biomedical Engineering 2000;28:351-362.

26. Ogle BM, Mooradian DL. Manipulation of remodeling pathways to enhance the mechanical properties of a tissue engineered blood vessel. J Biomech Eng 2002;124(6):724-733.

27. Girton TS, Oegema TR, Grassl ED, Isenberg BC, Tranquillo RT. Mechanisms of stiffening and strengthening in media-equivalents fabricated using glycation. J Biomech Eng 2000;122:216-223.

28. L'Heureux N, Paquet S, Labbe R, Germain L, Auger F. A completely biological tissue-engineered human blood vessel. FASEB J 1998;12:47-56.

29. L'Heureux N, Stoclet JC, Auger FA, Lagaud GJ, Germain L, Andriantsitohaina R. A human tissue-engineered vascular media: A new model for pharmacological studies of contractile responses. FASEB J 2001;15:515-524.

30. Niklason L, Gao J, Abbott W, Hirschi K, Houser S, Marini R, et al. Functional arteries grown in vitro. Science 1999;284(5413):489.

31. L'Heureux N, Dusserre N, Konig G, Victor B, Keire P, Wight TN, et al. Human tissue-engineered blood vessels for adult arterial revascularization. Nat Med 2006;12(3):361-365.

32. Shin'oka T, Matsumura G, Hibino N, Naito Y, Watanabe M, Konuma T, et al. Midterm clinical result of tissue-engineered vascular autografts seeded with autologous bone marrow cells. J Thorac Cardiovasc Surg 2005;129(6):1330-1338.

33. Hinds MT, Rowe RC, Ren Z, Teach J, Wu PC, Kirkpatrick SJ, et al. Development of a reinforced porcine elastin composite vascular scaffold. J Biomed Mater Res A 2006;77(3):458-469.

34. Badylak SF, Lantz GC, Coffey A, Geddes LA. Small intestinal submucosa as a large diameter vascular graft in the dog. Journal of Surgical Research 1989;47:74-80.

35. Dardik H. The second decade of experience with the umbilical vein graft for lower-limb revascularization. Cardiovascular Surgery 1995;3(3):265-269.

36. Hurt AV, Batello-Cruz M, Skipper BJ, Teaf SR, Sterling WA. Bovine caotid artery heterografts versus polytetrafluoroethylene grafts. The American Journal of Surgery 1983;146:844-847.

37. Marshall SE, Tweedt SM, Greene CH, Ballestas LY, Bunning KR. An alternative to synthetic aortic grafts using jejunum. Journal of Investigative Surgery 2000;13:333-341.

38. Schmit CE, Baier JM. Acellular vascular tissues: Natural biomaterials for tissue repair and tissue engineering. Biomaterials 2000;21:2215-2231.

39. Courtman DW, Errett BF, Wilson GJ. The role of crosslinking in modification of the immune response elicited against xenogenic vascular acellular matrices. J Biomed Mater Res 2001;55:576-586.

40. Berglund JD, Nerem RM, Sambanis A. Incorporation of intact elastin scaffolds in tissue-engineered collagen-based vascular grafts. Tissue Eng 2004;10(9-10):1526-1535.

41. Huang L, McMillan RA, Apkarian RP, Pourdeyhimi B, Conticello VP, Chaikof EL. Generation of synthetic elastin-mimetic small diameter fibers and fiber networks. Macromolecules 2000;33:2989-2997.

42. Li M, Mondrinos MJ, Gandhi MR, Ko FK, Weiss AS, Lelkes PI. Electrospun protein fibers as matrices for tissue engineering. Biomaterisl 2005;26:5999-6008.

43. Li M, Guo Y, Wei Y, MacDiarmid AG, Lelkes PI. Electrospinning polyaniline-contained gelatin nanofibers for tissue engineering applications. Biomaterials 2006 May;27(13):2705-2715.

44. Boland ED, Matthews JA, Pawlowski KJ, Simpson DG, Wnek GE, Bowlin GL. Electrospinning collagen and elastin: Preliminary vascular tissue engineering. Front Biosci 2004;9:1422-1432.

45. Stitzel J, Liu J, Lee SJ, Komura M, Berry J, Soker S, et al. Controlled fabrication of a biological vascular substitute. Biomaterials 2006;27(7):1088-1094.

46. Buttafoco L, Kolkman NG, Poot AA, Dijkstra PJ, Vermes I, Feijen J. Electrospinning collagen and elastin for tissue engineering small diameter blood vessels. J Control Release 2005;101(1-3):322-324.

47. Kwon IK, Kidoaki S, Matsuda T. Electrospun nano- to microfiber fabrics made of biodegradable copolyesters: Structural characteristics, mechanical properties and cell adhesion potential. Biomaterials 2005;26(18):3929-3939.

48. Humphrey JD. Mechaics of the arterial wall: Review and directions. Critical Reviews in Biomedical Engineering 1995;23:1-162.

49. Roach MR, Burton AC. The reason for the shape of the distensibility curves of arteries. Can J Biochem Physiol 1957;35:681-690.

50. Silver F, Horvath I, Foran DJ. Viscoelasticity of the vessel wall: The role of collagen and elastic fibers. Critical Reviews in Biomedical Engineering 2001;29(3):279-302.

51. Silver FH, Snowhill PB, Foran DJ. Mechanical behavior of vessel wall: A comparitive study of aorta, vena cava, and carotid artery. Annals of Biomedical Engineering 2003;31:793-803.

52. Lillie MA, Gosline JM. The viscoelastic basis for the tensile strength of elastin. International Journal of Biological Macromolecules 2002;30:119-127.

53. Clark JM, Glagov S. Transmural organization of the arterial media: The lamellar unit revisited. Arteriosclerosis 1985;5:19-34.

54. Dingemans KP, Telling P, Lagendijk JH, Becker AE. Extracellular matrix of the human aortic media: An ultrastructural histochemical and immunohistochemical study of the adult aortic media. The Anatomical Record 2000;258:1-14.

55. Wolinsky H, Glagov S. A lamellar unit of aortic medial structure and function in mammals. Circulation Reviews 1967;20:99-111.

56. Powell JT, Vine N, Crossman M. On the accumulation of D-aspartate in elastin and other proteins of the ageing aorta. Atherosclerosis 1992;97(2-3):201-208.

57. Li DY, Faury G, Taylor DG, Davis EC, Boyle WA, Mecham RP, et al. Novel arterial pathology in mice and humans hemizygous for elastin. J Clin Invest 1998;102(10):1783-1787.

58. Li DY, Brooke B, Davis EC, Mecham RP, Sorenson LK, Boak BB, et al. Elastin is an essential determinant of arterial morphogenesis. Nature 1998;393:276-280.

59. Wagenseil JE, Nerurkar NL, Knutsen RH, Okamoto RJ, Li DY, Mecham RP. Effects of elastin haploinsufficiency on the mechanical behavior of mouse arteries. Am J Physiol Heart Circ Physiol 2005;289:H1209-H1217.

60. Fulop T, Jacob MP, Khalil A, Wallach J, Robert L. Biological effects of elastin peptides. Pathol Biol (Paris) 1998;46(7):497-506.

61. Rucker RB, Dubick MA. Elastin metabolism and chemistry: Potential roles in lung development and structure. Environmental Health Perspectives 1984;55:179-191.

62. Rosenbloom J, Abrams WR, Mecham R. Extracellular matrix 4: The elastic fiber. FASEB J 1993;7:1208-1218.

63. Cox BA, Starcher BC, Urry DW. Communication: Coacervation of tropoelastin results in fiber formation. J Biol Chem 1974;249(3):997-998.

64. Wu WJ, Vrhovski B, Weiss AS. Glycosaminoglycans mediate the coacervation of human tropoelastin through dominant charge interactions involving lysine side chains. J Biol Chem 1999;274(31):21719-21724.

65. Bellingham CM, Woodhouse KA, Robson P, Rothstein SJ, Keeley FW. Self-aggregation characteristics of recombinantly expressed human elastin polypeptides. Biochim Biophys Acta 2001;1550(1):6-19.

66. Urry DW, Gowda DC, Parker TM, Luan CH, Reid MC, Harris CM, et al. Hydrophobicity scale for proteins based on inverse transition temperature. Biopolymers 1992;32:1243-1250.

67. Urry DW, Luan CH, Parker TM, Gowda DC, Prasad KU, Reid MC, et al. Temperature of polypeptide inverse temperature transition depends on mean residue hydrophobicity. J Am Chem Soc 1991;113:4346-4348.

68. Keeley FW, Bellingham CM, Woodhouse KA. Elastin as a self-organizing biomaterial: use of recombinantly expressed human elastin polypeptides as a model for investigations of structure and self-assembly of elastin. Philos Trans R Soc Lond B Biol Sci 2002;357(1418):185-189.

69. Alberts B, Johnson A, Lewis J, Raff M, Roberts K, Walter P. Molecular Biology of the Cell. 4th ed. New York, NY: Garland Science, 2002.

70. Mithieux SM, Weiss AS. Elastin. Adv Protein Chem 2005;70:437-461.

71. Garrett RH, Grisham CM. Biochemistry. 2 ed. Pacific Grove, CA: Brooks/Cole Thomas Learning, 1999.

72. Debelle L, Tamburro AM. Elastin: Molecular description and function. Int J Biochem Cell Biol 1999;31(2):261-272.

73. Ferrari FA, Cappello J. Protein Based Materials. Boston, MA: Birkhauser, 1997.

74. Petka WA, Harden JL, McGrath KP, Wirtz D, Tirrell DA. Reversible hydrogels from self-assembling artificial proteins. Science 1998;281:389-392.

75. Meyer DE, Chilkoti A. Genetically encoded synthesis of protein-based polymers with precisely specified molecular weight and sequence by recursive directional ligation: Examples from the elastin-like polypeptide system. Biomacromolecules 2002;3(2):357-367.

76. Nagarsekar A, Crissman J, Crissman M, Ferrari F, Cappello J, Ghandehari H. Genetic engineering of stimuli-sensitive silkelastin-like protien block copolymers. Biomacromolecules 2003;4:602-607.

77. Cappello J, Crissman J, Dorman M, Mikolajczak M, Textor G, Marquet M, et al. Genetic engineering of structural protein polymers. Biotechnol Progress 1990;6:198-202.

78. McGrath KP, Tirrell DA, Kawai M, Mason TL, Fournier MJ. Chemical and biosynthetic approaches to the production of novel polypeptide materials. Biotechnol Progress 1990;6:188-192.

79. Urry DW. Five axioms for the functional design of peptide-based polymers as molecualr machines and materials: Principles for macromolecular assembly. Biopolymers 1998;47(167-178).

80. Urry DW. Physical chemistry of biological free energy transduction as demonstrated by elastin protein-based polymers. J Phys Chem B 1997;101:11007-11028.

81. Chang DK, Urry DW. Molecular dynamics calculations on relaxed and extended states of the polypentapeptide of elastin. Chem Phys Letters 1988;147(4):395-400.

82. Wood SA, Lemons JE, Prasad KU, Urry DW. In vitro calcification and in vivo biocompatibility of the crosslinked polypentapeptide of elastin. J Biomed Mater Res 1986;20(3):315-335.

83. van Hest JC, Tirrell DA. Protein-based materials, toward a new level of structural control. Chem Commun 2001(19):1897-1904.

84. Sallach RE, Wei M, Biswas N, Conticello VP, Lecommandoux S, Dluhy RA, et al. Micelle density regulated by a reversible switch of protein secondary structure. J Am Chem Soc 2006;128(36):12014-12019.

85. Panitch A, Yamaoka T, Fournier MJ, Mason TL, Tirrell DA. Design and biosynthesis of elastin-like artificial extracellular matrix proteins containing periodically spaced fibronectin CS5 domains. Macromolecules 1999;32:1701-1703.

86. Welsh ER, Tirrell DA. Engineering the extracellular matrix: A novel approach to polymeric biomaterials. I. Control of the physical properties of artificial protein matrices designed to support adhesion of vascular endothelial cells. Biomacromolecules 2000;1(1):23-30.

87. Urry DW, Pattanaik A, Xu J, Woods TC, McPherson DT, Parker TM. Elastic protein-based polymers in soft tissue augmentation and generation. J Biomater Sci Polym Ed 1998;9(10):1015-1048.

88. Lee J, Macoscko CW, Urry DW. Mechanical properties of crosslinked synthetic elastomeric polypentapeptides. Macromolecules 2001;34:5968-5974.

89. Lee J, Macosko CW, Urry DW. Phase transition and elasticity of protein-based hydrogels. J Biomater Sci Polym Ed 2001;12(2):229-242.

90. Lee J, Macoscko CW, Urry DW. Swelling behavior of gamma-irradiation cross-linked elastomeric polypentapeptide-based hydrogels. Macromolecules 2001;34:4114-4123.

91. Bellingham CM, Lillie MA, Gosline JM, Wright GM, Starcher BC, Bailey AJ, et al. Recombinant human elastin polypeptides self-assemble into biomaterials with elastin-like properties. Biopolymers 2003;70(4):445-455.

92. Vieth S, Bellingham CM, Keeley FW, Hodge SM, Rousseau D. Microstructural and tensile properties of elastin-based polypeptides crosslinked with genipin and pyrroloquinoline quinone. Biopolymers 2007;85(3):199-206.

93. Girotti A, Reguera J, Rodriguez-Cabello JC, Arias FJ, Alonso M, Matestera A. Design and bioproduction of a recombinant multi(bio)functional elastin-like protein polymer containing cell adhesion sequences for tissue engineering purposes. J Mater Sci Mater Med 2004;15(4):479-484.

94. Martino M, Tamburro AM. Chemical synthesis of cross-linked poly(KGGVG), An elastin-like biopolymer. Biopolymers 2001;59(1):29-37.

95. Lee J, Macoscko CW, Urry DW. Elastomeric polypentapeptides cross-linked into matrixes and fibers. Biomacromolecules 2001;2:170-179.

96. Nowatzki PJ, Tirrell DA. Physcial properties of artificial extracellular matrix protein films prepared by isocyanate crosslinking. Biomaterials 2004;25:1261-1267.

97. Trabbic-Carlson K, Setton LA, Chilkoti A. Swelling and mechanical behaviors of chemically cross-linked hydrogels of elastin-like polypeptides. Biomacromolecules 2003;4:572-580.

98. McMillan RA, Lee TAT, Conticello VP. Rapid assembly of synthetic genes encoding protein polymers. Macromolecules 1999;32:3643-3648.

99. McMillan RA, Conticello VP. Synthesis and characterization of elastin-mimetic protein gels derived from a well-defined polypeptide precursor. Macromolecules 2000;33:4809-4821.

100. Zio KD, Tirrell DA. Mechanical properties of artificial protein matrices engineered for control of cell and tissue behavior. Macromolecules 2003;36:1553-1558.

101. Lim DW, Nettles DL, Setton LA, Chilkoti A. In situ cross-linking of elastin-like polypeptide block copolymers for tissue repair. Biomacromolecules 2008;9(1):222-230.

102. Lim DW, Nettles DL, Setton LA, Chilkoti A. Rapid cross-linking of elastin-like polypeptides with (hydroxymethyl) phosphines in aqueous solution. Biomacromolecules 2007;8(5):1463-1470.

103. Nagapudi K, Huang L, McMillan RA, Brinkman W, Conticello VP, Chaikof EL. Photomediated solid-state crosslinking of an elastin-mimetic recombinant protein polymer. Macromolecules 2002;35:1730-1737.

104. Rodríguez-Cabello JC, Reguera J, Girotti A, Arias FJ, Alonso M. Genetic engineering of protein-based polymers: The example of elastinlike polymers. Adv Polym Sci 2006;200:119-167.

105. Urry DW, Parker TM. Mechanics of elastin: Molecular mechanism of biological elasticity and its relationship to contraction. J Muscle Res Cell Motil 2002;23(5-6):543-559.

106. Vrhovski B, Weiss AS. Biochemistry of tropoelastin. Eur J Biochem 1998;258(1):1-18.

107. McHale MK, Setton LA, Chilkoti A. Synthesis and in vitro evaluation of enzymatically cross-linked elastin-like polypeptide gels for cartilaginous tissue repair. Tissue Eng 2005;11(11-12):1768-1779.

108. Narayanan AS, Page RC, Kuzan F, Cooper CG. Elastin cross-linking in vitro. Studies on factors influencing the formation of desmosines by lysyl oxidase action on tropoelastin. Biochem J 1978;173(3):857-862.

109. Bressan GM, Pasquali-Ronchetti I, Fornieri C, Mattioli F, Castellani I, Volpin D. Relevance of aggregation properties of tropoelastin to the assembly and structure of elastic fibers. J Ultrastruct Mol Struct Res 1986;94(3):209-216.

110. Heilshorn SC, DiZio KA, Welsh ER, Tirrell DA. Endothelial cell adhesion to the fibronectin CS5 domain in artificial extracellular matrix proteins. Biomaterials 2003;24(23):4245-4252.

111. Dinerman AA, Cappello J, Ghandehari H, Hoag SW. Swelling behavior of a genetically engineered silk-elastinlike protein polymer hydrogel. Biomaterials 2002;23(21):4203-4210.

112. Safley SA, Kapp LM, Tucker-Burden C, Hering B, Kapp JA, Weber CJ. Inhibition of cellular immune responses to encapsulated porcine islet xenografts by simultaneous blockade of two different costimulatory pathways. Transplantation 2005;79(4):409-418.

113. Tobias JW, Shrader TE, Rocap G, Varshavsky A. The N-end rule in bacteria. Science 1991;254:1324-1377.

114. Chang Y, Tsai CC, Liang HC, Sung HW. In vivo evaluation of cellular and acellular bovine pericardia fixed with a naturally occurring crosslinking agent (genipin). Biomaterials 2002;23(12):2447-2457.

115. Jayakrishnan A, Jameela SR. Glutaraldehyde as a fixative in bioprostheses and drug delivery matrices. Biomaterials 1996;17(5):471-484.

116. Gosline JM, French CJ. Dynamic mechanical properties of elastin. Biopolymers 1979;18(8):2091-2103.

117. Humphrey JD. Cardiovascular solid mechanics. New York: Springer, 2002.

118. Sacks MS. Biaxial mechanical evaluation of planar biological materials. J Elasticity 2000;61:199-246.

119. Carew EO, Garg A, Barber JE, Vesely I. Stress relaxation preconditioning of porcine aortic valves. Ann Biomed Eng 2004;32(4):563-572.

120. Carew EO, Barber JE, Vesely I. Role of preconditioning and recovery time in repeated testing of aortic valve tissues: validation through quasilinear viscoelastic theory. Ann Biomed Eng 2000;28(9):1093-1100.

121. Urry DW, Parker TM. Biocompatibility of the bioelastic materials, poly(GVGVP) and its gamma-irradiation cross-linked matrix: Summary of generic biological test results. J Bioactive Compatible Polym 1991;6:263-282.

122. Rincon AC, Molina-Martinez IT, de Las Heras B, Alonso M, Bailez C, Rodriguez-Cabello JC, et al. Biocompatibility of elastin-like polymer poly(VPAVG) microparticles: In vitro and in vivo studies. J Biomed Mater Res A 2006;78(2):343-351.

123. Hoban LD, Pierce M, Quance J, Hayward I, McKee A, Gowda DC, et al. Use of polypentapeptides of elastin to prevent postoperative adhesions: Efficacy in a contaminated peritoneal model. J Surg Res 1994;56(2):179-183.

124. Wei SM, Katona E, Fachet J, Fulop T, Jr., Robert L, Jacob MP. Epitope specificity of monoclonal and polyclonal antibodies to human elastin. Int Arch Allergy Immunol 1998;115(1):33-41.

125. Woodhouse KA, Klement P, Chen V, Gorbet MB, Keeley FW, Stahl R, et al. Investigation of recombinant human elastin polypeptides as non-thrombogenic coatings. Biomaterials 2004;25(19):4543-4553.

126. Meyer DE, Kong GA, Dewhirst MW, Zalutsky MR, A. C. Targeting a genetically engineered elastin-like polypeptide to solid tumors by local hypothermia. Cancer Res 2001;61:1548-1554.

127. Liu W, Dreher MR, Chow DC, Zalutsky MR, A. C. Tracking the *in vivo* fate of recombinant polypeptides by isotopic labeling. J Control Release 2006;114:184-192.

128. Betre H, Liu W, Zalutsky MR, Chilkoti A, Kraus VB, Setton LA. A thermally responsive biopolymer for intra-articular drug delivery. J Control Release 2006;115(2):175-182.

129. Mithieux SM, Rasko JEJ, Weiss AS. Synthetic elastin hydrogels derived from massive elastic assemblies of self-organized human protein monomers. Biomaterials 2004;25:4921-4927.

130. Cappello J, Crissman JW, Crissman M, Ferrari FA, Textor G, Wallis O, et al. In-situ self-assembling protein polymer gel systems for administration, delivery, and release of drugs. J Control Release 1998;53(1-3):105-117.

131. Hatefi A, Cappello J, Ghandehari H. Adenoviral gene delivery to solid tumors by recombinant silk-elastinlike protein polymers. Pharm Res 2007;24(4):773-779.

132. Megeed Z, Haider M, Li D, O'Malley BW, Jr., Cappello J, Ghandehari H. In vitro and in vivo evaluation of recombinant silk-elastinlike hydrogels for cancer gene therapy. J Control Release 2004;94(2-3):433-445.

133. Anderson JM. In vivo biocompatibility of implantable delivery systems and biomaterials. Eur J Pharm Biopharm 1994;40:1-8.

134. Hunt JA, Vince DG, Williams DF. Image analysis in the evaluation of biomaterials. J Biomed Eng 1993;15:39-45.

135. Andersson M, Suska F, Johansson A, Berglin M, Emanuelsson L, Elwing H, et al. Effect of molecular mobility of polymeric implants on soft tissue reactions: An *in vivo* study in rats. J Biomed Mater Res A 2008;84(3):652-660.

136. Butler K, Benghuzzui H, Tucci M, Cason Z. A comparsion of fibrous tissue formation surrounding intraperitoneal and subcutaneous implantation of ALCAP, HA, and TCP ceramic devices. Biomed Sci Instrum 1997;34:18-23.

137. Shin H, Quinten Ruhe P, Mikos AG, Jansen JA. In vivo bone and soft tissue response to injectable, biodegradable oligo(poly(ethylene glycol) fumarate) hydrogels. Biomaterials 2003;24(19):3201-3211.

138. Giavaresi G, Torricelli P, Fornasari PM, Giardino R, Barbucci R, Leone G. Blood vessel formation after soft-tissue implantation of hyaluronan-based hydrogel supplemented with copper ions. Biomaterials 2005;26(16):3001-3008.

139. Barbosa JN, Madureira P, Barbosa MA, Aguas AP. The influence of functional groups of self-assembled monolayers on fibrous capsule formation and cell recruitment. J Biomed Mater Res A 2006;76(4):737-743.

140. Nair A, Zou L, Bhattacharyya D, Timmons RB, Tang L. Species and density of implant surface chemistry affect the extent of foreign body reactions. Langmuir 2008;24(5):2015-2024.

141. Voskerician G, Gingras PH, Anderson JM. Macroporous condensed poly(tetrafluoroethylene). I. In vivo inflammatory response and healing characteristics. J Biomed Mater Res A 2006;76(2):234-242.

142. Montclare JK, Tirrell DA. Evolving proteins of novel composition. Angew Chem Int Ed Engl 2006;45(27):4518-4521.

143. Link AJ, Mock ML, Tirrell DA. Non-canonical amino acids in protein engineering. Curr Opin Biotechnol 2003;14(6):603-609.

144. Herrero-Vanrell R, Rincon AC, Alonso M, Reboto V, Molina-Martinez IT, Rodriguez-Cabello JC. Self-assembled particles of an elastin-like polymer as vehicles for controlled drug release. J Control Release 2005;102(1):113-122.

145. Dreher MR, Raucher D, Balu N, Michael Colvin O, Ludeman SM, Chilkoti A. Evaluation of an elastin-like polypeptide-doxorubicin conjugate for cancer therapy. J Control Release 2003;91(1-2):31-43.

146. Chilkoti A, Dreher MR, Meyer DE. Design of thermally responsive, recombinant polypeptide carriers for targeted drug delivery. Adv Drug Deliv Rev 2002;54(8):1093-1111.

147. Heilshorn SC, Liu JC, Tirrell DA. Cell-binding domain context affects cell behavior on engineered proteins. Biomacromolecules 2005;6(1):318-323.

148. Liu JC, Heilshorn SC, Tirrell DA. Comparative cell response to artificial extracellular matrix proteins containing the RGD and CS5 cell-binding domains. Biomacromolecules 2004;5(2):497-504.

149. Richman GP, Tirrell DA, Asthagiri AR. Quantitatively distinct requirements for signaling-competent cell spreading on engineered versus natural adhesion ligands. J Control Release 2005;101(1-3):3-12.

150. Sun XL, Haller CA, Wu X, Conticello VP, Chaikof EL. One-pot glyco-affinity precipitation purification for enhanced proteomics: The flexible alignment of solution-phase capture/release and solid-phase separation. J Proteome Res 2005;4(6):2355-2359.

151. Urry D, Pattanaik A, Accavitti MA, Luan CX, McPherson DT, Xu J, et al., editors. Handbook of Biodegradable Polymers: Harwood: Amsterdam, 1997.

152. Urry DW, Long MM, Cox BA, Ohnishi T, Mitchell LW, Jacobs M. The synthetic polypentapeptide of elastin coacervates and forms filamentous aggregates. Biochim Biophys Acta 1974;371(2):597-602.

153. Urry DW, Luan CH, Peng SQ. Molecular biophysics of elastin structure, function and pathology. Ciba Found Symp 1995;192:4-22.

154. Lu JR, Zhao XB, Yaseen M. Biomimetic amphiphiles: Biosurfactants. Curr Opin in Colloid & Int Sci 2007;12(2):60-67.

155. Lasch J. Interaction of detergents with lipid vesicles. Biochim Biophys Acta 1995;1241(2):269-292.

156. Helenius A, Simons K. Solubilization of membranes by detergents. Biochim Biophys Acta 1975;415(1):29-79.

157. Kapadia MR, Chow LW, Tsihlis ND, Ahanchi SS, Eng JW, Murar J, et al. Nitric oxide and nanotechnology: A novel approach to inhibit neointimal hyperplasia. J Vasc Surg 2008;47(1):173-182.

158. Rajangam K, Behanna HA, Hui MJ, Han X, Hulvat JF, Lomasney JW, et al. Heparin binding nanostructures to promote growth of blood vessels. Nano Lett 2006;6(9):2086-2090.

159. Holmes TC, de Lacalle S, Su X, Liu G, Rich A, Zhang S. Extensive neurite outgrowth and active synapse formation on self-assembling peptide scaffolds. Proc Natl Acad Sci U S A 2000;97(12):6728-6733.

160. Kisiday J, Jin M, Kurz B, Hung H, Semino C, Zhang S, et al. Self-assembling peptide hydrogel fosters chondrocyte extracellular matrix production and cell division: implications for cartilage tissue repair. Proc Natl Acad Sci U S A 2002;99(15):9996-10001.

161. Sargeant TD, Guler MO, Oppenheimer SM, Mata A, Satcher RL, Dunand DC, et al. Hybrid bone implants: Self-assembly of peptide amphiphile nanofibers within porous titanium. Biomaterials 2008;29(2):161-171.

162. Stroman PW, Dorvil JC, Marois Y, Poddevin N, Guidoin R. In vivo time course studies of the tissue responses to resorbable polylactic acid implants by means of MRI. Magn Reson Med 1999;42(1):210-214.

163. Mader K, Cremmilleux Y, Domb AJ, Dunn JF, Swartz HM. In vitro/in vivo comparison of drug release and polymer erosion from biodegradable P(FAD-SA) polyanhydrides--A noninvasive approach by the combined use of electron paramagnetic resonance spectroscopy and nuclear magnetic resonance imaging. Pharm Res 1997;14(6):820-826.

164. Mader K, Bacic G, Domb A, Elmalak O, Langer R, Swartz HM. Noninvasive in vivo monitoring of drug release and polymer erosion from biodegradable polymers by EPR spectroscopy and NMR imaging. J Pharm Sci 1997;86(1):126-134.

165. Puolakkainen P, Bradshaw AD, Kyriakides TR, Reed M, Brekken R, Wight T, et al. Compromised production of extracellular matrix in mice lacking secreted protein, acidic and rich in cysteine (SPARC) leads to a reduced foreign body reaction to implanted biomaterials. Am J Pathol 2003;162(2):627-635.

166. Senior JH. Fate and behavior of liposomes in vivo: A review of controlling factors. Crit Rev Ther Drug Carrier Syst 1987;3(2):123-193.

167. Meena R, Prasad K, Siddhanta AK. Effect of genipin, a naturally occurring crosslinker on the properties of kappa-carrageenan. Int J Biol Macromol 2007;41(1):94-101.

168. Lim DW, Choi SH, Park TG. A new class of biodegradable hydrogels stereocomplexed by enantiomeric oligo(lactide) side chains of poly(HEMA-*g*-OLA)s. Macromol Rapid Commun 2000;21:464-471.

169. Jeong B, Kibbey MR, Birnbaum JC, Won YY, Gutowska A. Thermogelling biodegradable polymers with hydrophilic backbones: PEG-g-PLGA. Macromolecules 2000;33:8317-8322.

170. Schwartz J, Zhang S. Peptide-mediated cellular delivery. Curr Opin in MolecTherap 2000;2(2):162-167.

171. Wilson JT, Cui W, Sun XL, Tucker-Burden C, Weber CJ, Chaikof EL. In vivo biocompatibility and stability of a substrate-supported polymerizable membrane-mimetic film. Biomaterials 2007;28(4):609-617.

172. Alsberg E, Kong HJ, Hirano Y, Smith MK, Albeiruti A, Mooney DJ. Regulating bone formation via controlled scaffold degradation. J Dent Res 2003;82(11):903-908.

173. Wakitani S, Goto T, Young RG, Mansour JM, Goldberg VM, Caplan AI. Repair of large full-thickness articular cartilage defects with allograft articular chondrocytes embedded in a collagen gel. Tissue Eng 1998;4(4):429-444.

174. Awad HA, Butler DL, Boivin GP, Smith FN, Malaviya P, Huibregtse B, et al. Autologous mesenchymal stem cell-mediated repair of tendon. Tissue Eng 1999 Jun;5(3):267-277.

175. Geiger M, Li RH, Friess W. Collagen sponges for bone regeneration with rhBMP-2. Adv Drug Deliv Rev 2003;55(12):1613-1629.

176. Wallace DG, Rosenblatt J. Collagen gel systems for sustained delivery and tissue engineering. Adv Drug Deliv Rev 2003;55(12):1631-1649.

177. Ruszczak Z. Effect of collagen matrices on dermal wound healing. Adv Drug Deliv Rev 2003;55(12):1595-1611.

178. van Wachem PB, van Luyn MJ, Olde Damink LH, Dijkstra PJ, Feijen J, Nieuwenhuis P. Biocompatibility and tissue regenerating capacity of crosslinked dermal sheep collagen. J Biomed Mater Res 1994;28(3):353-363.

179. Friess H, Zhu ZW, di Mola FF, Kulli C, Graber HU, Andren-Sandberg A, et al. Nerve growth factor and its high-affinity receptor in chronic pancreatitis. Ann Surg 1999;230(5):615-624.

180. Friess W, Uludag H, Foskett S, Biron R, Sargeant C. Characterization of absorbable collagen sponges as rhBMP-2 carriers. Int J Pharm 1999;187(1):91-99.

181. Zeeman R, Dijkstra PJ, van Wachem PB, van Luyn MJ, Hendriks M, Cahalan PT, et al. Crosslinking and modification of dermal sheep collagen using 1, 4-butanediol diglycidyl ether. J Biomed Mater Res 1999;46(3):424-433.

182. Gorham SD, Light ND, Diamond AM, Willins MJ, Bailey AJ, Wess TJ, et al. Effect of chemical modifications on the susceptibility of collagen to proteolysis. II. Dehydrothermal crosslinking. Int J Biol Macromol 1992;14(3):129-138.

183. Weadock KS, Miller EJ, Keuffel EL, Dunn MG. Effect of physical crosslinking methods on collagen-fiber durability in proteolytic solutions. J Biomed Mater Res 1996;32(2):221-226.

184. Han B, Jaurequi J, Tang BW, Nimni ME. Proanthocyanidin: a natural crosslinking reagent for stabilizing collagen matrices. J Biomed Mater Res A 2003;65(1):118-124.

185. Postlethwait RW, Dillon ML, Reeves JW. Experimental study of silk suture. Arch Surg 1962;84:698-702.

186. Greenwald D, Shumway S, Albear P, Gottlieb L. Mechanical comparison of 10 suture materials before and after in vivo incubation. J Surg Res 1994;56(4):372-377.

187. Altman GH, Diaz F, Jakuba C, Calabro T, Horan RL, Chen J, et al. Silk-based biomaterials. Biomaterials 2003;24(3):401-416.

188. Rehakova M, Bakos D, Vizarova K, Soldan M, Jurickova M. Properties of collagen and hyaluronic acid composite materials and their modification by chemical crosslinking. J Biomed Mater Res 1996;30(3):369-372.

189. Menon RS, Allen PS. Solvent proton relaxation of aqueous solutions of the serum proteins alpha 2-macroglobulin, fibrinogen, and albumin. Biophys J 1990;57(3):389-396.

190. Fullerton GD, Potter JL, Dornbluth NC. NMR relaxation of protons in tissues and other macromolecular water solutions. Magn Reson Imaging 1982;1(4):209-226.

191. Lee DH, Ko RK, Cho ZH, Kim SS. Applications of NMR imaging to the time-dependent swelling effect in polymers. Biomed Mater Eng 1996;6(5):313-322.

192. Constantinidis I, Stabler CL, Long R, Jr., Sambanis A. Noninvasive monitoring of a retrievable bioartificial pancreas in vivo. Ann N Y Acad Sci 2002;961:298-301.

193. Stabler CL, Long RC, Jr., Constantinidis I, Sambanis A. In vivo noninvasive monitoring of a tissue engineered construct using ^{1}H NMR spectroscopy. Cell Transplant 2005;14(2-3):139-149.

194. Stabler CL, Long RC, Sambanis A, Constantinidis I. Noninvasive measurement of viable cell number in tissue-engineered constructs in vitro, using ^{1}H nuclear magnetic resonance spectroscopy. Tissue Eng 2005;11(3-4):404-414.

195. Kellaway IW, Seale L, Spencer PS. The in vitro characterization and biostability of 99mTc-dextran and its accumulation within the inflamed paws of adjuvant-induced arthritic rats. Pharm Res 1995;12(4):588-593.

196. de Jong SJ, van Eerdenbrugh B, van Nostrum CF, Kettenes-van den Bosch JJ, Hennink WE. Physically crosslinked dextran hydrogels by stereocomplex formation of lactic acid oligomers: Degradation and protein release behavior. J Control Release 2001;71(3):261-275.

197. Akiyoshi K, Kobayashi S, Shichibe S, Mix D, Baudys M, Kim SW, et al. Self-assembled hydrogel nanoparticle of cholesterol-bearing pullulan as a carrier of protein drugs: Complexation and stabilization of insulin. J Control Release 1998;54(3):313-320.

198. Son S, Tanrikulu IC, Tirrell DA. Stabilization of bzip peptides through incorporation of fluorinated aliphatic residues. Chembiochem 2006;7(8):1251-1257.

199. Megeed Z, Cappello J, Ghandehari H. Genetically engineered silk-elastinlike protein polymers for controlled drug delivery. Adv Drug Deliv Rev 2002;54(8):1075-1091.

200. Chenite A, Chaput C, Wang D, Combes C, Buschmann MD, Hoemann CD, et al. Novel injectable neutral solutions of chitosan form biodegradable gels in situ. Biomaterials 2000;21(21):2155-2161.

201. Hassan CM, Peppas NA. Structure and morphology of freeze/thawed PVA hydrogels. Macromolecules 2000;33:2472-2479.

202. Wandrey C, Vidal DS. Purification of polymeric biomaterials. Ann N Y Acad Sci 2001;944:187-198.

203. Lee SY, Choi J, Han K, Song JY. Removal of endotoxin during purification of poly(3-hydroxybutyrate) from gram-negative bacteria. Appl Environ Microbiol 1999;65(6):2762-2764.

204. Choi J, Lee SY. Efficient and economical recovery of poly(3-hydroxybutyrate) from recombinant Escherichia coli by simple digestion with chemicals. Biotechnol Bioeng 1999;62(5):546-553.

205. Aida Y, Pabst MJ. Removal of endotoxin from protein solutions by phase separation using Triton X-114. J Immunol Methods 1990;132(2):191-195.

206. Fiske MJ, Fredenburg RA, VanDerMeid KR, McMichael JC, Arumugham R. Method for reducing endotoxin in Moraxella catarrhalis UspA2 protein preparations. J Chromatogr B Biomed Sci Appl 2001;753(2):269-278.

207. Salek-Ardakani S, Stuart AD, Arrand JE, Lyons S, Arrand JR, Mackett M. High level expression and purification of the Epstein-Barr virus encoded cytokine viral interleukin 10: Efficient removal of endotoxin. Cytokine 2002;17(1):1-13.

208. Fernando GJ, Murray B, Zhou J, Frazer IH. Expression, purification and immunological characterization of the transforming protein E7, from cervical cancer-associated human papillomavirus type 16. Clin Exp Immunol 1999;115(3):397-403.

209. Kim C, Ryu H. Immunologic reactivity of a lipopolysaccharide-protein complex of type A Pasteurella multocida in mice. J Vet Sci 2000;1(2):87-95.

210. Fletcher MA, McKenna TM, Quance JL, Wainwright NR, Williams TJ. Lipopolysaccharide detoxification by endotoxin neutralizing protein. J Surg Res 1993;55(2):147-154.

211. Adam O, Vercellone A, Paul F, Monsan PF, Puzo G. A nondegradative route for the removal of endotoxin from exopolysaccharides. Anal Biochem 1995;225(2):321-327.

212. Gui W, Xue L, Jing L, Ying L, Zhen S. Endotoxin removal in some medicines and human serum albumin solution by affinity membranes. Chromatography 2002;20(2):108-114.

213. Scheller J, Henggeler D, Viviani A, Conrad U. Purification of spider silk-elastin from transgenic plants and application for human chondrocyte proliferation. Transgenic Res 2004;13(1):51-57.

214. Lin M, Rose-John S, Grotzinger J, Conrad U, Scheller J. Functional expression of a biologically active fragment of soluble gp130 as an ELP-fusion protein in

transgenic plants: Purification via inverse transition cycling. Biochem J 2006;398(3):577-583.

215. Daniell H, Streatfield SJ, Wycoff K. Medical molecular farming: Production of antibodies, biopharmaceuticals and edible vaccines in plants. Trends Plant Sci 2001;6(5):219-226.

216. Scheller J, Leps M, Conrad U. Forcing single-chain variable fragment production in tobacco seeds by fusion to elastin-like polypeptides. Plant Biotechnol J 2006;4(2):243-249.

217. Scheller J, Guhrs KH, Grosse F, Conrad U. Production of spider silk proteins in tobacco and potato. Nat Biotechnol 2001;19(6):573-577.

218. Larrick JW, Thomas DW. Producing proteins in transgenic plants and animals. Curr Opin Biotechnol 2001;12(4):411-418.

219. Romanos MA, Scorer CA, Clare JJ. Foreign gene expression in yeast: A review. Yeast 1992;8(6):423-488.

220. Cregg JM, Vedvick TS, Raschke WC. Recent advances in the expression of foreign genes in *Pichia pastoris*. Biotechnology (N Y) 1993;11(8):905-910.

221. Srinivasan S, Barnard GC, Gerngross TU. A novel high-cell-density protein expression system based on Ralstonia eutropha. Appl Environ Microbiol 2002;68(12):5925-5932.

222. Toonkool P, Weiss AS. Expression of recombinant human tropoelastin in Saccharomyces cerevisiae containing synthetic gene with a high codon adaptation index coupled to the SUC2 invertase signal sequence. Acta Biotechnol 2001;2:189-193.

223. Fahnestock SR, Bedzyk LA. Production of synthetic spider dragline silk protein in *Pichia pastoris*. Appl Microbiol Biotechnol 1997;47(1):33-39.

224. Myllyharju J, Nokelainen M, Vuorela A, Kivirikko KI. Expression of recombinant human type I-III collagens in the yeast *Pichia pastoris*. Biochem Soc Trans 2000;28(4):353-357.

225. Olsen DR, Leigh SD, Chang R, McMullin H, Ong W, Tai E, et al. Production of human type I collagen in yeast reveals unexpected new insights into the molecular assembly of collagen trimers. J Biol Chem 2001;276(26):24038-24043.

226. Daly R, Hearn MT. Expression of heterologous proteins in Pichia pastoris: A useful experimental tool in protein engineering and production. J Mol Recognit 2005;18(2):119-138.

227. Cregg JM, Barringer KJ, Hessler AY, Madden KR. *Pichia pastoris* as a host system for transformations. Mol Cell Biol 1985;5(12):3376-3385.

228. Cregg JM. Gene expression systems: Using nature for the art of expression: Academic Press, 1999.

229. Higgins DR, Cregg JM. Methods in molecular biology: *Pichia* protocols: Humana Press, Inc, 1998.

230. Campbell RE, Tour O, Palmer AE, Steinbach PA, Baird GS, Zacharias DA, et al. A monomeric red fluorescent protein. Proc Natl Acad Sci U S A 2002;99(12):7877-7882.

231. Nguyen AW, Daugherty PS. Evolutionary optimization of fluorescent proteins for intracellular FRET. Nat Biotechnol 2005;23(3):355-360.

232. Kim SJ, Park H, Kim JK, Lee JY, Ahn K, Choe M, et al. Random changes of amino acid residues with expected frequency by saturated point mutagenesis. Mol Cells 2000;10(2):232-235.

233. Bzymek M, Lovett ST. Instability of repetitive DNA sequences: The role of replication in multiple mechanisms. Proc Natl Acad Sci U S A 2001;98(15):8319-8325.

234. Morag AS, Saveson CJ, Lovett ST. Expansion of DNA repeats in Escherichia coli: Effects of recombination and replication functions. J Mol Biol 1999;289(1):21-27.

235. Oberle I, Rousseau F, Heitz D, Kretz C, Devys D, Hanauer A, et al. Instability of a 550-base pair DNA segment and abnormal methylation in fragile X syndrome. Science 1991;252(5010):1097-1102.

236. Kraemer KH, Seidman MM. Use of supF, an Escherichia coli tyrosine suppressor tRNA gene, as a mutagenic target in shuttle-vector plasmids. Mutat Res 1989;220(2-3):61-72.

237. Ogihara Y, Ohsawa T. Molecular analysis of the complete set of length mutations found in the plastomes of Triticum-Aegilops species. Genome 2002;45(5):956-962.

238. Sinden RR, Zheng GX, Brankamp RG, Allen KN. On the deletion of inverted repeated DNA in Escherichia coli: Effects of length, thermal stability, and cruciform formation in vivo. Genetics 1991;129(4):991-1005.

239. Clare JJ, Rayment FB, Ballantine SP, Sreekrishna K, Romanos MA. High-level expression of tetanus toxin fragment C in Pichia pastoris strains containing multiple tandem integrations of the gene. Biotechnology (N Y) 1991;9(5):455-460.

240. Scorer CA, Buckholz RG, Clare JJ, Romanos MA. The intracellular production and secretion of HIV-1 envelope protein in the methylotrophic yeast Pichia pastoris. Gene 1993;136(1-2):111-119.

241. Daniell H, Guda C, McPherson DT, Zhang X, Xu J, Urry DW. Hyperexpression of a synthetic protein-based polymer gene. Methods Mol Biol 1997;63:359-371.

242. Barr KA, Hopkins SA, Sreekrishna K. Protocol for efficient secretion of HSA developed from Pichia pastoris. Pharm Eng 1992;12:48-51.

243. Wong Po Foo C, Kaplan DL. Genetic engineering of fibrous proteins: Spider dragline silk and collagen. Adv Drug Deliv Rev 2002;54(8):1131-1143.

244. Fahnestock SR, Irwin SL. Synthetic spider dragline silk proteins and their production in *Escherichia coli*. Appl Microbiol Biotechnol 1997;47(1):23-32.

245. Feschenko VV, Rajman LA, Lovett ST. Stabilization of perfect and imperfect tandem repeats by single-strand DNA exonucleases. Proc Natl Acad Sci U S A 2003;100(3):1134-1139.

246. Petit MA, Dimpfl J, Radman M, Echols H. Control of large chromosomal duplications in *Escherichia coli* by the mismatch repair system. Genetics 1991;129(2):327-332.

247. Albertini AM, Hofer M, Calos MP, Miller JH. On the formation of spontaneous deletions: The importance of short sequence homologies in the generation of large deletions. Cell 1982;29(2):319-328.

248. Waterham HR, Digan ME, Koutz PJ, Lair SV, Cregg JM. Isolation of the Pichia pastoris glyceraldehyde-3-phosphate dehydrogenase gene and regulation and use of its promoter. Gene 1997;186(1):37-44.

249. Goochee CF, Gramer MJ, Andersen DC, Bahr JB, Rasmussen JR. The oligosaccharides of glycoproteins: Bioprocess factors affecting oligosaccharide structure and their effect on glycoprotein properties. Biotechnology (N Y) 1991;9(12):1347-1355.

250. Hamilton SR, Bobrowicz P, Bobrowicz B, Davidson RC, Li H, Mitchell T, et al. Production of complex human glycoproteins in yeast. Science 2003;301(5637):1244-1246.

251. Chiba Y, Jigami Y. Production of humanized glycoproteins in bacteria and yeasts. Curr Opin Chem Biol 2007;11(6):670-676.

252. Hamilton SR, Davidson RC, Sethuraman N, Nett JH, Jiang Y, Rios S, et al. Humanization of yeast to produce complex terminally sialylated glycoproteins. Science 2006;313(5792):1441-1443.

253. Wu X, Sallach RE, Caves JM, Conticello VP, Chaikof EL. Mechanical stability and deformation responses of physically crosslinked protein-based materials. Biomacromolecules In review.

254. Nagapudi K, Brinkman WT, Thomas BS, Wright ER, Conticello VP, Chaikof EL. Protein-based thermoplastic elastomers. Macromolecules 2005;38:345-354.

255. Huang L, Apkarian RP, Chaikof EL. High-resolution analysis of engineered type I collagen nanofibers by electron microscopy. Scanning 2001 Nov-Dec;23(6):372-375.

256. Huang L, Nagapudi K, Apkarian RP, Chaikof EL. Engineered collagen-PEO nanofibers and fabrics. J Biomater Sci Polym Ed 2001;12(9):979-993.

257. Langer R, Tirrell DA. Designing materials for biology and medicine. Nature 2004;428(6982):487-492.

258. Tan E L, C. Effect of annealing on the structural and mechanical properties of electrospun polymeric nanofibers. Nanotechnology 2006;17:2649-2654.

259. Swuwanprateeb J. Rapid examination of annealing conditions for HDPE using indentation microhardness test Polym Test 2004;23:157-161.

260. Tiemprateeb S, Hemachandra K, Suwanprateeb J. A comparison of degree of properties enhancement produced by thermal annealing between polyethylene and calcium carbonate-polyethylene composites. Polym Test 2000;19:329-339.

261. Bodugoz-Senturk H, Choi J, Oral E, Kung JH, Macias CE, Braithwaite G, et al. The effect of polyethylene glycol on the stability of pores in polyvinyl alcohol hydrogels during annealing. Biomaterials 2008;29(2):141-149.

262. Suwanprateeb J, Tanner KE, Turner S, Bonfield W. Influence of sterilization by gamma irradiation and of thermal annealing on creep of hydroxyapatite-reinforced polyethylene composites. J Biomed Mater Res 1998;39:16-22.

263. Li G, Shrotriya V, Yao Y, Huang J, Yang Y. Manipulating regioregular poly(3-hexylthiophene): [6,6]-phenyl-C61-butyric acid methyl ester blends-route towards higher efficiency polymer solar cells. J Mater Chem 2007;17:3126-3140.

264. Sinclair AM, Elliott S. Glycoengineering: The effect of glycosylation on the properties of therapeutic proteins. J Pharm Sci 2005;94(8):1626-1635.

265. Formhals A, inventor. Process and appartus for preparing artificial threads, 1934.

266. Martin GE, inventor. Fibrillar product of electrostatically spun organic material, 1977.

267. Li D, Xia Y. Electrospinning: Reinvention of the wheel? Advanced Materials 2004;16:1151-1170.

268. MPC Industry Collegium Report. 2001;17:1-4.

269. Doshi J, Reneker DH. Electrospinning process and applications of electrospun fibers. Journal of Electrostatics 1995;35(2-3):151-160.

270. Reneker DH, Yarin AL, Fong H, Koombhongse S. Bending instability of electrically charged liquid jets of polymer solutions in electrospinning. J of App Phys 2000;87(9).

271. Fridrikh SV, Yu JH, Brenner MP, Rutledge GC. Controlling the fiber diameter during electrospinning. Phys Rev Lett 2003;90(144502):1-4.

272. Fong H, Chun I, Reneker DH. Beaded nanofibers formed during electrospinning. Polymer 1999;40:4585-4592.

273. Deitzel J. The effect of processing variables on the morphology of electrospun nanofibers and textiles. Polymer 2001;42:261-272.

274. Theron SA, Zussman E, Yarin AL. Experimental investigation of the governing parameters in the electrospinning of polymer solutions. Polymer 2004;45:2017-2030.

275. Kadler KE, Holmes DF, Trotter JA, Chapman JA. Collagen fibril formation. Biochem J 1996;316(1):1-11.

276. Silver FH, Kato YP, Ohno MW, A.J. Analysis of mammalian connective tissue: Relationship between hierarchical structures and mechanical properties. J Long Term Eff Med Implants 1992;2(2-3):165-198.

277. Brodsky B, Eikenberry, E. Supramolecular collagen assembilies. Ann NY Acad Sci 1985;460:73-84.

278. Brodsky B, Ramshaw JA. The collagen triple-helix structure. Matrix Biology 1997;15(8-9):545-554.

279. Beck K, Brodsky B. Supercoiled protein motifs: The collagen triple-helix and the alpha-helical coiled coil. Journal of Structural Biology 1998;122(1-2):17-29.

280. Mecham RP, Broekelmann TJ, Fliszar CJ, Shapiro SD, Welgus HG, Senior RM. Elastin degradation by matrix megalloproteinases. Cleavage site specificity and mechanisms of elastolysis. J Biol Chem 1997;272(29):18071-18076.

281. Silver FH, Garg AK. Handbook of Biodegradable Polymers. Amsterdam: Harwood, 1997.

282. Fagien S. Human-derived and new synthetic injectable materials for soft-tissue augmentation: Current status and role in cosmetic surgery. Plast Reconstr Surg 2000;105(7):2526-2528.

283. Stol M, Smetana K, Jr., Korbelar P, Adam M. Poly(HEMA)-collagen composite as a biomaterial for hard tissue replacement. Clin Mater 1993;13(1-4):19-20.

284. Rao KP. Recent developments of collagen-based materials for medical applications and drug delivery systems. J Biomater Sci Polym Edn 1995;7(7):623-645.

285. Parodi R, Carusi G, Santarelli G, Nanni F, Pingitore R, Brunel G. Guided tissue regeneration employing a collagen membrane in a human periodontal bone defect: A histologic evaluation. Int J Periodontics Restorative Dentistry 1997;17(3):282-291.

286. Purna SK, Babu M. Collagen based dressings--A review. Burns 2000;26(1):54-62.

287. Ellis DL, Yannas IV. Recent advances in tissue synthesis in vivo by use of collagen-glycosaminoglycan copolymers. Biomaterials 1996;17(3):291-299.

288. Hirano S, Zhang M, Nakagawa M, Miyata T. Wet spun chitosan-collagen fibers. Their chemical N-modifications, and blood compatibility. Biomaterials 2000;21(10):997-1003.

289. Fofonoff TW, Bell E, inventors. Method for spinning and processing collagen fiber, 1999.

290. Furukawa M, Takada M, Murata S, Sasayama A, inventors. Process for producing regenerated collagen fiber, 1994.

291. Breitender-Geleff S, Mallinger R, Bock P. Quantitation of collagen fibril cross-section profiles in aging human veins. Human Pathol 1990;21:1031-1035.

292. Merrilees MJ, Tiang KM, Scott L. Changes in collagen fibril diameter across artery wall including a correlation with glycosaminoglyan content. Connective Tissue Res 1987;16:237-257.

293. Buck R. Collagen fibril diameter in the common arotid artery of the rat. Connective Tissue Res 1987;16:121-129.

294. Matthews JA, Wnek GE, Simpson DG, Bowlin GL. Electrospinning of collagen nanofibers. Biomacromolecules 2002;3(2):232-238.

295. Zhong S, Teo WE, Zhu X, Beuerman R, Ramakrishna S, Yung LY. Formation of collagen-glycosaminoglycan blended nanofibrous scaffolds and their biological properties. Biomacromolecules 2005;6(6):2998-3004.

296. Zhong S, Teo WE, Zhu X, Beuerman RW, Ramakrishna S, Yung LY. An aligned nanofibrous collagen scaffold by electrospinning and its effects on in vitro fibroblast culture. J Biomed Mater Res A 2006;79(3):456-463.

297. Buttafoco L, Kolkman NG, Engbers-Buijtenhuijs P, Poot AA, Dijkstra PJ, Vermes I, et al. Electrospinning of collagen and elastin for tissue engineering applications. Biomaterials 2006;27(5):724-734.

298. Rho KS, Jeong L, Lee G, Seo BM, Park YJ, Hong SD, et al. Electrospinning of collagen nanofibers: Effects on the behavior of normal human keratinocytes and early-stage wound healing. Biomaterials 2006;27(8):1452-1461.

299. Lu Q, Ganesan K, Siminoescu DT, Vyavahare NR. Novel porous aortic elastin and collagen scaffolds for tissue engineering. Biomaterials 2004;25(22):5227-5237.

300. Ottani V, Raspanti M, Ruggeri A. Collagen structure and functional implications. Micron 2001;32:251-260.

301. McManus MC, Boland ED, Simpson DG, Barnes CP, Bowlin GL. Electrospun fibrinogen: Feasibility as a tissue engineering scaffold in a rat cell culture model. J Biomed Mater Res A 2006;81A(2):299-309.

302. Urry DW. Protein elasticity based on the confromation of sequential polypeptides: The biological elastic fiber J Protein Chem 1984;3:403-436.

303. Brinkman WT, Nagapudi K, Thomas BS, Chaikof EL. Photo-cross-linking of type I collagen gels in the presence of smooth muscle cells: mechanical properties, cell viability, and function. Biomacromolecules 2003;4(4):890-895.

304. Dong CM, Wu X, Caves J, Rele SS, Thomas BS, Chaikof EL. Photomediated crosslinking of C6-cinnamate derivatized type I collagen. Biomaterials 2005;26(18):4041-4049.

305. Kagan HM, Tseng L, Trackman PC, Okamoto K, Rapaka RS, Urry DW. Repeat polypeptide models of elastin as substrates for lysyl oxidase. Journal of Biological Chemistry 1980;255(8):3656-2659.

306. Kidoaki S, Kwon IK, Matsuda T. Mesoscopic spatial designs of nano- and microfiber meshes for tissue-engineering matrix and scaffold based on newly devised multilayering and mixing electrospinning techniques. Biomaterials 2005;26(1):37-46.

307. Vaz CM, van Tuijl S, Bouten CV, Baaijens FP. Design of scaffolds for blood vessel tissue engineering using a multi-layering electrospinning technique. Acta Biomater 2005;1(5):575-582.

308. Smith LA, Ma PX. Nano-fibrous scaffolds for tissue engineering. Colloids Surf B Biointerfaces 2004;39(3):125-131.

309. Stitzel JD, Pawlowski KJ, Wnek GE, Simpson DG, Bowlin GD. Arterial smooth muscle cell proliferation on a novel biomimicking biodegradable vascular graft scaffolding. J Biomater Appl 2001;16:22-33.

310. Keen C, Wnek G, Baumgarten CM, Newton D, Bowlin GL, Simpson DG. Tissue engineered skeletal muscle. New York, NY: Marcel Dekker, 2004.